

Air-path control of clean diesel engines : for disturbance rejection on NOx, PM and fuel efficiency

Citation for published version (APA):

Criens, C. H. A. (2014). *Air-path control of clean diesel engines : for disturbance rejection on NOx, PM and fuel efficiency*. [Phd Thesis 1 (Research TU/e / Graduation TU/e), Mechanical Engineering]. Technische Universiteit Eindhoven. <https://doi.org/10.6100/IR769972>

DOI:

[10.6100/IR769972](https://doi.org/10.6100/IR769972)

Document status and date:

Published: 01/01/2014

Document Version:

Publisher's PDF, also known as Version of Record (includes final page, issue and volume numbers)

Please check the document version of this publication:

- A submitted manuscript is the version of the article upon submission and before peer-review. There can be important differences between the submitted version and the official published version of record. People interested in the research are advised to contact the author for the final version of the publication, or visit the DOI to the publisher's website.
- The final author version and the galley proof are versions of the publication after peer review.
- The final published version features the final layout of the paper including the volume, issue and page numbers.

[Link to publication](#)

General rights

Copyright and moral rights for the publications made accessible in the public portal are retained by the authors and/or other copyright owners and it is a condition of accessing publications that users recognise and abide by the legal requirements associated with these rights.

- Users may download and print one copy of any publication from the public portal for the purpose of private study or research.
- You may not further distribute the material or use it for any profit-making activity or commercial gain
- You may freely distribute the URL identifying the publication in the public portal.

If the publication is distributed under the terms of Article 25fa of the Dutch Copyright Act, indicated by the "Taverne" license above, please follow below link for the End User Agreement:

www.tue.nl/taverne

Take down policy

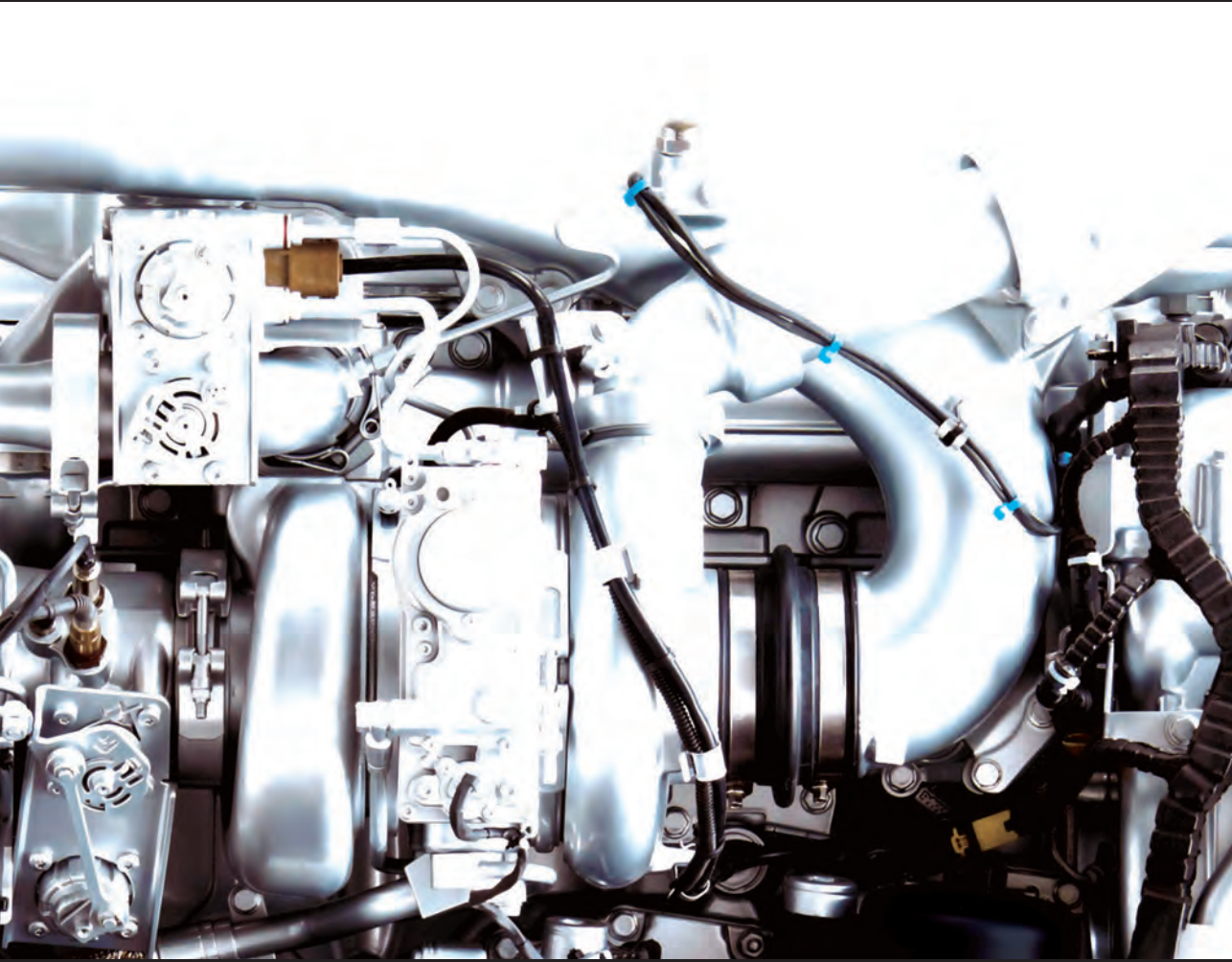
If you believe that this document breaches copyright please contact us at:

openaccess@tue.nl

providing details and we will investigate your claim.

Air-Path Control of Clean Diesel Engines

for disturbance rejection on NO_x , PM and fuel efficiency



Chris Criens

Air-Path Control of Clean Diesel Engines

for disturbance rejection on NO_x, PM and fuel efficiency



This research was financially supported by the HighTech Automotive Systems (HTAS), Further Emission Reduction, Vehicle Efficiency gains and Neutral Thermal loading (FERVENT) program.

disc

The research reported in this thesis is part of the research program of the Dutch Institute of Systems and Control (DISC). The author has successfully completed the educational program of the Graduate School DISC.

Air-Path Control of Clean Diesel Engines for disturbance rejection on NO_x , PM and fuel efficiency

by Chris Criens

Eindhoven: Technische Universiteit Eindhoven, 2014 - Proefschrift

A catalogue record is available from the Eindhoven University of Technology Library.

ISBN: 978-90-386-3575-0

NUR: 951

Typeset by the author using L^AT_EX2e

Cover design: Chris Criens

Cover picture: DAF Trucks N.V. Imagebank, PACCAR MX-13 - EURO 6

Reproduction: Ipskamp Drukkers B.V., Enschede, The Netherlands

Copyright ©2013 by C.H.A. Criens. All rights reserved.

Air-Path Control of Clean Diesel Engines

for disturbance rejection on NO_x, PM and fuel efficiency

PROEFSCHRIFT

ter verkrijging van de graad van doctor aan de
Technische Universiteit Eindhoven, op gezag van de
rector magnificus, prof.dr.ir. C.J. van Duijn, voor een
commissie aangewezen door het College voor
Promoties in het openbaar te verdedigen
op donderdag 13 maart 2014 om 16.00 uur

door

Christiaan Henricus Antonius Criens

geboren te Roermond

Dit proefschrift is goedgekeurd door de promotoren en de samenstelling van de promotiecommissie is als volgt:

Voorzitter:	prof.dr. L.P.H. de Goey
Promotor:	prof.dr.ir. M. Steinbuch
Copromotor:	dr.ir. F.P.T. Willems
Leden:	prof.dr. L. del Re (Johannes Kepler Universität Linz) prof.dr.ir. J. Schoukens (Vrije Universiteit Brussel) dr. L. Eriksson (Linköping University) prof.dr.ir. P.M.J. Van den Hof
Adviseurs:	dr.ir. T.A.C. van Keulen

Contents

Contents	v
Glossary	ix
1 Introduction	1
1.1 Requirements on the Air-Path Control System	6
1.2 State of the Art of Engine Control	8
1.2.1 Production Engines	8
1.2.2 Literature	10
1.3 Opportunities for Improvement	11
1.4 Approach	12
1.5 Main Contributions	14
1.6 Overview of this Thesis	16
2 Fundamentals of Diesel Engines and Combustion	19
2.1 The EURO VI Engine Layout	19
2.1.1 Fuel Path	20
2.1.2 Air Path	21
2.1.3 Exhaust Aftertreatment	22
› Selective Catalytic Reduction	23
› Diesel Particulate Filter	23
2.2 Emission Formation and Fuel Efficiency	24
2.2.1 Combustion Process	24
2.2.2 Emission Formation	26
› Nitrogen Oxides	26
› Particulate Matter	27

2.2.3	Fuel Efficiency	28
2.2.4	Simultaneously Low NO _x , PM and BSFC?	31
2.3	Emission Legislation	32
2.3.1	EURO VI Legislation	34
	› Stationary Testing	34
	› Transient Testing	35
	› Not-To-Exceed Tests	35
	› In-Service Conformity	37
	› Implications for Engine Design and Control	38
3	Literature Overview	41
3.1	Controlled Outputs	42
3.1.1	Track Boost Pressure and Fresh Air Flow	42
3.1.2	Minimize NO _x Emissions	43
3.1.3	EGR Rate and Air-Fuel Ratio	44
3.1.4	Direct Emission Control	45
3.2	Model Predictive Control	46
3.3	Transient Control	50
3.4	Discussion	52
4	Modeling, Identification and Analysis	59
4.1	Introduction	59
4.2	Measurement Setup	63
4.2.1	Engine	63
4.2.2	Actuators	64
4.2.3	Sensors	64
4.3	Design of the Input Signal	65
4.3.1	Multisine	65
4.3.2	Influence of Input Quantization	68
4.4	Analysis of the Identification Accuracy	69
4.4.1	Frequency Response Function	71
4.4.2	Accuracy of the Frequency Response Function	72
4.4.3	Classification of Nonlinearities	74
4.4.4	Time-Domain Validation	77
4.5	Frequency Response Function Measurement Results	82
4.6	Discussion	85
4.7	Conclusions	86

5	Feedback Control for Disturbance Rejection	89
5.1	Introduction	89
5.2	Control Problem	90
5.3	Conceptual Design	93
5.3.1	Actuators	93
5.3.2	Controlled Outputs	95
5.3.3	Input-Output Controllability	96
5.3.4	Control Design	96
5.3.5	Simulation Result	97
5.4	Experimental Design	102
5.4.1	Selection of Controlled Outputs	102
5.4.2	Input-Output Analysis	107
5.4.3	Control Design	111
	› Decoupling	112
	› Feedback Control Design	113
5.4.4	Experimental Results	117
6	Control on the Full Speed-Load Range	125
6.1	Feedback Control	127
6.1.1	NO _x Measurement	128
6.1.2	Decoupling	129
6.1.3	PI control	132
6.1.4	Implementation	134
	› Nominal Inputs and Setpoint Values	134
	› Safety	135
6.1.5	Experimental Results	136
6.2	Feed-Forward Control	138
6.2.1	Control Design	140
6.2.2	Tuning Process	141
6.2.3	Torque Step Experiments	143
6.3	Experimental WHTC Tests	145
7	Conclusions & Recommendations	151
7.1	Conclusions	151
7.1.1	Disturbance Rejection	151
7.1.2	Design Effort	152
7.1.3	Summary of the Main Results	153
	› Identification	153

› Disturbance Rejection	154
› Full Operating Range	155
7.2 Recommendations for Future Research	156
7.2.1 Improved Air Path Control	156
› Control Algorithm	156
› Controlled Outputs	157
› Experiments	158
› Transients	158
7.2.2 Modeling	159
7.2.3 Integrated Engine Control	160
Bibliography	163
Summary	171
Samenvatting	175
Dankwoord	179
Curriculum Vitae	183

Glossary

ACEA Association des Constructeurs Européens d'Automobiles; English: European Automobile Manufacturers Association

AFR Air-Fuel Ratio

AMOX AMmonia OXidation catalyst

a.u. arbitrary units

AVL Anstalt für Verbrennungskraftmaschinen List

BDC Bottom Dead Center

BLA Best Linear Approximation

BMEP Brake Mean Effective Pressure

BPV Back Pressure Valve

BSFC Brake Specific Fuel Consumption

CA50 Crank Angle at which 50% of the combustion heat is released

CO Carbon monoOxide

CO₂ Carbon diOxide

CR Common-Rail

DFT Discrete Fourier Transform

DOC Diesel Oxidation Catalyst

DOE Design Of Experiments

DPF Diesel Particulate Filter

ECE R49 Regulation No. 49 of the Economic Commission for Europe

ECU Engine Control Unit

EEA European Environment Agency

EGR Exhaust Gas Recirculation

ESC European Stationary Cycle

ETC European Transient Cycle

EU European Union

FERVENT Further Emission Reduction, Vehicle Efficiency gains and Neutral Thermal loading

FRF Frequency Response Function

HC Hydro Carbons

HCCI Homogeneous Charge Compression Ignition

HD Heavy Duty

HTAS HighTech Automotive Systems

IDFT Inverse Discrete Fourier Transform

IJPT International Journal of PowerTrains

IMC Internal Model Control

IMEP Indicated Mean Effective Pressure

FMEP Friction Mean Effective Pressure

LPV Linear Parameter Varying

LQG Linear Quadratic Gaussian

LTC Low Temperature Combustion

LTI Linear Time Invariant

MAF fresh Mass Air Flow

MAP Manifold Absolute Pressure, (also: Manifold Air Pressure)

MIMO Multi-Input Multi-Output

MISO Multi-Input Single-Output

MPC Model Predictive Control

NEDC New European Driving Cycle

NL NonLinear

NMHC Non-Methane Hydro Carbons

NO_x Nitrogen Oxides

-
- OBD** On-Board Diagnostics
- ODE** Ordinary Differential Equations
- PCCI** Premixed Charge Compression Ignition
- PC** Personal Computer
- PEMS** Portable Emission Measurement System
- PI** Proportional Integral controller
- PID** Proportional Integral Derivative controller
- PM** Particulate Matter
- PMEP** Pumping Mean Effective Pressure
- PN** Particle Number
- ppm** parts per million
- RGA** Relative Gain Array
- RMS** Root Mean Square
- RPM** Revolutions Per Minute
- SCR** Selective Catalytic Reduction
- SISO** Single-Input Single-Output
- SOI** Start Of Injection
- SVD** Singular Value Decomposition
- SQP** Sequential Quadratic Programming
- TDC** Top Dead Center
- THC** Total HydroCarbon
- TITO** Two-Input Two-Output
- TNO** Nederlandse organisatie voor Toegepast-Natuurwetenschappelijk Onderzoek
- TU/e** Eindhoven University of Technology
- UEGO** Universal Exhaust Gas Oxygen
- US** United States
- VGT** Variable Geometry Turbine
- WNTE** World-harmonized Not-To-Exceed
- WHSC** World-Harmonized Steady-state Cycle
- WHTC** World Harmonized Transient Cycle

1 Introduction

The goal of this research is to design a control system for heavy-duty diesel engines that is capable of combining a low fuel consumption with low emissions of Nitrogen Oxides (NO_x) and Particulate Matter (PM). In addition, these properties should be maintained when disturbances are present. A feature of the to be designed control system should be that the required design effort is low. The relevance of such a control system is further detailed in this introduction.

Fuel efficiency and reliability made diesel engines the most popular means of propulsion for commercial Heavy-Duty (HD) trucks. In spite of their fuel efficiency and accordingly low CO_2 emissions, diesel engines are known to cause more pollution than gasoline engines (Guzzella and Amstutz, 1998). The lean diffusion combustion in diesel engines produces more PM and makes the use of three-way catalysts ineffective, resulting in higher NO_x emissions.

The 2013 report of the European Environment Agency (EEA) on emissions in the European Union (EU) between 1990 and 2011 (European Environment Agency, 2013), provides data on the recent evolution of harmful emissions in the EU. Road transport is one of the main contributors to these emissions. In 2011, 40% of the total NO_x emissions originated from road transport, equally divided between passenger cars and commercial HD vehicles. Also, 17% of the total fine PM emissions originated from road transport, slightly more from passenger cars than from HD vehicles. To protect man and his environment against the air pollution caused by these emissions, the EU restricts these emissions via legislation. As a result, the total emissions of NO_x decreased with 48% between 1990 and 2011. For the PM emissions, a 20% reduction was achieved between 2000 and 2011. The

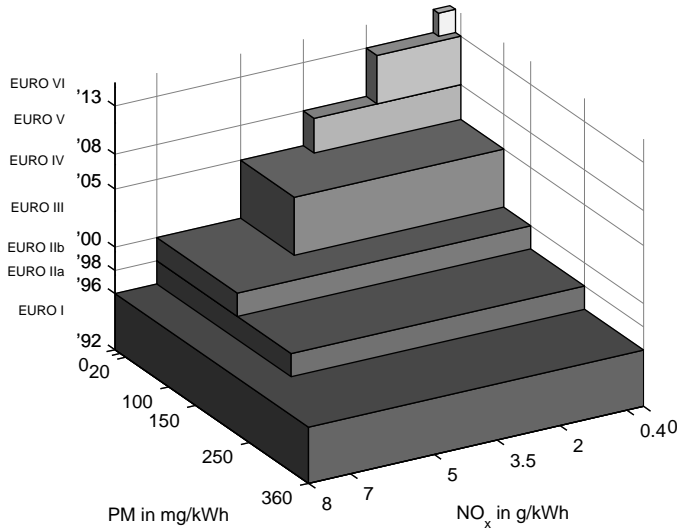


Figure 1.1: The evolution of the heavy-duty steady-state emission limits for NO_x and PM in the European Union. Data source: DieselNet (2013).

EU goal for 2020 is to achieve a further 42% and 22% decrease in the overall NO_x and PM emissions, respectively, with the 2005 emissions as the baseline.

Figure 1.1 shows the evolution of the limits for NO_x and PM emissions of HD diesel engines in the European Union. With EURO VI, the emission limits have reached near zero impact levels. Moreover, to increase the practical impact of the tightened legislation, World harmonized Not-To-Exceed (WNTe) and in-service conformity emission limits are introduced with EURO VI (see Section 2.3.1 for more details). The drive cycle, ambient conditions, fuel composition, production tolerances and ageing can all influence the produced emissions. This makes guaranteeing compliance with in-service emission limits particularly challenging.

Considering the NO_x and PM emission goal for 2020, the low emission limits in EURO VI and the natural phasing out of EURO III, EURO IV and EURO V vehicles, further drastic cuts in the allowed emission levels are not expected in the near future. Instead, legislation restricting the CO₂ emissions, or almost equivalently, the fuel consumption, is anticipated. In the United States (US), fuel consumption legislation for 2014-2018 engines is already finalized. Up until the introduction of increasingly stringent emission legislation, a trend was observed

that fuel economy improved in newer vehicles. Because reducing the emissions of NO_x and PM required the implementation of measures that conflict with fuel efficiency, this trend has stopped, despite the advancements in technology. Fuel consumption is, and has been, a major competitive factor for truck manufacturers. Any cost effective solution to reduce the fuel consumption is therefore readily adopted in production vehicles (ACEA, 2010). When needed for compliance with legislation, fuel-reduction technologies that have not proven to be cost-effective will be implemented as well.

For engine manufacturers, the increasingly stringent legislation requires constant innovation of their engines. Complying with emission legislation in a cost effective manner and with minimum impact on the fuel consumption, resulted in the adoption of several new hardware components. A typical EURO VI engine comprises components that provide control over the air intake and fuel injection, and reduce the emissions via exhaust gas aftertreatment. Figure 1.2 lists the components typically available in a modern EURO VI HD diesel engine.

To utilize the flexibility provided by the new components and release their full potential, a digital, electronic control system is used. This system provides settings for each component, based on the actual engine speed, torque demand and sensor measurements. Along with the increase in the number of components, the complexity of this control system increased as well. The time and effort needed to design and calibrate a control system that achieves optimal, or at least satisfactory, engine performance increased significantly.

In this thesis, control design for the diesel engine air path is considered. Air-path control is particularly interesting. It is challenging and time consuming to calibrate using current control methods. Moreover, the air path contains a variety of sensors and actuators, which means that within the current hardware constraints, various control layouts are possible. The main actuators in the air path are the Variable Geometry Turbine (VGT) and Exhaust Gas Recirculation (EGR) valve. Figure 1.3 shows the air path of an EGR diesel engine including a VGT and EGR valve.

Exhaust Gas Recirculation (EGR) is used in diesel engines to reduce the NO_x emissions. By diluting the intake air with cooled exhaust gas, the combustion temperature is lowered, which reduces the NO_x formation. The combination of a

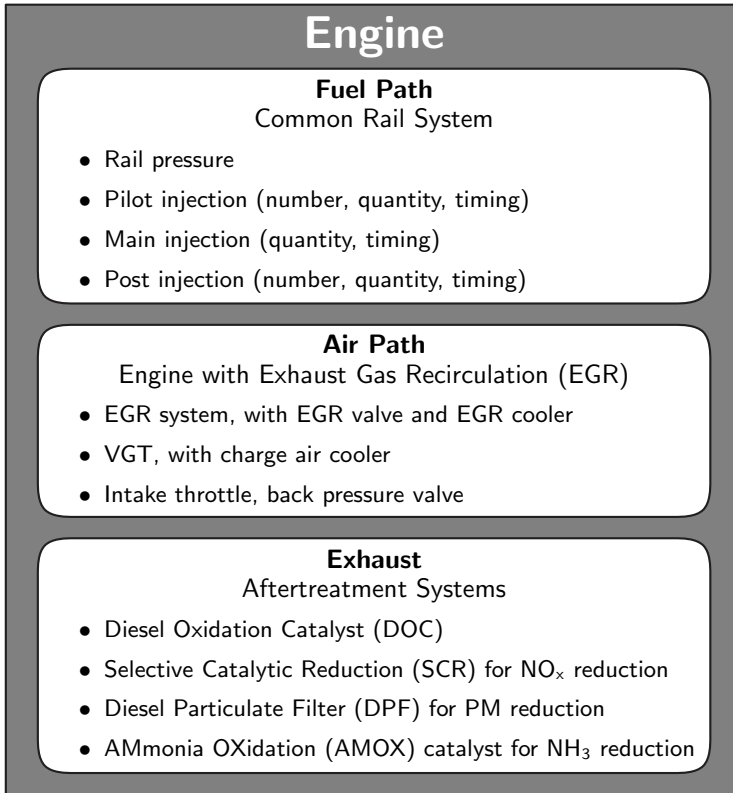


Figure 1.2: Subsystems of a typical, heavy-duty EURO VI engine.

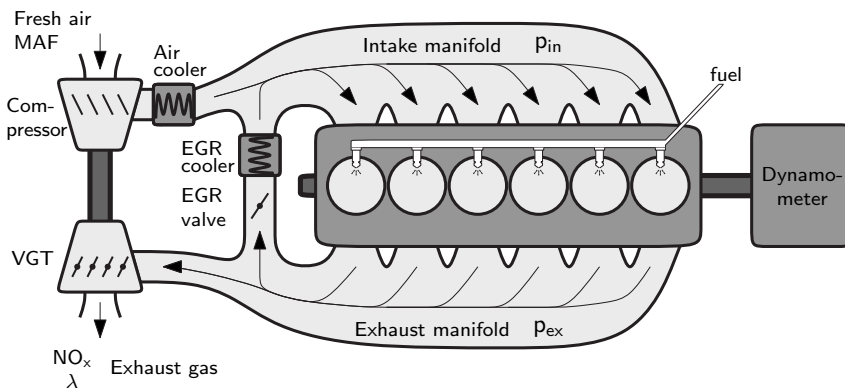


Figure 1.3: A schematic representation of the layout of the air path of the studied EGR engine.

VGT and EGR valve provides control over the flows of fresh air and exhaust in the engine. This affects the NO_x and PM emissions as well as the fuel efficiency. More details on the functioning of the VGT and EGR are provided in Section 2.1.2.

For EURO VI, emission control has gained importance. The allowed emission limits were drastically reduced, which makes tight compliance with legislation increasingly important to minimize the fuel consumption. Moreover, to ensure in-service conformity, which is required for EURO VI, the effects of disturbances and uncertainties in the engine have to be accounted for. Via the VGT and EGR valve actuators, the air-path controller affects the NO_x and PM emissions and the fuel consumption. The air-path controller is therefore a key part of the design of a fuel efficient, EURO VI compliant diesel engine.

Air-path control for diesel engines is considered challenging. Several conflicting and tight requirements are present (Alberer et al., 2012). Minimizing the engine-out NO_x emissions can result in excessive PM emissions and vice versa. To achieve EURO VI compliance, both emission species must be maintained within tight bounds. To be economically viable, the fuel consumption must be minimized. The dynamic behavior of the air path can be characterized as coupled, nonlinear and nonminimum phase. These characteristics complicate control design. Also, the external disturbances and internal uncertainties that are present affect both the outputs of the system and the dynamic input-output response. A successful control design should have regard for all the above aspects.

The use of EGR, controlled via the EGR valve and VGT, is not limited to current EURO VI engines. Advanced combustion concepts such as Low Temperature Combustion (LTC), Homogeneous Charge Compression Ignition (HCCI) and Premixed Charge Compression Ignition (PCCI) also rely heavily on the use of EGR. Engines using these combustion concepts are currently being investigated in academic literature. They have the potential to combine extremely low emissions with a high fuel efficiency. In particular for HCCI and PCCI engines, very high EGR rates are necessary for proper functioning. EGR is used to reduce the otherwise excessive combustion rate and can also be used to control the combustion phasing. For these engines, control is even more important than for the EURO VI diesel engines considered in this thesis. Their operation is not naturally stable, which makes the use of feedback control a necessity.

1.1 Requirements on the Air-Path Control System

The main purpose of a diesel engine in a commercial vehicle is to provide propulsion. The control system provides some essential tasks in achieving this in the best way possible.

On a high level, the goals of a diesel engine control system are as follows.

- **Drivability** Achieve a satisfactory level of drivability, i.e., comply with the drivers torque demand.
- **Legislation** Comply with the EURO VI emission legislation, both for type approval and in use.
- **Fuel consumption** Minimize the operational costs of the vehicle, which are largely determined by the fuel consumption.
- **Constraints** Remain within limits for safety, noise and durability.

The control system is not the only factor that determines whether or not the above goals are met. The synergy between the engine hardware, its control system and the external conditions determines the achieved engine performance. As a subsystem of the overall engine control system, the air-path controller can provide a partial contribution to achieving the above goals. The following list provides the main aspects where the air-path controller can contribute.

- **Enable overall low emissions and low fuel consumption** The air path affects the engine-out NO_x and PM emissions as well as the fuel efficiency. The air-path controller should therefore apply settings that result in simultaneously low NO_x and PM emissions and a low fuel consumption.
- **Improve the robustness** The real-world emissions of a diesel engine are affected by disturbances and uncertainties such as ambient conditions, fuel composition, production tolerances and ageing. In particular for EURO VI engines, where not-to-exceed and in-service conformity limits are enforced, reducing the effects of these disturbances and uncertainties on the NO_x and PM emissions is important for tight compliance with the limits set in legislation.

- **Decrease the turbo lag** The turbocharger is responsible for providing the fresh air flow that is required to generate a high brake torque. When the torque demand is low, the turbocharger speed is low as well. Due to its inertia, the turbocharger cannot instantly speed up and provide the boost pressure and air flow needed to generate the peak torque. Consequently, when the driver demands a fast change from low to high torque, turbo lag is observed, while the turbocharger speeds up. In an engine equipped with a VGT and EGR system, the EGR flow and pressures in the intake and exhaust manifold can be influenced by the VGT and EGR valve. This can result in a faster acceleration of the turbine and an additional increase in the fresh air flow ahead of the increase in turbine speed. Control using the VGT and EGR valve therefore affects the observed turbo lag.

The control design in this thesis focusses on performance with respect to the above aspects. For a practical integration into a production engine, other aspects are relevant as well.

- **Design time** An increase in the design time and effort results in an increase in the costs associated with control design. Moreover, the time to market of new engines increases. The increase in flexibility due to additional actuators and sensors resulted in a significant increase in control design effort. It is even expected that by 2020, the effort associated with control design exceeds the effort associated with the design of the engine hardware. Considering this, the effort needed for control design is a considerable factor to take into account.
- **Computational complexity** The computational power of a modern Engine Control Unit (ECU) and the memory available for storage are limited. The footprint on the ECU should therefore be small and be compatible with current production ECUs.
- **Use currently available hardware** Research engines can be equipped with an extensive sensor set and additional actuators. In production engines, the means are much more limited. Size, cost-effectiveness and reliability limit the availability of sensors and actuators and a control design should fit within these restrictions.

- **Flexibility** Engines will have different modes that are selected depending on the current requirements, e.g., during warm-up, the engine will be controlled differently than during normal operation. A control system should be able to cope with this and remain functional.
- **General applicability** The control design method should be applicable for a range of engine topologies. Moreover, the controller should work without further modification on a full production series during the complete live cycle of the engines.
- **Integration into the control system** As shown in Figure 1.2, the air-path control system constitutes only a part of the engine control system. In consequence, a synergy with the other parts of the control system is required.

The practical considerations above are important and will be kept in mind during control design. Compliance with these aspects is flexible, e.g., when a significant improvement of the fuel efficiency can be achieved, a failure to meet any of the above practical aspects may be justified.

1.2 State of the Art of Engine Control

1.2.1 Production Engines

The control systems that are used in production engines are typically confidential and undisclosed. The details of the state-of-the-art control systems as applied in production engines are therefore not available.

It is however known that production control systems rely heavily on so called engine maps (Stewart et al., 2010) to control the engine. These maps provide settings for all actuators depending on the speed-load operating point of the engine. By means of Design Of Experiment (DOE), they can be calibrated efficiently. Also, when using a nominal engine, under nominal and steady-state conditions, an engine map is a nonconservative control method, i.e., under these conditions control via a well-calibrated engine map is sufficient to achieve optimal performance.

When disturbances are present or the engine is in a transient state, i.e., the engine speed or torque is not constant, an engine map that provides settings based

on the operating point is no longer sufficient for optimal performance. Therefore, additional maps are implemented that adapt the base engine map using sensor measurements as input. Although they are based on sensor data, the adaptations are usually of the feed-forward type, i.e., the sensor measurement is not directly affected by the actuator setting that is adapted. This type of control design can theoretically be nonconservative. Suppose that all engine states, external disturbances and uncertain parameters are accurately measured. And also that based on all these measurements, a multidimensional map is created that contains the optimal settings for each actuator. This type of control is nonconservative and optimal performance is achieved.

In a practical setting, achieving optimal performance using the method described above is not a feasible approach. First of all, not all measurements that are theoretically required are available. But also, the control design effort will be enormous. For example, even using only five internal and three external measurements, and a grid density of 10 control settings per measurement, a total of 10^8 actuator settings have to be calibrated and stored for each actuator. The exponential increase in the complexity when the number of measurements or actuators increases makes this method of control prohibitively complex, when optimal performance is strived for.

To reduce the control design effort, subsystems are identified that are calibrated individually, largely neglecting possible interactions. This reduces the complexity, but also introduces conservatism. Despite this, the control design effort is immense (Stewart et al., 2010; Pachner et al., 2012; Henningsson, 2012; Guzzella and Amstutz, 1998). Moreover, when sensors and actuators are added to the engine, the complexity rapidly increases even further.

In addition to map-based feed-forward control, feedback control is also applied in production engines. Feedback control can make the achieved performance more robust against disturbances. Also, feedback control can be an effective way of reducing the performance requirements on the feed-forward control system, because it can compensate for the remaining inaccuracies. This potentially reduces the required calibration effort. Details of the applied feedback strategies are not disclosed. Considering the increasing design time that is widely reported, it can be concluded that thus far, a feedback control solution that provides a reduction in calibration effort and accurate disturbance compensation is not available.

1.2.2 Literature

In literature, diesel engine control and also air-path control are extensively studied. A brief review is presented here, with a more elaborate version in Chapter 3. To determine the state of the art in current academic research on control using the VGT and EGR valve, two paths are distinguished. First, the use of new control algorithms is proposed to make control design more efficient, improve on the achieved performance, or both. Second, the use of new control problems with different output combinations, often using different, newly available sensors is proposed. This results in new control problems that may better reflect the actual high-level objectives as listed in Section 1.1. Generally, the use of feedback control is widespread in academic literature.

In terms of control schemes used for air-path control, the current state of the art is arguably Model Predictive Control (MPC). Several versions of MPC for air-path control have been proposed as listed in Section 3.2. MPC allows for a systematic and optimal control design procedure that can take into account nonlinear system behavior, and constraints on the actuator range and internal engine states. This makes MPC very suitable for air-path control from a performance perspective. In consequence of the complexity of the MPC algorithm, several simplifications are needed to enable an experimental demonstration on an engine. These simplifications complicate the control design and can hamper the performance obtained by the controller. The differences between the papers listed in Section 3.2 are mostly found in the simplifications that are used. Variations are found in the considered constraints, the modeling method used to take into account the nonlinear engine behavior, prediction and control horizon, and the algorithm used to synthesize the controller.

The studied control problems found in literature evolve towards more direct control of emissions. Initially control designs used control of fresh Mass Air Flow (MAF) and Manifold Absolute Pressure (MAP). Sensors to measure these quantities are present by default in the air path of a production engine. Sensors for measuring PM emissions are lacking in current HD production engines, and the use of a NO_x sensor is often dismissed due to the slow sensor dynamics of the available NO_x sensors. Direct control of NO_x and PM (using a research opacity sensor to determine PM) is used in Tschanz et al. (2013). Earlier works often also thrive towards direct emission control, but use substitute measurements, e.g., EGR rate

instead of NO_x , and λ instead of PM. In terms of controlled outputs, a very elaborate study is done in Karlsson et al. (2010), where Indicated Mean Effective Pressure (IMEP), combustion phasing, maximum pressure derivative, NO_x emissions and exhaust opacity are controlled. This work also employs MPC control, but in a simplified linear version, which is applicable only at a single speed-load operating point.

1.3 Opportunities for Improvement

With the goals of this research in mind: enable low average emissions and a low average fuel consumption, improve the robustness and decrease the turbo lag. And also considering the current issues with the high control design effort, the state-of-the-art is reviewed to distinguish opportunities for improvement.

In terms of performance potential, MPC is a very suitable control technology. Moreover, it is very flexible in terms of modeling and can work with a wide range of optimization criterions. However, with robustness as a main goal, MPC falls short. Stability, or robust stability, a basic aspect of any practical control algorithm, is not guaranteed by default. Moreover, the approaches presented in the literature show that the computational complexity of the resulting control law pushes the boundaries of what is possible with current ECU hardware. Considering this, the presented MPC approaches are not very suitable to reduce the control design effort in a practical setting. A systematic, low-complexity control design is likely to improve upon this.

In terms of the considered outputs, it has been shown that the classical approach of MAF-MAP control is not effective for disturbance rejection on the engine-out NO_x and PM emissions. Even high-end control algorithms that achieve accurate tracking of MAF-MAP do not necessarily improve the performance on the high-level objectives. In Chapter 5 of this thesis, it is shown that control of NO_x and PM, using the air-path actuators, is not compatible with robust stability and may deteriorate the fuel efficiency in a low emission engine. Control solutions that take into account both fuel efficiency and emissions are scarce in literature, with Henningsson (2012) and Wahlström et al. (2010) as the main contributions. The work of Henningsson (2012) is intended as an academic showcase and is not suitable for implementation due to the control algorithm and the use of sensors

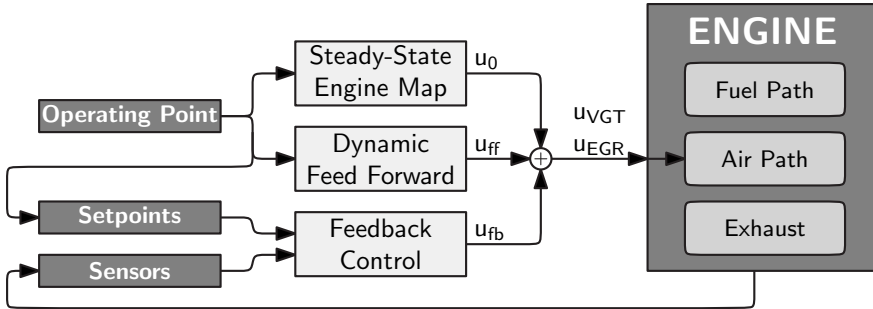


Figure 1.4: An overview of the proposed control scheme.

that are available only on research engines. The work of Wahlström et al. (2010) does not use the currently available emission sensors and aims mostly to minimize the pumping work. Disturbance rejection on NO_x and PM emissions as well as fuel efficiency can improve on the current approaches found in literature.

1.4 Approach

The control structure that is proposed in this thesis consists of three parts. First, a base engine map defining nominal VGT and EGR settings based on engine speed and torque request, and corresponding setpoints. Second, a feedback controller to reduce the effects of disturbances. Third, a dynamic feed-forward controller to improve the torque response and reduce the PM emissions during torque transients. This control layout is illustrated in Figure 1.4.

The steady-state engine map, which is a map with input settings, u_0 , for all speed-load operating points, is available a priori and its design is not discussed in this work. Although it largely determines the actual performance of the engine, standard Design Of Experiments (DOE) techniques are adequate to calibrate the parameters in the engine map. Using DOE, optimal settings for stationary engine speed and load can be found in a reasonable amount of time. Feed-forward by means of a map is very flexible and, when a dense enough grid is used, it is nonconservative for stationary performance under nominal conditions.

The feedback controller is the main part of the new control design. Its purpose is to adapt the VGT and EGR valve, such that the optimal tradeoff between

NO_x , PM and fuel efficiency is maintained as closely as possible when disturbances are present. Moreover, the feedback controller keeps the NO_x and PM emissions close to their nominal values, to ensure tight compliance with emission legislation. By applying feedback control, the effects of uncertainties and disturbances are compensated for. The external disturbances include, e.g., ambient changes in temperature, pressure and humidity, and differences in fuel quality and composition. Also, engine temperature variations, aging, production tolerances, fouling of the engine and aftertreatment system, and actuator imperfections and hysteresis affect the achieved emissions and fuel efficiency. To make feedback control most effective, outputs are selected that are directly related with the high-level objectives. The NO_x emissions, PM emissions and fuel efficiency are represented by NO_x emissions, air-fuel equivalence ratio, λ , and pressure difference between the intake and exhaust manifold, Δp , respectively. The output value that is obtained under nominal conditions is used as a setpoint value. When the feedback controller actively maintains the outputs close to their respective setpoint values, the effects of changing conditions on the emissions and fuel efficiency is counteracted. The design of the feedback controller is further discussed in Chapter 5.

During transient engine operation, the combination of the engine map with feedback control is no longer sufficient. To ensure a fast torque response and reduce the PM emissions when a large increase in torque demand is applied, additional functionality is needed. For this reason a dynamic feed-forward controller is implemented. This controller takes additional control actions based on the variation of the torque demand. This speeds up the response of the fresh air flow and turbine speed. A simple structure with a small number of parameters is used such that manual tuning on a dynamometer test setup is possible. With the extensive emission measurement capabilities available on a dynamometer setup, the feed-forward parameters can be calibrated to achieve a desirable combination of NO_x emissions, PM emissions and torque response.

Apart from the performance of the controller, the design effort is also a bottleneck in the design process. Both the proposed feedback controller and feed-forward controller require a short design time. The design of the feedback controller is completely model based. This shifts the design effort from manual calibration on an engine towards model design and identification. The multisine identification procedure elaborated in Chapter 4 offers a time-efficient identification procedure.

The resulting linear Frequency Response Function (FRF) models are directly suitable for the design of the proposed feedback controller. Moreover, the identification procedures allows an extensive analysis of the accuracy of the identified models. The effects of nonlinearities and noise are quantified separately, which provides confidence in the accuracy of the resulting models and identification procedure. Based on the FRF models, a control design consisting of decoupling and classical control design is proposed. It is shown that despite the nonlinear behavior, a linear controller is effective. This results in a feedback controller with both a low design and implementation effort. The calibration of the dynamic feed-forward controller is performed manually on a dynamometer test setup. Here, the design effort is low due to the small number of parameters (four) that require calibration.

1.5 Main Contributions

The main contributions of this work are: a new feedback and feed-forward control design method; multisine FRF identification and analysis applied to the diesel engine air path; a representative testing procedure. To achieve a reduction in the control design time, this aspect is taken into consideration in all parts of the control design process. This is explained below in more detail.

- **New feedback control strategy** A new choice of controlled outputs is made. The NO_x sensor, λ sensor are combined with a measurement of the pressure difference between intake and exhaust manifold, Δp . These outputs have a direct relation with the performance measurements of a diesel engine. This selection is aimed at improving the robustness of the engine. Robustness has two interpretations in this context. First, maintaining closed-loop stability in case of uncertainty of the input-output response. Second, maintaining the performance (emissions, fuel consumption, torque response) when disturbances are present. Both aspects of the robustness improve as a result of this selection. It is shown that with this new selection of controlled outputs, a linear feedback controller can be used in almost the complete operating range. This is a significant simplification over alternative control methods, which reduces the complexity of the controller and reduces the design time.

-
- **New feed-forward control strategy** The feed-forward controller has a new structure, which is efficient to implement and easy to calibrate. A dynamometer test setup that is equipped with emission measurement equipment and torque sensors is used during calibration. Using a small number of parameters, manual tuning for optimal performance is possible. Combined with the measurement equipment available on a dynamometer setup, direct optimization of the high-level objectives can be achieved. Compared with previous approaches, the design complexity and possibility for direct optimization of the high level objectives are improvements.
 - **Time-efficient and accurate system identification** Linear system identification using multisine excitation signals was used to model the input-output dynamics. The local behavior and accuracy of the identification were extensively analyzed. This analysis includes the ability to quantify to what extent the local behavior is linear. Moreover, the effects of noise and nonlinearity are separated from the identified models and individually quantified. It was found that using 10 minutes of measurement time, an accurate local model can be identified at a single speed-load operating point. The identified models naturally include both sensor and actuator dynamics, which is important for the intended application: the design of feedback controllers. Also, the ability to model any measured output, including emissions, is an advantage; the emissions are very difficult to model using first-principles models. Both the multisine FRF identification procedure and the analysis are not found in literature for the application of engine control. Moreover, when the operating point is fixed, the accuracy of the resulting models is very high, compared with alternative modeling approaches found in literature.
 - **Representative testing procedure** The control design presented in this thesis is demonstrated and tested experimentally on a EURO VI type engine. The performance is validated while additional disturbances are applied as well as using the World Harmonized Transient Cycle (WHTC). This cycle is designed to be a realistic representation of actual world-wide usage of engines in commercial vehicles and is also used in the EURO VI emission test procedure. Although in industrial practise the use of realistic test cycles is common, in academia, controllers are often evaluated on simplified test cycles only.

1.6 Overview of this Thesis

The remainder of this thesis is organized as follows.

Chapter 2 contains background information regarding diesel engines and in particular emission formation and legislation.

In Chapter 3, an overview and review of relevant academic literature in the field of air-path control and diesel engine control is presented.

Chapter 4 considers modeling, identification and analysis of the dynamic behavior of the air-path. The chapter elaborates on the identification procedure, accuracy of the resulting models and sources of distortion. The contents of this chapter are also submitted for journal publication.

Chapter 5 deals with feedback control for disturbance rejection around a single speed-load operating point. The purpose of this controller is to reduce the effect that disturbances and uncertainties have on the achieved emissions and fuel efficiency. In this chapter, the selection of both sensors and actuators is discussed. Also, the properties of the control problem are analyzed. A feedback controller is designed and its ability to counteract disturbances is experimentally validated.

In Chapter 6, the design procedure of a controller to be used with varying engine speed and load is detailed and executed. The results of Chapter 4 and Chapter 5 are used and in addition a dynamic feed-forward controller is designed. The resulting controller is suitable for transient operation in the complete speed-load operating range. A time efficient design process is an important consideration for the controller in this chapter. The performance of the engine using this controller is evaluated on the WHTC.

The thesis ends with conclusions and directions for future research. The presented control design and performance are reviewed and suggestions for further improvements are provided. Also, suggestions for further integration of the air-path controller into the engine control structure are made.

2 Fundamentals of Diesel Engines and Combustion

This chapter details the working principles of a modern diesel engine. The layout of a modern HD EURO VI diesel engine is described in Section 2.1. Section 2.2 is dedicated to diesel combustion, emission formation and fuel consumption and how the available actuators can influence these parameters. The current emission legislation is detailed in Section 2.3.

2.1 The EURO VI Engine Layout

Various layouts and additional subsystems can be considered for a EURO VI engine. In this section the layout of the studied EURO VI engine is described. The functionality of the engine hardware outside of the cylinder block is subdivided into three parts, which are all interconnected, but all serve different purposes: the fuel path, air path and aftertreatment. Figure 2.1 illustrates this.

The main purpose of a HD diesel engine is provide propulsion for the vehicle. For this, chemical energy that is stored in diesel fuel is converted into heat during

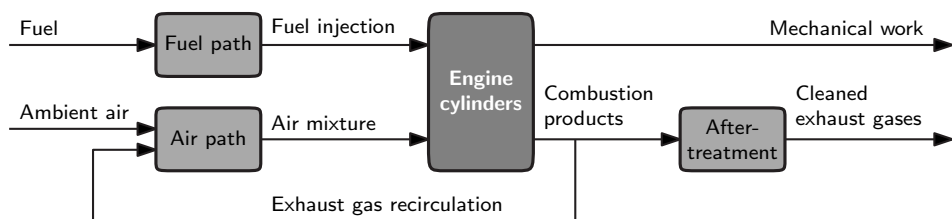


Figure 2.1: A block scheme of the high-level layout of a diesel engine.

combustion in the cylinders. As a result of the heat release, the temperature and pressure of the air-exhaust-fuel mixture within this cylinder increase. During expansion of the mixture, the high pressure adds mechanical work to a moving piston, which ultimately provides the desired propulsion to the wheels of the vehicle.

This process should occur with a high conversion ratio of the chemical energy stored in the fuel into the mechanical work that drives the wheels. Moreover, the composition of the produced exhaust gas should comply with the EURO VI legislation. This is realized by precise timing and dosing of the fuel injection, controlling the amount and composition of the intake air mixture and cleaning the exhaust gases. The following sections detail the hardware components that achieve this.

2.1.1 Fuel Path

To inject the fuel, a Common-Rail (CR) fuel injection system is used. In a CR system, a single accumulator (common rail) is used to store fuel at a high pressure. From this accumulator, fuel is distributed to the fuel injectors. The fuel in the rail is stored at a high, controllable pressure. Pressures up to and sometimes over 2500 bar can be achieved and are controlled by the engine ECU. High pressures are beneficial for the atomization of the injected fuel, which increases the combustion efficiency and decreases the PM emissions, but also require additional power for the fuel pump.

Fuel injectors are also controlled by the ECU and are used to inject the high-pressure fuel from the rail into the cylinders. Combined with a common rail, multiple injections with controllable start and end of injection are possible. A main injection can be combined with a smaller pilot injection to reduce the combustion noise and emissions. In a modern CR system, even multiple pilot injections and post injections per cycle are possible.

2.1.2 Air Path

The purpose of the air path is to provide a fresh air-exhaust mixture of the desired composition and with sufficient oxygen into the cylinders. To achieve this, a compressor, charge air cooler, intake and exhaust valves, Variable Geometry Turbine (VGT), Exhaust Gas Recirculation (EGR) valve, EGR cooler, Back Pressure Valve (BPV) and intake throttle can be used. Figure 1.3 shows the basic layout of an EGR engine, including most parts mentioned above. In addition to what is shown in Figure 1.3, an intake throttle can be placed before the compressor, and a BPV after the turbine. The intake and exhaust valves are located at the cylinders.

In a turbocharged engine, disregarding EGR for the moment, air enters through the air intake. The density of the air is first increased by the compressor and is secondly further increased by the charge-air cooler. When the intake valves open, the high-density air is aspirated into the cylinders, where it is used for combustion. Due to the increased air density, more oxygen is available and consequently, more fuel can be efficiently combusted in the cylinders. Thus increasing the maximum torque that can be produced by the engine. After combustion, the exhaust valves open and the exhaust gas flows through a turbine, where the excess energy in the exhaust gas is used to power the turbine.

When the turbine is of the VGT type, the nozzle geometry at the inlet of the turbine can be varied. This way, the flow properties of the turbine can be influenced. Modifying the inlet directly affects the turbine power, pressure in the exhaust manifold and flow through the turbine. The VGT can therefore be used in an air-path control system.

The considered engine is equipped with a high-pressure, cooled EGR system. Therefore, a part of the exhaust gas is recirculated. It flows via a controllable EGR valve and EGR cooler from the exhaust manifold into the intake manifold. By adding cooled exhaust gas to the intake air, the composition, specific heat capacity and total mass of the intake air mixture can be influenced. This affects the combustion process and thus the produced emissions. EGR is used in particular for reducing the engine-out NO_x emissions. The pressure difference between the intake and exhaust manifold is the driving force for the EGR flow. Therefore, both the VGT and the EGR valve affect the EGR flow. Similarly, when the amount

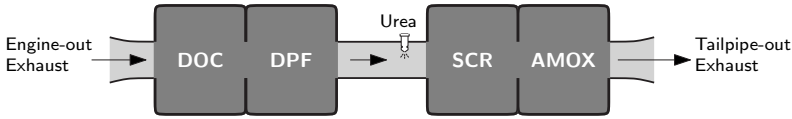


Figure 2.2: The parts of a typical HD EURO VI exhaust aftertreatment system; the Diesel Oxidation Catalyst (DOC), Diesel Particulate Filter (DPF), Selective Catalytic Reduction (SCR) and AMmonia OXidation catalyst (AMOX)

of recirculated exhaust gas is increased, the turbine flow and the intake air flow reduce. The VGT and EGR therefore naturally form a coupled system.

The optional use of an intake throttle and BPV adds flexibility to the use of the turbine, but also induces additional pumping work when (partially) closed. Partially closing the intake throttle will reduce the intake flow and intake manifold pressure and thereby increase the EGR flow. Closing the BPV (partially) reduces the turbine power and increases the back pressure. This also reduces the flow of fresh air and exhaust and increases the EGR flow. These effects can be desired, e.g., for engine braking, or to increase the EGR flow beyond what can be achieved using the VGT. Also, the increased exhaust gas temperature resulting from the use of a BPV can increase the efficiency of the exhaust gas aftertreatment system.

2.1.3 Exhaust Aftertreatment

In this thesis, engine-out emissions rather than tailpipe-out emissions are considered. The difference between these two is caused by the aftertreatment system. To achieve EURO VI compatible emissions, some form of aftertreatment is necessary as with currently applied technology, the engine-out emissions exceed the EURO VI acceptable emission levels. A typical aftertreatment system, shown in Figure 2.2, combines a Selective Catalytic Reduction (SCR) system to reduce NO_x and a Diesel Particulate Filter (DPF) to filter PM. In addition, a Diesel Oxidation Catalyst (DOC) is used to reduce the amount of CO and HC in the exhaust gas and convert NO into NO_2 and an AMmonium OXidation catalyst (AMOX) is used to oxidize the ammonia slip from the SCR.

Selective Catalytic Reduction

The SCR system is the commonly used NO_x reduction system in HD EURO VI engines. In an SCR system, ammonia, which is supplied via urea, reacts with NO and NO_2 to form nitrogen and water. To make this reaction possible with a high conversion efficiency, a catalyst material, often zeolite, and an elevated exhaust temperature are required. With favorable conditions for this reaction, NO_x conversion efficiencies of 95 % and above can be achieved.

The main disadvantages of an SCR system are added costs for the equipment, the costs of the urea consumption, possible ammonium slip and the required high exhaust temperature. The ammonium slip is typically small, but to achieve this, a control system to carefully dose the urea flow and an AMOX catalyst are needed. When the exhaust temperature is increased to increase the SCR efficiency, more energy is present in the exhaust gas, which induces a fuel penalty. More details on the SCR system are provided in the reference (Willems and Cloudt, 2011) and the references therein.

Diesel Particulate Filter

A DPF filters PM from the exhaust gas and stores it in the filter. A DPF can remove over 98 % of the PM from the exhaust gas. To avoid clogging of the filter, which would cause an increased back pressure, the filter is regenerated by oxidizing the stored particulates. This regeneration is done in part passively, when NO_2 in the exhaust gasses reacts with the particulates. Also active regeneration is used, for this, the exhaust gas temperature is artificially increased at times, by burning additional fuel. With the resulting high exhaust gas temperature, the excess oxygen in the exhaust gas oxidizes the particulates stored in the DPF.

High engine-out PM emissions often combine with a reduced fuel efficiency for two reasons. First, the engine-out PM emissions are the result of incomplete combustion, i.e., not all chemical energy that is available in the injected fuel is used effectively to generate heat. Second, active regeneration of the DPF induces a fuel penalty. Therefore, even with a DPF that filters PM with a very high efficiency, low engine-out PM emissions should be aimed for. Additional information on the DPF system can be found in, e.g., (Koji and Kazuhiro, 2012) and the references therein.

2.2 Emission Formation and Fuel Efficiency

To effectively control a clean diesel engine, knowledge of emission formation and fuel efficiency and an understanding of how the available actuators affect these aspects is a prerequisite. A brief overview is provided in this section. More information on emission formation can be found in, e.g., Seykens (2010). This section describes the combustion process in diesel engines and how this process can be affected via the available actuators. Also, the basic principles of NO_x and PM formation, and the conversion of chemical energy into mechanical work are detailed.

2.2.1 Combustion Process

In a diesel engine, an air-exhaust mixture is brought to high pressure and temperature inside a cylinder by means of compression by a piston. When diesel fuel is injected into this cylinder, it combusts as a result of the high temperature and pressure. The combustion further increases the pressure and temperature of the in-cylinder mixture. Therefore, the work transfer from the in-cylinder gases to the piston during the subsequent expansion stroke exceeds the work transfer from the piston to the in-cylinder gases during the compression stroke and mechanical work is created.

Figure 2.3 shows a schematic representation of the pressure and cylinder volume during a four-stroke diesel cycle. During the intake stroke, the piston moves from Top Dead Center (TDC) to Bottom Dead Center (BDC) and aspirates the fresh air-exhaust mixture from the intake manifold. In the compression stroke, the piston moves from BDC to TDC. After Intake Valve Closing (IVC), the in-cylinder air-exhaust mixture is compressed via isentropic compression, increasing both its pressure and temperature. Close to TDC, the fuel injection and, subsequently, the combustion start (SOC). The heat that is generated by the combustion further increases the in-cylinder pressure. When the piston moves from TDC to BDC during the expansion stroke, the mechanical work is generated. At the end of this stroke the exhaust valve opens (EVO). The piston again moves to BDC and the exhaust gases are expelled through the exhaust valve.

The chemical energy of the fuel is released during combustion. Combustion in diesel engines occurs in two stages. When the fuel spray is injected into the cylinder, a portion of the fuel mixes with oxygen during the ignition delay. When

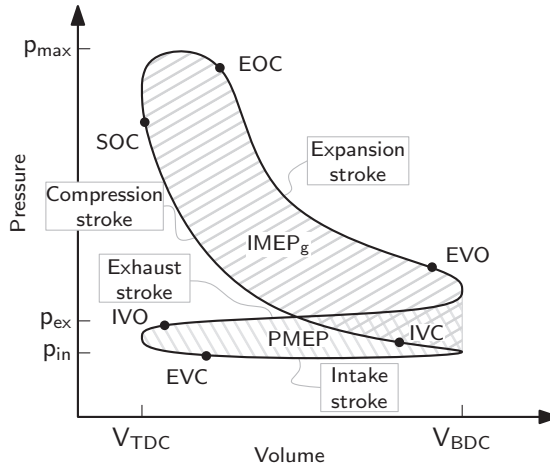


Figure 2.3: A schematic PV-diagram. The labels inside the graph indicate: Intake Valve Opening (IVO), Exhaust Valve Opening (EVO), Intake Valve Closing (IVC), Exhaust Valve Closing (EVC), Start Of Combustion (SOC), End Of Combustion (EOC). The labels on the axes indicate: Volume at Top Dead Center (V_{TDC}), Volume at Bottom Dead Center (V_{BDC}), intake manifold pressure (p_{in}), exhaust manifold pressure (p_{ex}), maximum pressure (p_{max}).

this portion ignites, it oxidizes rapidly in a premixed flame. After this premixed combustion phase, the remaining main portion of the fuel oxidizes in a mixing-controlled diffusion flame.

Figure 2.4 shows a schematic representation of a diesel diffusion flame. Diffusion combustion in a diesel engine is an inhomogeneous process, i.e., the nature of the combustion varies spatially. The combustion starts in a premixed zone (different from the initial premixed combustion) where air that mixed with the fuel spray partially oxidizes the fuel. The products resulting from this initial combustion form the interior of the flame. When these combustion products mix with the air-exhaust mixture in the cylinder, they further oxidize and release the remainder of their chemical energy. This mixing-controlled diffusion flame forms the flame exterior.

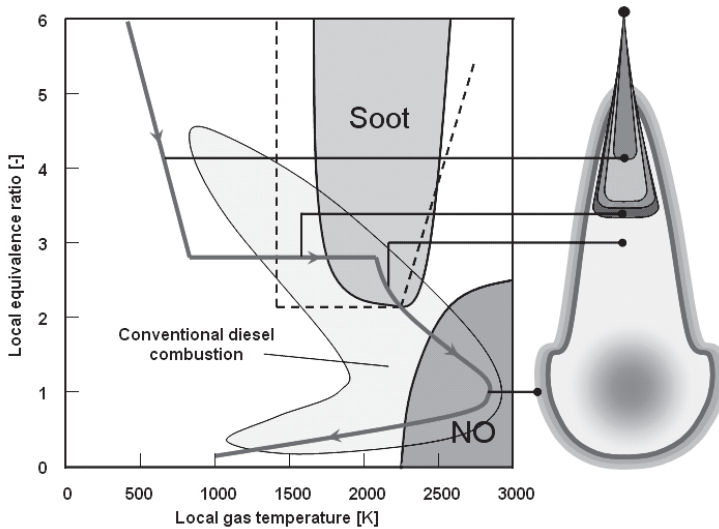


Figure 2.4: Diffusion combustion of a diesel spray. On the left: the effect of the local temperature and fuel-air equivalence ratio, i.e., $1/\lambda$, on the formation of soot (PM) and NO_x . The line indicates the temperature-equivalence ratio combinations that are present during diesel combustion. On the right: a steady-state diesel flame, with premixed combustion and diffusion combustion. The figure is taken from: Seykens (2010), where additional details on the assumptions used for the creation of this figure can be found.

2.2.2 Emission Formation

Nitrogen Oxides

Nitrogen Oxides (NO_x) are formed during combustion, when nitrogen and oxygen, which are both present in the fresh intake air, react. This reaction takes place as a result of the high temperatures and pressures during combustion. The NO_x formation reaction is very sensitive to temperature; at 2000 K, a 1% increase in temperature increases the formation rate of NO_x with 20% (Seykens, 2010). Particularly in the area surrounding the diffusion flame, a high temperature is combined with an oxygen-rich air-fuel mixture. These conditions are ideal for high NO_x formation.

To influence the NO_x formation rate, either the temperature, or the availability of oxygen has to be modified. The main NO_x reduction method is Exhaust

Gas Recirculation (EGR), i.e., cooled exhaust gas that is recirculated and mixed with the intake air. This reduces the in-cylinder temperature reached during combustion by increasing the specific heat capacity of the intake air mixture. Also, the inert exhaust gases dilute the air-mixture, which lowers the oxygen concentration. All these aspects reduce the NO_x formation rate. Because this slows down the combustion, decreases the peak temperature and involves pumping work, using EGR decreases the fuel efficiency, but when used moderately, this effect is small. The fuel injection also affects the NO_x emissions. The Start Of Injection (SOI) can be retarded to move the combustion center further away from TDC. This reduces the peak temperature, resulting in a lower NO_x formation rate. Because this moves the pressure peak away from TDC, this also decreases the fuel efficiency.

External conditions influence the NO_x formation as well, which is investigated in Van Helden et al. (2004). In this reference the influences of ambient humidity, ambient temperature, variations in fuel properties, engine-to-engine variations, wear and maintenance state are investigated. Significant variations are found. When the ambient humidity increases, the NO_x emissions decrease: an increase of water vapor in the ambient air by 1 g/kg decreases the NO_x emissions by 1%. An increase in manifold air temperature of 1 °C increases NO_x by 0.6% to 1.2%. With all effects combined, the effects are considerable and variations in NO_x of up to 35% are anticipated as a result of climate variations, when compared with standard laboratory conditions.

Particulate Matter

Particulate Matter (PM) is the particulate residue in the exhaust gas. It consists mainly of soot, but also contains quantities of other small particles. The soot is formed in the fuel-rich interior of the diffusion flame. After the premixed combustion at the start of the diffusion flame, a mixture of combustion products remains at a high temperature inside the diffusion flame. These products form small nuclei that agglomerate into soot particles. Most of this soot is oxidized in the diffusion flame. However, when the soot remains in a region with insufficient oxygen or temperature for combustion until the end of the combustion stroke, it will not oxidize and end up in the exhaust. Soot emissions therefore increase when the injected fuel mass increases. Also, when the engine speed increases, the time

that is available for combustion decreases and, consequently, the PM emissions increase.

Soot formation is an intermediate step in the combustion process and can only be avoided by fundamentally changing the combustion type, e.g., using HCCI or PCCI combustion. In conventional diesel engines, the amount of PM is best reduced by increasing the soot oxidization, rather than preventing soot formation. Measures that improve the conditions for rapid and complete combustion of the injected fuel decrease the PM emissions. These measures include: increasing the atomization of the fuel spray by increasing the injection pressure, advancing the SOI and increasing the oxygen-fuel equivalence ratio.

2.2.3 Fuel Efficiency

The fuel efficiency of an engine is expressed as Brake Specific Fuel Consumption (BSFC), i.e., the ratio between the fuel mass flow and the resulting brake power, and is typically expressed in g/kWh:

$$\text{BSFC} = \frac{\dot{m}_{\text{fuel}}}{P} = \frac{m_{\text{fuel,inj}} N_{\text{cyl}}}{4\pi \tau}, \quad (2.1)$$

with the fuel mass flow, \dot{m}_{fuel} , the break power, P , the fuel mass per injection, $m_{\text{fuel,inj}}$, the number of cylinders, N_{cyl} and the brake torque, τ .

To further specify the generation of torque in a diesel engine, the Brake Mean Effective Pressure (BMEP) is considered, which is instrumental for understanding torque generation in diesel engines. The BMEP of a four-stroke engine can be expressed as a function of the brake torque, τ , and engine displacement, V_e :

$$\text{BMEP} = \frac{4\pi \tau}{V_e}. \quad (2.2)$$

The BMEP can be decomposed into two parts:

$$\text{BMEP} = \text{IMEP} + \text{FMEP}, \quad (2.3)$$

with the Indicated Mean Effective Pressure (IMEP) and the Friction Mean Effective Pressure (FMEP). IMEP can be defined as:

$$\text{IMEP} = \frac{1}{V_e} \oint_{\text{cycle}} p dV, \quad (2.4)$$

the circular integral over the four-stroke engine cycle, with the in-cylinder pressure, p , and the actual cylinder volume, V . For analysis, it is insightful to further decompose the IMEP:

$$\text{IMEP} = \frac{1}{V_e} \overbrace{\int p dV}^{\text{IMEP}_g} + \frac{1}{V_e} \overbrace{\int p dV}^{\text{PMEP}} \quad (2.5)$$

compression,
expansion
intake,
exhaust

with the gross Indicated Mean Effective Pressure (IMEP_g) and the Pumping Mean Effective Pressure (PMEP). IMEP_g can be observed in Figure 2.3 as the area filled using a rising hatch pattern. This is where the fuel is effectively converted into mechanical energy. PMEP can be observed in Figure 2.3 as the area filled using a falling hatch pattern. The cross-hatched area is part of both PMEP and IMEP_g . Typically, PMEP has a negative value and, consequently, a detrimental effect on the produced torque. FMEP is the equivalent pressure needed to overcome the engine friction and always has a negative value. It is not caused by the in-cylinder pressure and can therefore not be observed in Figure 2.3. To specify how the available actuators affect the torque generation and fuel efficiency, the effects of the available actuators on the IMEP_g , PMEP and FMEP are detailed.

The main factor contributing to IMEP_g is the injected fuel amount. During combustion this is converted into heat. The resulting increase in pressure then drives the pistons and the engine. This process can be optimized by maximizing the combustion efficiency¹ and optimizing the timing of the combustion. Increasing the combustion efficiency moves the line between End Of Combustion (EOC) and Exhaust Valve Opening (EVO) upwards in Figure 2.3. Centering the combustion timing closer to TDC extends the area of IMEP_g towards the top left of the figure in Figure 2.3.

The combustion efficiency can be increased by increasing the fuel atomization via an increased injection pressure, reducing the EGR fraction, increasing the amount of oxygen and optimizing the timings and amounts of the pilot and main injection.

¹The combustion efficiency is defined here as the ratio between the amount of heat released during combustion and the heating value of the injected fuel.

A heat release closer to TDC also increases IMEP_g . This can be achieved by increasing the combustion speed and correctly timing the combustion. The combustion timing can be influenced directly using the injection timing. Because the ignition delay depends on in-cylinder conditions such as temperature and air-exhaust composition, these should be accounted for when determining the injection timing. The combustion speed can be increased by reducing the EGR fraction and increasing the injection pressure.

The above measures for increasing the IMEP_g all result in an increase in engine-out NO_x emissions. Improving the BSFC via an increased IMEP_g therefore increases the NO_x emissions and a tradeoff between BSFC and NO_x needs to be made.

The PMEP causes a net work transfer between the piston and the in-cylinder gases during the inlet and exhaust strokes. This is mainly attributed to the pressure difference between the intake and exhaust manifold. Assuming the in-cylinder pressure during the intake and exhaust stroke is equal to the pressure in the intake and exhaust manifold, respectively, the PMEP is approximated with:

$$\text{PMEP} = \frac{1}{V_e} \oint_{\substack{\text{intake,} \\ \text{exhaust}}} p dV \approx p_{\text{in}} - p_{\text{ex}}, \quad (2.6)$$

where p_{in} and p_{ex} represent the intake and exhaust manifold pressure, respectively. When the exhaust manifold pressure is higher than the intake manifold pressure, which is required for a positive EGR flow, the pumping work constitutes a loss to the BMEP. Exceptions are possible in turbocharged engines, where, theoretically, the intake pressure can exceed the exhaust pressure and PMEP can positively contribute to the BMEP. The air-path actuators that affect the intake and exhaust manifold pressures affect the PMEP and, thereby, the BMEP and BSFC. The VGT, EGR valve, intake throttle and exhaust throttle all affect the PMEP. Because these actuators also affect the engine-out emissions and temperature, again a tradeoff between emissions and fuel efficiency should be made.

The FMEP is mainly affected by the engine speed and engine hardware. Its effect on the BSFC is most notable when the brake torque is low. The engine speed is determined by the vehicle speed and gear ratio. The actuators available for engine control do not have a significant effect on the engine speed and, consequently, the FMEP.

2.2.4 Simultaneously Low NO_x, PM and BSFC?

From the above sections on NO_x, PM and BSFC, it can be concluded that several conditions for minimal NO_x, PM and BSFC are conflicting. Changing an actuator setting to improve one aspect will come at a cost of a deterioration in another aspect. Making an engine more fuel efficient will therefore not coincide with reducing its engine-out NO_x and PM emissions.

Particularly after calibrating the engine, the tradeoff between emissions and fuel efficiency will be pronounced. The engine calibration will be designed such that minimum fuel efficiency is combined with low engine-out emissions, resulting in tailpipe emissions that fit within the requirements of legislation. Any method for reducing the emissions without deteriorating the fuel consumption, or vice versa, will be exploited in this calibration. Further simultaneous improvements by means of control should therefore not be expected.

This situation changes when disturbances are taken into consideration. As a result of disturbances, the emissions and fuel consumption change and the achieved tradeoff shifts. Because the NO_x production increases exponentially with temperature, the increase in NO_x due to an increase in temperature exceeds the decrease in NO_x due to a decrease in temperature of the same magnitude. Similarly, the increase in PM due to a decrease in λ exceeds the decrease in PM due to an increase in λ of the same magnitude. Therefore, the average NO_x and PM emissions are expected to increase as a result of disturbances.

Also, as a result of disturbances the exhaust emissions are uncertain. To comply with legislation despite this uncertainty, margins between the limits set in legislation and the achieved emissions have to be implemented to ensure in-service conformity. For this, both the NO_x and PM emissions have to be reduced. In consequence of the tradeoff between emissions and fuel consumptions, an increase in the fuel consumption has to be permitted to realize this.

With improved feedback control, this situation can be mediated. When the actual engine performance is measured, the inputs can be adapted by means of feedback control to counteract the disturbances and keep the emissions and fuel consumption close to nominal. This can reduce the detrimental effect of disturbances on the average emissions. Moreover, when the emissions remain

closer to nominal, the margins between the nominal emissions and the limits set in legislation can be reduced. The decrease of the average emissions and the opportunity for reduced margins can both be exploited to further improve the fuel efficiency.

2.3 Emission Legislation

The European Union (EU) defines emission legislation for the entire EU region. Because lowering the exhaust emissions requires more complex and more costly hardware and can induce an increase of the fuel consumption, legislation is needed as an incentive for producing cleaner engines. Without requirements in legislation, clean engines are not economically viable. Legislation is therefore a necessary driving factor for innovation in diesel engines.

In this thesis, the European emission legislation is considered. In other parts of the world, different, but often similar, emission legislation is used to limit the exhaust emissions of on-road vehicles. A similar trend with tightening legislation is observed worldwide. In the US, e.g., the latest legislation, US2010, requires similar exhaust emissions as EURO VI.

Legislation for heavy-duty diesel engines defines limits for several exhaust gas quantities: Carbon mono Oxide (CO), Total HydroCarbon (THC), Hydro Carbons (HC), Non-Methane Hydro Carbons (NMHC), Ammonia (NH₃), Nitrogen Oxides (NO_x), Particulate Matter (PM) and Particle Number (PN). For diesel engines, the most restricting limits in practice are for NO_x and PM. The evolution of the limits for these quantities, according to European legislation, is depicted in Figure 1.1.

The emission test procedure is specified in legislation as well. Up to EURO II, the emissions were tested using steady-state test cycles. Such a test cycle consists of a sequence of stationary engine modes with predefined engine speed and torque at each mode. With the introduction of EURO III, transient test cycles were included. For a transient test, a predefined engine speed and torque trajectory is completed on a dynamometer test setup. With EURO VI, the test procedures changed again to require low exhaust emissions under a wider range of conditions; not-to-exceed emission limits and in-service conformity tests using a Portable Emission Measurement System (PEMS) are added. More details on EURO VI are

Table 2.1: The evolution of the steady-state emission limits for heavy-duty diesel engines in the European Union. For EURO III, IV and V, also smoke limits were defined. Source: (DieselNet, 2013).

	Year	Test	CO	HC	NO _x	PM	PN
			g/kWh	g/kWh	g/kWh	g/kWh	#/kWh
EURO I	1992	ECE R49	4.5	1.1	8	0.36	-
EURO IIa	1996	ECE R49	4	1.1	7	0.25	-
EURO IIb	1998	ECE R49	4	1.1	7	0.15	-
EURO III	2000	ESC	2.1	0.66	5	0.1	-
EURO IV	2005	ESC	1.5	0.46	3.5	0.02	-
EURO V	2008	ESC	1.5	0.46	2	0.02	-
EURO VI	2013	WHSC	1.5	0.13	0.4	0.01	8·10 ¹¹

Table 2.2: The evolution of the transient emission limits for heavy-duty diesel engines in the European Union. Source: (DieselNet, 2013).

	Year	Test	CO	NMHC	NO _x	PM	PN
			g/kWh	g/kWh	g/kWh	g/kWh	#/kWh
EURO III	2000	ETC	5.45	0.78	5	0.16	-
EURO IV	2005	ETC	4	0.55	3.5	0.03	-
EURO V	2008	ETC	4	0.55	2	0.03	-
EURO VI	2013	WHTC	4	0.16	0.46	0.01	6·10 ¹¹

provided in Section 2.3.1. The emission limits and corresponding test cycles are listed in Tables 2.1 and 2.2. With every update of the legislation, the emission limits got increasingly stringent. With the current EURO VI legislation, the steady-state emission limits for NO_x and PM are reduced by 80 % and 50 %, respectively, compared with EURO V (2008-2013). When EURO VI is compared with EURO I (1992-1996), the NO_x and PM limits are reduced with 95 % and 97 %, respectively, resulting in comparatively near-zero values.

Table 2.3: The EURO VI emissions limits.

	CO	THC	NO_x	NH₃	PM	PN
	g/kWh	g/kWh	g/kWh	ppm	g/kWh	#/kWh
WHSC	1.5	0.13	0.4	10	0.01	$8 \cdot 10^{11}$
WHTC	4	0.16	0.46	10	0.01	$6 \cdot 10^{11}$
WNTE	2	0.22	0.6	-	0.016	-
In-service conformity	6	0.24	0.69	-	-	-

2.3.1 EURO VI Legislation

Currently, the EURO VI legislation is applicable in the European Union. With the introduction of EURO VI, both the emission limits and test procedures have changed. The most important changes with respect to EURO V are a drastic reduction of the limits for NO_x and PM, a change from European test cycles to worldwide test cycles and the introduction of in-service conformity and not-to-exceed limits. In this section, the most relevant parts of the EURO VI legislation for commercial vehicles (European Commission, 2011) are summarized. Apart from restricting exhaust emissions, EURO VI also dictates requirements for On-Board Diagnostics (OBD) to monitor the produced emissions on road going vehicles. The requirements on the OBD are found in (European Commission, 2011), but are not detailed in this thesis.

To test for EURO VI type approval, a combination of stationary tests, transient test cycles, not-to exceed limits and on-road tests using PEMS are conducted. For each test, emission limits are specified as listed in Table 2.3. Furthermore, in-service conformity tests are conducted during the useful life of the vehicle.

Stationary Testing

The steady-state emissions are tested on the World-Harmonized Steady-state Cycle (WHSC). This cycle contains a sequence of stationary engine modes with predefined engine speed and brake torque. The modes are maintained for a predefined interval length and connected via 20 second linear ramps in engine speed and torque. The WHSC cycle is shown in Figure 2.5 and the limits for the average emissions produced during this cycle are provided in Table 2.3.

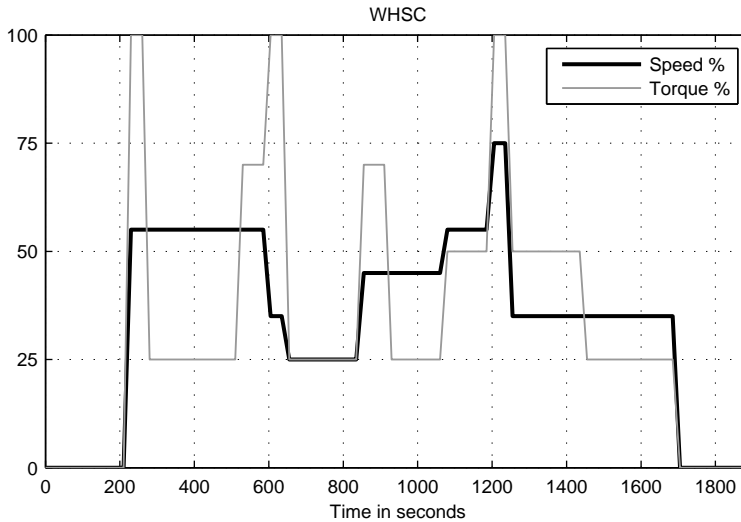


Figure 2.5: The WHSC; the stationary test cycle used for the EURO VI emission tests.

Transient Testing

The World Harmonized Transient Cycle (WHTC), shown in Figure 2.6, is a transient test cycle, designed to be representative for the global use of engines in commercial vehicles. It consists of an 1800s engine speed and torque trajectory that contains parts representative for urban, rural and motorway driving and includes idling and coasting. Two types of WHTC tests are conducted: cold start and hot start. Depending on the type of emission aftertreatment system, that can either operate continuous or require periodic regeneration, the hot-start test procedure is adapted such that a representative measurement is obtained. The weighted average emissions over the cold and hot tests are calculated, where 14% and 86% weights for the cold-start test and the average of the hot-start tests are used, respectively. The emission limits for the weighted average emissions over the WHTC tests are provided in Table 2.3.

Not-To-Exceed Tests

The World-harmonized Not-To-Exceed (WNTE) limits specify off-cycle maximum emissions that are active in a part of the speed-load operating range. The WNTE

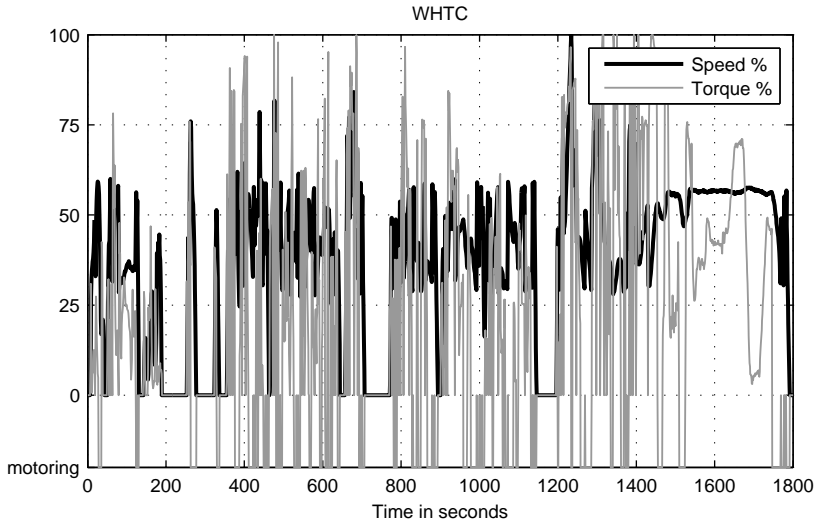


Figure 2.6: The WHTC; the transient test cycle used for the EURO VI emission tests. The conversion between torque and speed expressed in % into Nm and RPM, respectively, is defined in (European Commission, 2011).

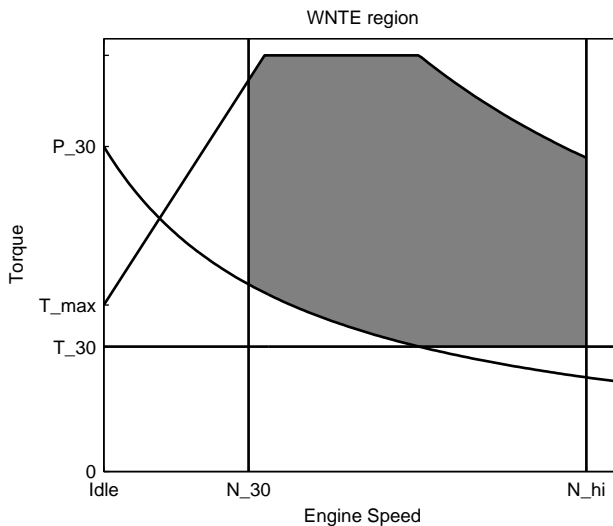


Figure 2.7: The WNTe region for the EURO VI emission tests. P₃₀ denotes 30 % of the peak power, T₃₀ denotes 30 % of the peak torque. N₃₀ denotes the engine speed at 30 % of the speed range between idle speed and N_{hi}; N_{hi} denotes the highest engine speed where at least 70 % of the maximum power is available.

limits must be complied with, regardless of the drive cycle, both during transient and steady-state conditions. The WNTE area is bounded by a minimum and maximum engine speed and minimum torque and minimum power. The area is shown in Figure 2.7 and defined in (European Commission, 2011).

Compliance with the WNTE limits must be shown both on a dynamometer and on a vehicle. The cycles for these tests are not rigidly defined and contain aspects of randomness. The dynamometer test procedure consists of a series of stationary points connected via 20 s ramps that are randomly chosen within a grid in the WNTE area. The vehicle test procedure involves driving in urban, rural and motorway conditions using a PEMS. When the engine is within the WNTE area for at least 30 s, a WNTE event is constituted. The emissions during the WNTE dynamometer tests and of the WNTE events during vehicle testing must comply with the limits in Table 2.3. The WNTE emission limits are higher than for the WHTC and WHSC, but the uncertainty in the test cycle makes the test procedure more challenging. The use of random cycles prevents adapting the calibration for low emissions only during the cycle tests.

In-Service Conformity

The in-service conformity tests are conducted during the useful life of the vehicle, i.e., 700 000 km or seven years. For the tests, a truck equipped with additional emission measurement equipment, i.e. PEMS, is driven on the road. The vehicle must be operated under normal conditions; bounds on the ambient conditions and payload are specified in (European Commission, 2011). The trip must be at least 90 minutes long and contain urban, rural and motorway driving and the work performed should be at least five times the work performed during a WHTC. Only the gaseous emissions are restricted by the in-service conformity legislation, i.e., the PM emissions are not restricted or measured in this test. Compared with the WHTC tests, the emissions limits are less strict; a relative increase of 50 % is allowed in CO, THC, NMHC, CH₄ and NO_x. The test is challenging nonetheless, because ageing, an unknown drive cycle and ambient conditions all influence and possibly increase the resulting emissions.

Implications for Engine Design and Control

To comply with EURO VI legislation, modifications are made to both the hardware and the software of the engine. The introduction of stricter emission limits requires a combination of combustion control systems and aftertreatment technology (Gense et al., 2006) and hence more complex hardware. To comply with the WNTE limits and in-service conformity limits, engine control strategies gain importance. The change from ESC and ETC to WHSC and WHTC test cycles does not require any fundamental changes for diesel engines.

Engines of the EURO V generation typically used SCR to achieve compliance with the EURO V NO_x limits. To further reduce the NO_x emissions, SCR is combined with EGR in EURO VI engines. To control the flow of EGR, a combination of an EGR valve and VGT is used. The use of these two actuators greatly enhances the flexibility of the air-path control system. Combined with SCR, low tailpipe NO_x emissions in compliance with EURO VI levels can be achieved.

To comply with the WNTE and in-service conformity limits, the engine control system has to guarantee low emissions for a wide range of conditions, including changing ambient conditions, ageing, production tolerances and an unknown drive cycle. This makes the use of control strategies that are able to reduce the effects of disturbances and uncertain conditions on the emissions increasingly relevant. Feedback control therefore gained importance with the introduction of EURO VI.

Also, the tightened emission legislation has an indirect effect on control during torque transients. To comply with the lowered NO_x emission limits, increased EGR rates (Körfer et al., 2008) are used. And, as a consequence of this, the air-fuel equivalence ratio, λ , is reduced. The amount of excess oxygen affects the natural ability of the engine to quickly respond to an increase in torque demand. The reduction of λ deteriorates the natural torque response. Control algorithms to quickly increase the fresh air flow during torque transients therefore gain importance when lower engine-out NO_x levels are required.

The combination of SCR deNO_x aftertreatment systems and a low emission diesel engine enables the design of control systems that interact with both systems simultaneously. This can be beneficial for both systems. The diesel engine can be controlled such that the exhaust gas is conditioned for efficient aftertreatment. Also, the allowed engine-out NO_x levels can be varied depending on the current

state (temperature) of the aftertreatment system. Willems et al. (2013) shows the potential benefits of such a control design. This temperature has to be in a certain range, depending on the chosen catalyst material, to achieve a high NO_x conversion efficiency. When the aftertreatment temperature is in this range, the BSFC can be reduced by allowing for increased engine-out NO_x emissions, which are compensated for by the increased aftertreatment efficiency. In this thesis, only engine-out emissions are considered; the interactions with aftertreatment are not exploited in the proposed controllers and not further elaborated in this thesis.

3 Literature Overview

This chapter presents a review of recent academic literature on control of diesel engines, focussing on air-path control and emission control. Control for diesel engines using the VGT and EGR has been explored extensively in academic literature. Various control problems are formulated and solved, resulting in a variety of control types. This section discusses a selection of the available literature, aimed at determining the path to the current state of the art of air-path control. Research in this field is actively ongoing, as can be concluded from Figure 3.1. The novelty of the published approaches can often be found in a new control goal, typically via new controlled outputs, or a different control algorithm for improved performance on a previously studied control problem. The focus of this overview is control using VGT and EGR, but some contributions included here extend this choice of actuators or substitute one for another actuator.

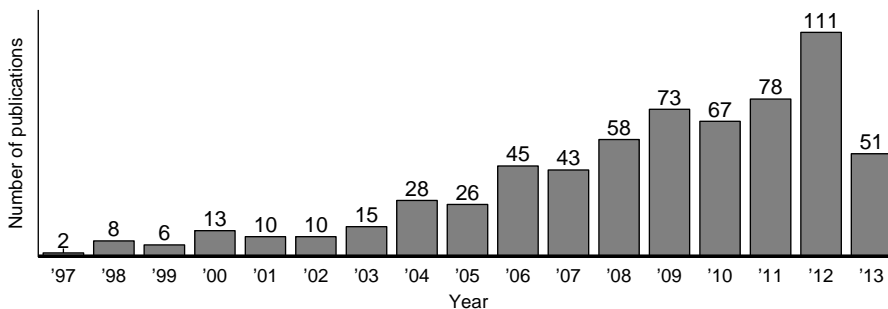


Figure 3.1: The number of publications found using a Google Scholar™ search on "EGR, VGT, diesel". For '13, the results up to 28-6-2013 are included.

In 1998, an overview paper was published detailing the state-of-art of air-path control: (Guzzella and Amstutz, 1998). The combination of VGT and EGR control was, at this point, an emerging technology. The reference (Dekker and Sturm, 1996) is mentioned, where the EGR valve is controlled in open loop and is either fully open or closed. The VGT is used to control either the intake or exhaust manifold pressure. Also, papers are mentioned where the use of a Universal Exhaust Gas Oxygen (UEGO) sensor is explored to measure and control λ , for better control of the emissions. In the outlook of Guzzella and Amstutz (1998), a way to speed up the calibration process is mentioned as the most urgently needed improvement in engine control. Since 1998, several changes in control strategies can be observed. In this chapter, first various control problems that are found in literature are discussed, which are ordered by the selection of controlled outputs. Section 3.2 is dedicated to engine control using Model Predictive Control (MPC), which gained a lot of attention in recent literature. Control during torque transients is often treated as a separate subject; the control techniques used for transient control are discussed in Section 3.3. A number of remaining challenges are identified in Section 3.4. The articles discussed in this chapter are listed in Tables 3.1, 3.2, 3.3, which can be found at the end of this chapter.

3.1 Controlled Outputs

3.1.1 Track Boost Pressure and Fresh Air Flow

The default approach for feedback control of the engine air path is to control the fresh Mass Air Flow (MAF) with the EGR valve and the intake Manifold Absolute Pressure (MAP, alternatively expanded as Manifold Air Pressure) with the VGT.

Sensors that measure the actual MAF and MAP are available on typical HD diesel engines. Moreover, the MAF and MAP largely determine the flows and, thereby, the mixtures in the air path. Control of MAF and MAP outputs to reference values reduces the uncertainty on the intake air-exhaust mixture and also reduces the actuator uncertainty due to production tolerances ageing and hysteresis. This way, MAF-MAP control eliminates part of the uncertainty in the emission formation. Moreover, the MAF is important for the torque response, improved control of MAF can therefore also make the torque response more consistent.

The coupled nature of the actions of VGT and EGR makes the use of the SISO control loops used in Dekker and Sturm (1996) conservative. More advanced control algorithms can improve the tracking performance, which implies that the achieved engine performance improves as well. This motivates the use of complex control structures such as Model Predictive Control (MPC) (Ferreau et al., 2007; Ortner and Del Re, 2007; Stewart et al., 2010; Zhao et al., 2013), Linear Parameter Varying control (LPV) (Jung and Glover, 2006; Wei and Del Re, 2007) or sliding mode control (Brahma, 2005). In van Nieuwstadt et al. (2000) and Wahlstrom and Eriksson (2013), it is shown that the choice of setpoints and controlled outputs is, however, more important for the achieved engine performance than the choice of the control algorithm that tracks the setpoints. In Wahlstrom and Eriksson (2013), a comparison is made between three controllers: MPC control of MAF and MAP is compared with MPC control of EGR rate and the oxygen-fuel equivalence ratio, λ_O , and PID control of EGR rate and λ_O . The EGR rate and λ_O are closely related with NO_x and PM emissions, respectively. The MAF and MAP controller using MPC is outperformed by the other two controllers in terms of maintaining the EGR rate and λ_O close to their nominal values. By extension, this implies that MAF and MAP are not a favorable choice of controlled outputs, when maintaining the emissions close to nominal is aimed for.

3.1.2 Minimize NO_x Emissions

In Stefanopoulou et al. (2000), a controller is designed aimed at minimizing the NO_x emissions, while preventing visible smoke. Minimizing NO_x is achieved by maximizing the EGR ratio, also denoted burned gas rate, in the intake manifold. To keep the PM emissions at an acceptable level and prevent visible smoke, a lower bound on the air-fuel ratio of 25 (1.7 times more lean than stoichiometry) is maintained. It is observed that control at a Pareto optimal point of burned gas rate and λ results in a rank-deficient local static input-output response, when the burned gas fraction and air-fuel ratio are used as outputs.

The burned gas rate and air-fuel ratio are not readily available for feedback control on their experimental setup. A control scheme is proposed, where the nominal stationary MAF and MAP values that correspond with the desired burned gas rate and air-fuel ratio are used as controlled outputs for feedback control. The VGT and EGR are used as actuators. To account for the observed rank deficiency,

feedback control is applied only in the input direction that corresponds with maximum gain in the burned gas rate and air-fuel ratio. It is shown that limiting control to one direction significantly decreases the actuator usage, but only has a minor impact on the achieved burned gas rate and air-fuel ratio.

3.1.3 EGR Rate and Air-Fuel Ratio

A more direct relation between the controlled outputs and the actual performance measures improves the effectiveness of a feedback controller. The EGR rate can be used as a substitute measurement for NO_x emissions, when an actual NO_x measurement is not available. Increasing the EGR rate increases the thermal heat capacity of the intake mixture and decreases the availability of oxygen. Both effects lower the NO_x formation rate. The EGR rate is considered representative for the effect the air path has on the NO_x emissions. The air-fuel ratio is used as a substitute for PM measurements. Increasing the air-fuel ratio increases the soot combustion, resulting in lower PM emissions. Both the relation between NO_x and EGR rate and between PM and air-fuel ratio were also remarked in Sections 2.2.2.1 and 2.2.2.2, respectively.

In Jankovic et al. (2000), a nonlinear feedback controller is designed to track the EGR rate and air-fuel ratio using the VGT and EGR valve. The constructive Lyapunov approach and a third-order nonlinear model are used to design the controller. The controller is implemented on an experimental dynamometer setup and is shown to provide a fast air-fuel ratio response.

In Wahlström et al. (2010), a control scheme is proposed that minimizes the pumping work under certain conditions. The pumping work is the net work transfer between the piston and the cylinder gases during the inlet and exhaust stroke. Reducing the pumping work is beneficial for the fuel economy of a diesel engine, which was also noted in Section 2.2.3. The pumping work is minimized by keeping the VGT fully opened as long as the EGR rate exceeds its setpoint value; and opening the EGR valve as much as possible, while satisfying a lower limit on the oxygen-fuel equivalence ratio, λ_O . The value λ_O is used as a substitute for the PM emissions and should be more representative for the PM emissions than the more common λ measurement based on the fresh air flow. In case the λ_O value that is obtained using this controller is lower than otherwise achieved, the

pumping work decreases. Although lowering the air-fuel ratio might also reduce the combustion efficiency, the net effect should be beneficial for the fuel economy.

3.1.4 Direct Emission Control

To reduce the effect of disturbances and uncertainties on the produced emissions, direct feedback control of the measured engine-out emissions has the best performance potential.

Körfer et al. (2008) presents a feedback control method using a NO_x sensor. Two PID control loops are designed. The first loop is used to control either the intake pressure or the exhaust pressure via the VGT. The second loop is used to control the NO_x concentration via the EGR valve. These input-output systems physically interact and output-decoupling is used to reduce the effects of interaction in the control loops. A series of models, sensors and observer-like structures is used to generate the pressure setpoints and improve the accuracy of the NO_x measurement. The performance of the controller is demonstrated on an unspecified torque step with a ramp time close to 3.5 s. Accurate tracking of both the NO_x concentration and the exhaust pressure is achieved in 7 s after the start of the transient.

In Alfieri (2009), a NO_x concentration sensor is combined with a λ sensor for control of the emissions, where the λ sensor is used as an indicator for PM emissions. This study does not use the EGR valve for control, instead the injection timing and the VGT are used as actuators. Because the injection timing has a negligible influence on λ , a triangular input-output system is obtained, which is convenient for Multi-Input Multi-Output (MIMO) control design, as coupling between the inputs and outputs no longer affects the stability. Successful tracking of the NO_x concentration and λ is obtained. However, the use of the injection timing for emission control using these outputs is questionable. Even when λ remains constant, changing the injection timing changes the PM emissions, as shown in, e.g., Guzzella and Amstutz (1998). PM control is therefore not achieved. Moreover, controlling NO_x by shifting the injection timing influences the thermal efficiency as well as the exhaust temperature (Guzzella and Amstutz, 1998; Brahma, 2005). Using this control scheme can therefore have a detrimental effect on the fuel efficiency.

In Tschanz et al. (2013), the principle of direct emission control is further developed. Direct control of measured NO_x and PM emissions is implemented. To measure the PM emissions, a smoke sensor is used in the experimental setup. Such a sensor is neither available currently nor suitable for use in production HD diesel engines. To reduce the effects of the dynamic response of the emission measurements, two linear observers are implemented. These observers combine the emission measurements with an emission model based on the measured engine speed, fuel quantity and deviations in the burned gas rate, boost pressure, start of injection and swirl-valve position. A cascaded control structure using four actuators is proposed. The observed PM emissions are closed-loop controlled using the swirl valve. The observed NO_x concentration is controlled in a cascaded fashion. The controller adapts the SOI, but also uses integral action to adjust a lookup-table with setpoint values for the EGR rate. A lower level controller is implemented that uses the EGR valve and VGT to control the intake manifold pressure and EGR rate. This method successfully achieves emission control and improves on the work of Alfieri (2009). However, the proposed control strategy is applicable only in the low load, low speed part of the operating range, due to the limited influence of the swirl valve outside of this range. Also, reachability issues that can occur when the emission setpoint is not feasible are not addressed. Particularly with low, close to Pareto optimal, setpoints for the emissions, reachability can easily be compromised by disturbances or uncertainties.

3.2 Model Predictive Control

Several recent papers use Model Predictive Control (MPC) to control the air path of a diesel engine. MPC can provide a flexible, systematic framework for optimal control. It can handle nonlinear dynamics, input saturation and constraints on, e.g., emissions, turbine speed or boost pressure, which are difficult to take into account using conventional feedback control methods. Moreover, an MPC controller combines feedback of measured signals with predictive (feed forward) control. This can improve the response to known disturbances.

The challenge for MPC is an implementation including all the above features. The optimal control problem requires simplifications to make its solution solvable and implementable in real time within the computational and memory constraints

of the available controller hardware. As a result, several alternative implementations are found in literature.

In Herceg et al. (2006), nonlinear MPC is applied in simulation. A third-order nonlinear mean-value model is used to describe the system dynamics. The goal is to track setpoints for the intake and exhaust pressure, and turbine power, while also satisfying constraints on the intake and exhaust pressure. The proposed nonlinear MPC method solves this problem directly and online, resulting in an implicit MPC implementation. A 0.1 s and 0.9 s control and prediction horizon were used. The controller is only suitable for simulation; due to the computational effort needed to run the controller it cannot be implemented in real time.

In Ferreau et al. (2007), an MPC controller is used to control MAF and MAP. The model used to describe the engine dynamics consists of two local linear submodels for low and high engine speed, respectively. Using an advanced quadratic programming algorithm, a control horizon of 0.25 s (five samples) and a prediction horizon of 5 s can be implemented in real time.

Ortner and Del Re (2007) also use an MPC controller to control MAF and MAP. The model used to describe the engine dynamics consists of twelve local linear submodels, covering the full speed-load range. To remain within memory and CPU speed bounds, the control horizon was limited to one sample. The prediction horizon was set to 5 s. With the new controller, an increase of the engine-out NO_x emissions with 36 %, and a decrease of the PM emissions with 46 % are achieved on the NEDC, when compared with the production engine controller.

García-Nieto et al. (2008) implement nonlinear MPC to track MAF and MAP. The model used for control design consists of a series of fifteen local linear submodels, where each submodel consists of two second-order models. The controller was designed using a control horizon of one second (ten samples) and a prediction horizon of five seconds and is implemented on a Pentium PC.

Ortner et al. (2009) also use nonlinear MPC to track setpoints on MAF and MAP. Four first-order LPV models, using VGT and engine speed as scheduling variables, describe the engine dynamics. The nonlinear MPC controller uses a control horizon of 0.15 s (three samples) and a prediction horizon of six seconds and is only tested in simulation.

In Stewart et al. (2010), MPC is proposed as a systematic method of control design. A control design framework is presented that also includes mean-value modeling and identification. They propose that the systematic, model-based approach to control design that MPC uses is a more time efficient method than conventional tuning and calibration of engine maps. The presented control design methodology consists of scheduled, explicit linear MPC. They do not directly specify an engine configuration, sensors or actuators.

In Alberer and Del Re (2010), linear MPC, designed using a high-order linear model, is tested both in simulation and in experiments. The VTG, EGR valve and fuel rate are the considered actuators, the intake and exhaust oxygen concentration, and engine torque are used as outputs. Limited by computational power, the control horizon for the experiments consists of four samples distributed within a three second (150 samples) prediction horizon. The experiment shows a potential for reduced transient emissions, compared with the production engine controller. But the experimental comparison that is shown is limited to a single transient and not fully convincing. The increase of fuel flow during the presented transient was slowed down, indicating that the torque response is slower. Moreover, the equilibria at the start and end of the transient were not entirely consistent in the compared cases.

In Karlsson et al. (2010), the SOI, fuel-injection duration, EGR valve and VGT are used to control several outputs linked with high-level objectives. The considered outputs are the Indicated Mean Effective Pressure (IMEP), combustion phasing, maximum pressure derivative, engine-out NO_x concentration and exhaust opacity. The first three outputs are derived from the measured in-cylinder pressure trace of a single cylinder. The operating range is limited to a small area around a single speed-load operating point. Therefore, the input-output behavior of the engine can be modeled with a single linear dynamic model, which enables the application of linear MPC. The designed controller uses the engine cycles 0, 2 and 4 as the control horizon and a prediction horizon of 100 engine cycles. A controller is designed that minimizes a weighted quadratic sum of tracking errors, where tracking of IMEP, combustion phasing, opacity, NO_x and VGT position is implemented. For NO_x the setpoint is zero, which is not physically possible; effectively, the quadratic NO_x emissions are minimized in the weighted sum. Fuel efficiency was not optimized explicitly, because a linear model cannot suitably

describe the change in fuel efficiency close to its optimum as the input-output gain changes sign there.

In Wang et al. (2011), two MPC control algorithms are compared. Both control designs use the VGT and EGR valve to control MAF and MAP. The first design uses a multi-linear model similar to Ortner and Del Re (2007), a control horizon of one sample, a prediction horizon of 120 samples, and a sample rate of 0.05 s. The second controller uses an LPV model similar to Ortner et al. (2009), a control horizon of three samples, a prediction horizon of 120 samples, and a sample rate of 0.05 s. It is found that the second controller achieves the best tracking performance.

In Wahlstrom and Eriksson (2013), two MPC controllers using a different output selection (MAF, MAP vs. λ_O , burned gas rate, pumping losses) are compared with each other and a PID based controller using (λ_O , burned gas rate, pumping losses) in simulation. A series of local linear models are used for MPC control design, with a control horizon of two samples and a prediction horizon of 50 samples. The controllers are compared in simulation using a mean-value model. It is concluded that the MPC controller based on MAF and MAP is the least effective in controlling emissions. The other MPC controller has a small advantage over the PID controller with the same inputs and outputs, reducing the error in the EGR rate with 10 % and the pumping work with 1 %, while having a similar error in λ_O .

In Zhao et al. (2013), explicit MPC control of both the air path and the fuel path is considered. An air-path controller using the EGR valve and VGT is designed for tracking of MAF and MAP. Also, a fuel-path controller using the SOI, rail pressure and ratio between pilot and main injection mass is designed for tracking of the exhaust temperature, NO_x concentration and CA50 (crank Angle at which 50 % of the combustion heat is released). A series of 20 local linear models with orders ranging between 2 and 6 is used for the design of the MPC controller. The control and prediction horizons are 2 and 8 samples respectively, with a sample rate of 0.1 s. The performance of the air-path and fuel-path controllers is evaluated separately on step tests. During the air-path controller test, the fuel-path actuators are fixed and vice versa. The tracking performance of the air-path controller is tested using torque steps from 375 Nm to 475 Nm at 1550 RPM with ramp times of 2 s and 10 s. The performance is compared with control using fixed actuator settings. In this test, an improved tracking performance is shown. In comparison with most other works discussed here, the tracking performance can be considered

poor; a slow bandwidth and visible oscillations are observed. The performance of the fuel-path controller is evaluated using a torque step from 375 Nm to 475 Nm at 1550 RPM with a ramp time of 5 s. The performance is compared with the ECU controller. The ECU controller does not follow the setpoints, whereas the new MPC controller does. With the MPC controller, control of the CA50 signal is accurate, but slow response times and poor tracking are observed in the the NO_x and exhaust temperature responses.

3.3 Transient Control

In literature, control solutions dedicated to improve the engine behavior during tip-in transients can be found. A tip-in transient is a sudden increase in the driver torque demand. In a turbocharged diesel engine, a large tip-in transient from low to high torque requires a large change in the intake air flow. To achieve this, the compressor speed has to increase accordingly, which cannot be realized instantaneously due to the inertia of the turbocharger. The turbocharger therefore becomes a bottleneck during these large transients. To achieve a satisfactory torque response, the fresh air flow and hence turbocharger speed have to increase quickly, which requires control actions. Several control solutions for this problem are described in literature.

In Dekker and Sturm (1996), it is proposed to completely close the EGR valve when a large tip-in transient is detected. When the EGR valve is closed, the VGT is used to keep the exhaust pressure at or below the maximum allowed pressure. This control strategy minimizes the response time of the air path, resulting in the fastest possible pedal response. On the other hand, the EGR flow is stopped completely, maximizing the NO_x emissions. Also, maximizing the exhaust manifold pressure maximizes the pumping work, lowering the momentary BSFC.

In Chauvin et al. (2008), a motion planning strategy is proposed for transient control of the air path of an HCCI diesel engine. Using some unconventional assumptions such as that the turbocharger is in steady state, a second-order mean-value model is derived. A smooth, monotonic, third-order polynomial trajectory for the boost pressure and burned gas fraction in the intake manifold is designed, which leads from the initial state to a target state. Using model inversion, taking into account the input constraints, the fresh air and EGR flow corresponding with

these trajectories are derived. Conventional PID controllers are used to adapt the EGR valve and VGT to track these trajectories.

In Alfieri (2009), two feed-forward strategies for the EGR valve are considered. The first strategy is based on a approximation of the static system inverse. It calculates a desired EGR valve setting using measurements of the EGR mass flow, EGR temperature, intake manifold pressure and exhaust manifold pressure. This strategy is dismissed, because it causes unwanted oscillations during simulation tests. The second strategy adds a correction to the EGR valve setting based on the estimated deviation of the actual λ , combined with a linear gain. The linear gain is used as a tuning parameter to obtain a desirable response. The second strategy is tested experimentally and performs adequately.

In Section 3.2, Alberer and Del Re (2010) is discussed, which also focuses on transient performance and shows a potential for reduced emissions.

The transient control methods mentioned above do not directly optimize a performance criterion explicitly based on the emissions, fuel efficiency and torque response. Even though these measures are considered the most important during load transients. Using optimal control, direct optimization of these high-level objectives is possible, which is also studied in the literature.

In Alberer and Del Re (2009), an objective function of torque tracking, NO_x and PM emissions is optimized with fuel flow, EGR valve and VGT as inputs. The iterative optimization procedure uses an actual engine to evaluate the objective function. Due to the time needed for optimization, only a single transient is considered. The optimal control signals are compared with a standard controller, the NO_x peak is significantly reduced, the opacity peak is effectively erased and the torque response shows a minor deterioration. Unfortunately, the initial states (initial oxygen concentration) in the compared transients are not equal. It is therefore not clear to what extent the achieved improvement is due to the improved control actions.

In Benz (2010), optimal control using the VGT and EGR valve and fuel actuators is studied. Sequential Quadratic Programming (SQP) is used for numerical optimization of the engine performance in transient operation. The objective function consists of a combination of the predicted emissions and torque response.

Using a mean-value model, a potential for an improved emission tradeoff and improved transient response is shown. The optimal input trajectories, however, do not have smooth characteristics.

In Sequenz et al. (2011), the squared deviation from nominal of PM and NO_x emissions is minimized using numerical optimization. The trajectories of the EGR valve, VGT and crank angle of 50 % mass fraction burnt are used as input variables for the optimization. The latter input is available only indirectly and is controlled using the injection angle. The optimal results show a much smaller peak in PM, combined with an increase in NO_x emissions.

3.4 Discussion

In current literature, a wide variety of choices for sensor selection, actuator selection and control algorithms is made. Nonetheless, a control structure that completely meets all the demands listed in Section 1.1 is not found and further challenges remain.

- **Reduce the average BSFC and engine-out emissions** to reduce the demands on the aftertreatment system and improve the fuel economy. It is difficult to quantify to what extent this is possible by only making changes to the control system, when a production control system is used as a benchmark. When no disturbances are present, or all disturbances are compensated for by means of feed-forward maps, open-loop map-based control does not introduce conservatism. In this thesis, a potential for net performance improvement by remaining close to the nominally optimal performance is aimed for. This should reduce the occurrence of excessive emission deviations and the associated increase of the average emissions.
- **Increase the robustness of the the engine performance**, i.e., reduce the effect disturbances have on the achieved emissions and fuel efficiency. This is particularly relevant due to the introduction of in-service conformity emission limits in the EURO VI legislation. The problem of remaining tightly within the emission limits, while minimizing the BSFC remains to be solved. Control of emissions is studied in Tschanz et al. (2013) and Karlsson et al. (2010), but both methods cannot be applied in the full speed-load operating range

and require sensors that are only available for research. In this thesis the robustness is improved by remaining close to the nominal emissions and fuel consumption that were found optimal during calibration. Moreover, a production engine sensor layout is used and the full speed-load range is considered.

- **Improve tip-in transient** emissions and torque response. A practical that enables the optimization of a combination of emissions, fuel efficiency and torque response by means of control was not found in literature. In this thesis, a feed-forward control method is presented, which is aimed at achieving this.
- **Reduce the design, calibration and implementation effort** to reduce the engine design time and development costs. The trend for more systematic control designs mainly resulted in the use of more complex, rather than easy to implement, control structures. Moreover, a correlation between the use of computational resources by the controllers and a reduction in emissions or fuel consumption is not observed. In this thesis, the focus is therefore on reducing the complexity of the design to achieve the desired low design, calibration and implementation effort.

Table 3.1: Literature overview part 1.

Reference	Controlled outputs	Actuators	Algorithm	Goal
Dekker and Sturm (1996)	EGR flow, p_{ex}	EGR valve, VGT	PID	Active air-path control
Guzzella and Amstutz (1998)	-	-	-	Literature overview
Stefanopoulou et al. (2000)	MAF, MAP	EGR valve, VGT	Scheduled PID	Minimize NO _x emissions
Jankovic et al. (2000)	EGR rate, λ	EGR valve, VGT	Inverse Lyapunov	Improve tracking
van Nieuwstadt et al. (2000)	MAF, MAP	EGR valve, VGT	PID	Comparison
van Nieuwstadt et al. (2000)	MAF, est. MAF	EGR valve, VGT	PID	Comparison
van Nieuwstadt et al. (2000)	MAF, MAP	EGR valve, VGT	SISO PI	Comparison
van Nieuwstadt et al. (2000)	MAF, p_{ex}	EGR valve, VGT	Lyapunov	Comparison
van Nieuwstadt et al. (2000)	MAF, EGR flow	EGR valve, VGT	PID	Comparison
Brahma (2005)	MAF, p_{ex}	EGR valve, VGT	Sliding mode	Maintain λ and NO _x -BSFC tradeoff
Jung and Glover (2006)	MAF, MAP	EGR valve, VGT	LPV	Reduce calibration
Herceg et al. (2006)	p_{in} , p_{ex} , F_{turb}	EGR valve, VGT	MPC	Show MPC performance potential
Wei and Del Re (2007)	MAF, MAP	EGR valve, VGT	LPV	Improve tracking, reduce calibration
Ferreau et al. (2007)	MAF, MAP	EGR valve, VGT	MPC	Improve tracking
Ortner and Del Re (2007)	MAF, MAP	EGR valve, VGT	MPC	Improve tracking

Table 3.2: Literature overview part 2.

Reference	Controlled outputs	Actuators	Algorithm	Goal
Körper et al. (2008)	NO_x , ppm, p_{im}/p_{ex}	EGR valve, VGT	Decoupling, linearization, PID	Systematic control design
García-Nieto et al. (2008)	MAF, MAP	EGR valve, VGT	MPC	Improve tracking
Chauvin et al. (2008)	p_{in} , EGR rate	EGR valve, VGT	Motion planning	Transient control
Alberer and Del Re (2009)	NO_x , ppm, PM, torque	EGR valve, VGT, \dot{m}_{fuel}	Input trajectory optimization	Optimal transient emissions
Alfieri (2009)	NO_x , ppm, λ_O	VGT, SOI	IMC	Control NO_x and PM
Ortner et al. (2009)	MAF, MAP	EGR valve, VGT	MPC	Improve Tracking
Alberer and Del Re (2010)	Intake and exhaust oxygen	EGR valve, VGT	MPC	Reduce transient emissions
Stewart et al. (2010)	Not specified	EGR valve, VGT	MPC	Systematic air-path control design
Wahlström et al. (2010)	EGR rate, λ_O	EGR valve, VGT	Switched, scheduled PID	Minimize pumping work
Karlsson et al. (2010)	In-cylinder pressure, NO_x , ppm, smoke	EGR valve, VGT, SOI, p_{rail} , \dot{m}_{fuel}	MPC	Explore MPC possibilities
Benz (2010)	NO_x flow, PM, torque	EGR valve, VGT, \dot{m}_{fuel}	Input trajectory optimization	Minimize transient emissions
Sequenz et al. (2011)	NO_x flow, PM, CA_{50} (via SOI)	EGR valve, VGT	Input trajectory optimization	Optimal transient emissions
Wang et al. (2011)	MAF, MAP	EGR valve, VGT	MPC	Compare tracking performance

Table 3.3: Literature overview part 3.

Reference	Controlled outputs	Actuators	Algorithm	Goal
Wahlstrom and Eriksson (2013)	MAF, MAP	EGR valve, VGT	MPC	Compare outputs and control algorithms
Wahlstrom and Eriksson (2013)	EGR rate, λ_O	EGR valve, VGT	MPC, PID	Compare outputs and algorithms
Tschanz et al. (2013)	$\text{NO}_{x,\text{ppm}}$, smoke	Swirl valve, SOI, EGR rate (via EGR valve and VGT)	Internal model control	Control NO_x and PM
Zhao et al. (2013)	MAF, MAP, T_{exh} , $\text{NO}_{x,\text{ppm}}$, CA50	EGR valve and VGT, SOI, p_{rail} , R_{fuel}	MPC	Air-path and fuel-path control
Criens et al. (2013b)	specific NO_x , PM, Δp	EGR valve, VGT	PID	Disturbance rejection
This thesis	specific NO_x , λ , Δp	EGR valve, VGT	PID	Robustly maintain performance

4 Modeling, Identification and Analysis

Abstract

In this chapter¹, multisine frequency response function identification is used for non-parametric modeling of the air path of a turbocharged diesel engine around a fixed operating point. The Variable Geometry Turbine (VGT) and Exhaust Gas Recirculation (EGR) valve are used as inputs. The nitrogen oxide emissions, air-fuel equivalence ratio and pressure difference between the intake and exhaust manifold are the considered outputs. A time-efficient and accurate identification procedure for this input-output system is devised, analyzed and executed experimentally for a range of operating points. The analysis quantifies the individual effects of noise and nonlinearities and shows to what extent the local engine behavior can be captured by a linear model.

4.1 Introduction

Stringent legislation of Nitrogen Oxide (NO_x) and Particulate Matter (PM) emissions implies a need for tight control of the combustion conditions in heavy-duty diesel engines. Due to the tightening emission legislation, the complexity and the number of actuators of diesel engines increased significantly in recent years (Pachner et al., 2012). This rapid evolution in engine dynamics requires new control

¹This chapter is accepted as a paper for publication in a special issue on *Engine Combustion Optimisation and Control* in the *International Journal of Powertrains (IJPT)*, title: *A Control Oriented Multivariable Identification Procedure for Turbocharged Diesel Engines*, authors: Chris Criens, Thijs van Keulen, Frank Willems and Maarten Steinbuch (Criens et al., 2013a). The contents are slightly adapted to match the thesis style

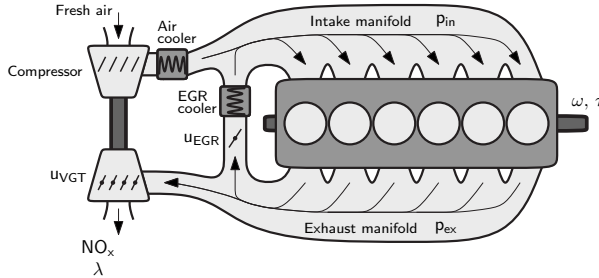


Figure 4.1: A schematic representation of the engine layout.

techniques and corresponding control-relevant modeling techniques. A common heavy-duty engine configuration, depicted in Figure 4.1, enables control over both the oxygen quantity and concentration of oxygen in the intake air mixture, using a valve for Exhaust Gas Recirculation (EGR) and a Variable Geometry Turbine (VGT). This combination of actuators effectively enables control over both the NO_x and PM emissions. Simultaneously, these actuators influence the fuel consumption (Wahlström, 2009). The controlled engine should meet the emission legislation with minimum fuel consumption, while uncertainties are present in, e.g., ambient conditions, production tolerances and aging. A multivariable control design is required to govern the EGR valve and VGT position in a coordinated fashion. Sensors are available to measure the NO_x and oxygen concentration and several other quantities. The input-output behavior, from the actuators to the sensor signals mentioned above, exhibits nonlinear behavior, sign changes and non-minimum phase behavior (Wahlström, 2009), which complicates control design. In order to effectively design a controller, an accurate and control relevant model is required.

The models that are used for VGT-EGR control design are often of the mean-value type (Wahlström, 2009; Stefanopoulou et al., 2000; Del Re et al., 2009; Guzzella and Onder, 2004; Jankovic et al., 2000; Stewart et al., 2010; Wahlström and Eriksson, 2011). These nonlinear first-principles models use lumped volumes for the manifolds and averaging of the reciprocating behavior of the engine to approximate the engine dynamics using low-order Ordinary Differential Equations (ODE). Due to the nonlinear dynamics and the ODE description (which typically includes maps or polynomial relations to represent physical relations) the identification procedure for mean-value models can be complex (Pachner et al., 2012; Wahlström, 2009; Ferreau et al., 2007; Wahlström and Eriksson, 2011). Furthermore, the

formation of emissions during combustion, if included in the model, is based on complex empirical or phenomenological relations (Benz, 2010; Seykens, 2010; Hirsch et al., 2010). Finally, for feedback control design, the entire dynamic input-output behavior is important; sensor and actuator dynamics must be taken into account. In mean-value models sensor and actuator dynamics are often neglected (Wahlström, 2009; Stefanopoulou et al., 2000; Guzzella and Onder, 2004; Jankovic et al., 2000; Kolmanovsky et al., 1999; Wahlström and Eriksson, 2011), which limits their accuracy (Guardiola et al., 2012).

In contrast with the nonlinear mean-value models, control design for the air path is often based on linear and quasi-linear techniques. Numerous examples of, e.g., linear control, scheduled linear control, Linear Parameter Varying (LPV) control or Model Predictive Control (MPC) are available in academic literature (Stewart et al., 2010; Ferreau et al., 2007; van Nieuwstadt et al., 2000; Ortner and Del Re, 2007; Tschanz et al., 2013). For these control designs, the nonlinear engine behavior is reduced to a series of linear submodels, where each submodel describes the engine behavior in a part of the speed-load operating range. Since the controllers are designed using the local linear properties, they do not make full use of the actual nonlinear system description. It can therefore be beneficial to directly determine the local linear input-output response from identification data. This has the advantage that averaging in time and lumping of volumes is no longer needed to describe the system in terms of an ODE and actuator and sensor dynamics are naturally included in the model.

For control design, linear black-box modeling is used in a small number of papers, e.g., in Ferreau et al. (2007) and Ortner and Del Re (2007). Contributions on (quasi)-linear modeling are found as well. A notable contribution on black-box modeling of diesel engines is Henningsson et al. (2012), where local parametric linear models are identified and clustered depending on the dynamic response. In Wei and Del Re (2007), a low-order black-box LPV model is identified. In Verma (2013), the local accuracy of mean-value models is compared with a linear model and measurements in both the time and frequency domain.

In this chapter, it is proposed to use Frequency Response Function (FRF) measurements for identifying the local linear response of the diesel engine air path. FRF measurements are often used to make a control-relevant non-parametric model of the system dynamics (Ljung, 1999). When broadband multisine excitation

signals are used for measuring the FRF, optimal identification accuracy in minimal measurement time is obtained (Pintelon and Schoukens, 2001). Also, the nonlinear influences in the system can be detected and quantified. This is particularly relevant for our application, because the air-path is known to be highly nonlinear. Because this modeling method does not rely on predetermined first-principles models, the modeled outputs can be chosen flexibly. Any output that can be measured during an identification experiment, including emissions, can be modeled this way. For the application of air-path modeling and analysis, this approach is unique in the literature. The work of Stamati et al. (2012) is related, however, in Stamati et al. (2012) multisine excitation is used to determine the parameters of a mean-value model of a diesel engine air path.

Two main difficulties arise when frequency response measurements, i.e., linear black-box modeling, are used for modeling engine dynamics. First, the description of the system dynamics in terms of an FRF is limited to linear dynamics. Second, black-box models typically require more measurement data for their identification than gray-box mean-value models (Pachner et al., 2012). In this chapter both issues are addressed.

The main contribution of this chapter is the application and analysis of multisine FRF identification of a diesel engine air path. A systematic and efficient procedure for the application of multisine FRF identification is presented. This results in a MIMO model describing the local input-output dynamics, with the VGT and EGR valve as inputs and NO_x , air-fuel equivalence ratio and pressure difference between intake and exhaust manifold as outputs. The accuracy of the FRF identification is extensively analyzed; the accuracy is quantified and different sources of distortion are distinguished and quantified. This analysis reveals how accurate the linear behavior is determined, as well as to what extent the actual local behavior of the air path can be captured using a linear model. It is shown that, using ten minutes of measurement data, the linear engine dynamics for a single operating point are accurately captured. The models and analysis are presented mostly in the frequency domain, which is particularly relevant for linear feedback control design. Compared with alternative methods, the identified models represent the local engine behavior with a high accuracy, as is shown in Section 4.6.

The remainder of this chapter is structured as follows. Section 4.2 describes the measurement setup, including sensors and actuators. Section 4.3 describes the

design of the multisine identification experiment. In Section 4.4, the accuracy of the identification method is analyzed. The nonlinear behavior of the system is explicitly included in the analysis and both quantified and classified. It is shown that the engine dynamics can largely be described using linear FRF models. Also, a time-domain validation is performed to illustrate the accuracy in the time domain. Section 4.5 presents FRF measurements on a grid of speed-load operating points. This shows the variation of the dynamic response over the entire operating range. In Section 4.6, the limitations and possible extensions of the modeling approach are discussed. The chapter ends with conclusions.

4.2 Measurement Setup

4.2.1 Engine

The test engine is a modern 6-cylinder heavy-duty diesel engine, equipped with a common-rail injection system, cooled, high-pressure EGR and a VGT. The engine is mounted on an electric dynamometer. This dynamometer governs the engine speed, ω . Also, the dynamometer provides additional measurements, such as the produced net torque, τ . As demonstrated in Section 4.5, the local dynamic behavior changes at different operating points of the engine (combination of ω and τ).

To control the air path, an Exhaust Gas Recirculation (EGR) valve and a Variable Geometry Turbine (VGT) are available. In a VGT, an actuator is available to adjust the guide vanes in the turbine inlet, which changes the flow properties of the turbine. Figure 4.1 shows a schematic representation of the engine focusing on the air path.

The engine was calibrated before the start of the dynamic identification experiments. The actuator settings for nominal, stationary operation were extracted from this calibration. The excitation signal used for identification was added to these nominal EGR and VGT settings. A dSPACE Autobox[®] was used as an I/O board for both controlling the actuators and collecting the sensor signals with a sampling interval of $T_s = 0.01$ s.

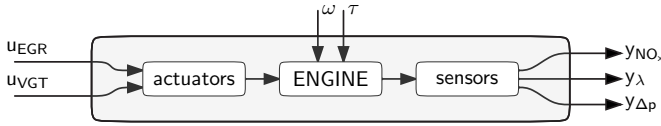


Figure 4.2: The studied input-output relations of the engine in a block scheme. The torque, τ , is controlled via the fuel flow.

4.2.2 Actuators

For identification of the dynamic behavior of the engine air path, two actuators are of main interest: the EGR valve and VGT actuator. These actuators will be controlled by the dSPACE Autobox[®]. Any other available actuators, e.g., the fuel injection equipment or exhaust throttle valve, are not included in this dynamic identification and are controlled by the engine ECU, although it is possible to extend or change the identification procedure to include other actuator configurations. Both the EGR valve and VGT position are electrically actuated. The input signals to these actuators:

$$u = \{u_{VGT}, u_{EGR}\}, \quad (4.1)$$

both have a range between 0 % and 100 %, with a quantization resolution of 0.5 % and 0.1 % for u_{VGT} and u_{EGR} , respectively. Internal control loops in the actuators control the VGT and EGR valve to the requested settings.

4.2.3 Sensors

The identification procedure is demonstrated on three different outputs: the engine-out NO_x emissions, y_{NO_x} , engine-out air-fuel equivalence ratio, y_λ , and the pressure difference between intake and exhaust manifold, $y_{\Delta p}$. The latter two measurements are selected because of their link with the PM emissions and fuel efficiency, respectively. These measurements provide insight into the behavior and performance of the engine air path and are relevant for control design (Wahlström et al., 2010; Alfieri, 2009; Criens et al., 2013b). The outputs are denoted:

$$y = \{y_{\text{NO}_x}, y_\lambda, y_{\Delta p}\}. \quad (4.2)$$

The y_{NO_x} measurement is based on the engine-out NO_x sensor. This sensor measures NO_x levels in ppm. They are converted to g/kWh using the the engine

speed, injected fuel mass, dynamometer torque measurement² and a measurement of the exhaust mass flow. The second signal, y_λ , is derived from the oxygen concentration sensor measurement. Both the NO_x sensor and λ sensor are placed downstream of the turbine, as shown in Figure 4.1. The third measurement signal, $y_{\Delta p}$, is the pressure difference between the intake and exhaust manifold. Both the intake, p_{in} , and exhaust manifold pressure, p_{ex} , are measured in kPa and $y_{\Delta p}$ is calculated using: $y_{\Delta p} = p_{\text{ex}} - p_{\text{in}}$. Figure 4.2 summarizes the input-output relations in a block scheme.

4.3 Design of the Input Signal

The result of the identification experiment and the available analysis methods depend largely on the input signal. In Section 4.3.1, the design of the multisine input signal is detailed. Then in Section 4.3.2, the effect of input quantization on the experiment is discussed.

4.3.1 Multisine

A multisine signal is particularly useful as an excitation signal for FRF identification. The frequency content can be chosen flexibly and multisine identification combines minimum measurement time with maximum identification accuracy. When the excitation frequencies are selected suitably, multisine identification can also be used to detect, classify and quantify nonlinear behavior (Pintelon and Schoukens, 2001). This is particularly useful due to the fact that the engine dynamics are known to be nonlinear.

A multisine signal consists of a sum of sinusoidal signals. Realization k of a multisine signal for input m is defined as:

$$u_m^{[k]}(t) = \sum_{n=1}^{N_m} A_{m,n} \sin\left(2\pi f_0 l_{m,n} t + \phi_{m,n}^{[k]}\right) \quad (4.3)$$

with amplitudes $A_{m,n}$, excitation frequencies $f_0 l_{m,n}$ and phase $\phi_{m,n}^{[k]}$. The spectral lines are selected from $l_{m,n} \in \mathbb{N}$, where \mathbb{N} is the set of nonnegative integers. When

²A torque measurement is not typically available on diesel engines. This sensor can be replaced with an estimate, e.g., using the fuel flow, to enable control of NO_x in g/kWh when the engine is not installed on a dynamometer.

the multisine signal is constructed according to this definition, a periodic signal with period length $T = 1/f_0$ is obtained. It was found that selecting $T = 600$ s, gives accurate identification results, which is analyzed in Section 4.4. A total of N_m spectral lines are present in the multisine. The subscript m is used to distinguish between the EGR and VGT input, i.e., $m \in \{\text{EGR}, \text{VGT}\}$ in the rest of the chapter.

In aid of the analysis of the identification accuracy, a random multisine is used. For each realization k , a different phase $\phi_{m,n}^{[k]}$ is chosen randomly in the interval $[-\pi, \pi)$. Figure 4.3 shows a realization of the multisine excitation signal in both the frequency and time domain. For the identification experiments, this signal is added to the nominal VGT and EGR valve positions. In the next subsections, the choices made for the frequencies, $f_0 l_{m,n}$, and amplitudes, $A_{m,n}$ are discussed and motivated.

Excitation Frequencies

Two considerations are made when choosing the excitation frequencies: first, the identification of nonlinearities and second, the distribution of uncertainties of the FRF.

For identification of nonlinear behavior, it is beneficial to use only odd multiples of f_0 in the excitation signal (Vanhoenacker et al., 2001). The odd and even harmonic content of the measured output signals will then distinguish between the effects of odd and even nonlinear behavior. Moreover, when only odd frequencies (odd multiples of f_0) are used in the input signal, even nonlinearities do not disturb the FRF measurement, which is beneficial for an accurate measurement of the linear behavior.

These arguments for using only odd frequencies do not hold when only even multiples of f_0 are used. Using even frequencies exclusively will render both even and odd nonlinear distortions at even frequencies; their effects can no longer be separated and both will distort the FRF measurement. For an accurate measurement, it is therefore not recommended to use even frequencies.

A property that is often encountered in dynamic systems is that the features that determine the FRF (resonances, poles and zeros) are distributed approximately logarithmically over the frequency space. To obtain a similar accuracy over

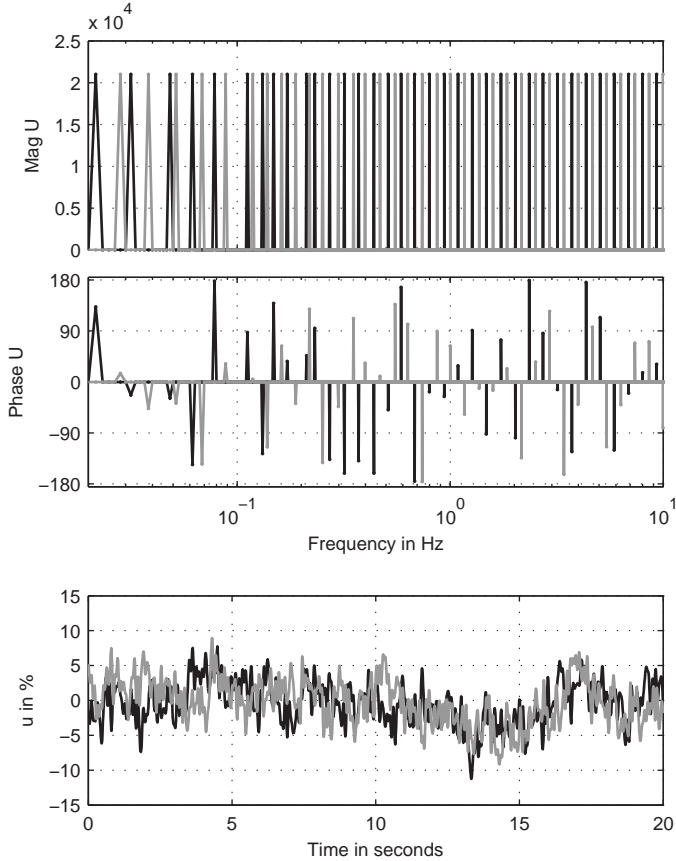


Figure 4.3: The multisine excitation signal. From top to bottom: the magnitude spectrum; phase spectrum; and first 20s of the 600s excitation signal. In black u_{VGT} , in gray u_{EGR} .

the entire frequency range, which is desired, the excitation frequencies, $f_0 l_{m,n}$ should then also be distributed logarithmically over the frequency range. For the experiments, the ideal logarithmic frequency distribution is approximated by a quasi-logarithmic distribution that fits Equation (4.3) by rounding $l_{m,n}$ to the nearest odd spectral line such that $l_{m,n} \in (2N+1)$. The number of excitation frequencies in the excitation signals for the VGT and EGR equals: $N_{\text{VGT}} = N_{\text{EGR}} = 35$. The highest excitation frequency is 10 Hz, which is well beyond the expected bandwidth of a closed-loop controlled system.

Particularly at frequencies over 1 Hz, the logarithmic distribution of excitation frequencies on the linear frequency grid of the Discrete Fourier Transform (DFT) is very sparse. For identification of nonlinear effects, a more dense linear distribution is preferred over the sparse logarithmic distribution (Vanhoenacker et al., 2001). However, for our purposes, an accurate detection of the low frequency linear behavior has a higher priority than an accurate detection of the high frequency nonlinear behavior. Therefore, the logarithmic distribution is preferred.

To separate the response due to excitation of the EGR valve from the response due to excitation of the VGT actuator, two non-overlapping grids of spectral lines, $l_{m,n}$, are used for the inputs. This enables a separation of the linear effects of the individual inputs in the frequency domain and only one experiment is needed to identify the Multi-Input Multi-Output (MIMO) system. In Dobrowiecki and Schoukens (2007), it is shown that the level of nonlinear distortions for MIMO FRF measurements using non-overlapping frequency grids is similar to that of an optimized experiment using multiple experiments.

Excitation Amplitude

The amplitude $A_{m,n}$ of the individual sinusoids is chosen such that the amplitude of the combined multisine signal, $u_m^{[k]}(t)$, is similar to the expected amplitude of the input signal when a feedback controller for EGR and VGT is active. In this way, the nonlinear effects that arise during identification are similar to those that are present during feedback operation. This consideration resulted in a constant amplitude of $A_{m,n} = 0.7\%$ of the maximum actuator position for both inputs and all excited frequencies.

4.3.2 Influence of Input Quantization

The amplitude of the individual sinusoids is chosen $A_{m,n} = 0.7\%$, whereas the quantization in the VGT actuator allows only steps of 0.5% . Consequently, the values in the smooth multisine signal are rounded towards the nearest integer multiple of 0.5% . Therefore, concerns arise regarding the smoothness and accuracy of the quantized signal that excites the VGT actuator.

To evaluate the influence of quantization of the VGT input, a smooth multisine signal is compared with a simulated quantized multisine signal. The relative power

of the difference between the quantized multisine, $u_{q,\text{VGT}}^{[k]}$, and the actual, smooth multisine, $u_{\text{VGT}}^{[k]}$, is calculated as follows:

$$e_q^{[k]} = \frac{\sum_{n=1}^N \left| u_{q,\text{VGT}}^{[k]}(t_n) - u_{\text{VGT}}^{[k]}(t_n) \right|^2}{\sum_{n=1}^N \left| u_{\text{VGT}}^{[k]}(t_n) \right|^2}, \quad (4.4)$$

where $N = T/T_s = 60000$ equals the number of samples in the excitation signal, measured in discrete time, t_n , and n denotes the sample number. In the frequency domain, the relative power of the difference between $U_{q,\text{VGT}}^{[k]}$ and $U_{\text{VGT}}^{[k]}$, evaluated only at $l_{\text{VGT},n}$, the excited spectral lines in $U_{\text{VGT}}^{[k]}$, is:

$$e_{q,\text{exc}}^{[k]} = \frac{\sum_{n=1}^{N_{\text{VGT}}} \left| U_{q,\text{VGT}}^{[k]}(l_{\text{VGT},n}) - U_{\text{VGT}}^{[k]}(l_{\text{VGT},n}) \right|^2}{\sum_{n=1}^{N_{\text{VGT}}} \left| U_{\text{VGT}}^{[k]}(l_{\text{VGT},n}) \right|^2}. \quad (4.5)$$

The capital U denotes the Fourier transform of the input u . The parameter $e_q^{[k]}$ quantifies the total error, whereas $e_{q,\text{exc}}^{[k]}$ only takes into account the error at the measurement frequencies. The difference between $e_q^{[k]}$ and $e_{q,\text{exc}}^{[k]}$ is the energy of the quantized input signal at non-excited frequency lines.

For the multisine signal shown in Figure 4.3, the values $e_q^{[1]} = 2.425 \cdot 10^{-3}$ and $e_{q,\text{exc}}^{[1]} = 6.316 \cdot 10^{-6}$ are obtained³. Both $e_q^{[1]}$ and $e_{q,\text{exc}}^{[1]}$ are much smaller than one. This means that the relative influence of quantization on the frequency content of the input signal is very small. The influence of quantization on the identification experiment is therefore not explicitly taken into account during the further analysis.

4.4 Analysis of the Identification Accuracy

Before using multisine excitation to measure FRFs, the accuracy of the identification procedure is studied using a more extensive identification procedure. A series of experiments using multiple periods of multiple random-phase multisine realizations is performed at a single operating point (1455 rpm and 120 mg/inj). The

³The exact values of both $e_q^{[k]}$ and $e_{q,\text{exc}}^{[k]}$ depend on the phase realization, k , of the multisine signal, but they have approximately the same value for all phase realizations.

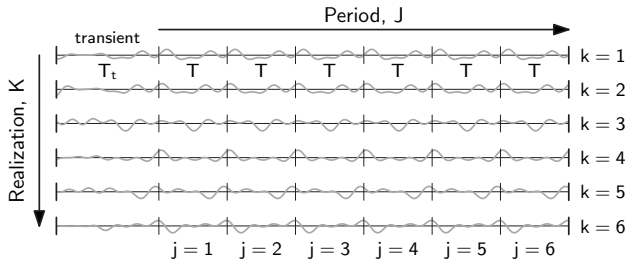


Figure 4.4: Scheme of the analysis experiment. For every phase realization k of the multisine signal, $J = 6$ periods are measured and a total of $K = 6$ different phase realizations of the multisine signal are used. Before measuring the periodic response, a waiting time of T_t is introduced to prevent startup transients from disturbing the periodic measurement (Schoukens et al., 2005).

extended procedure is constructed to analyze the effects of noise and nonlinearities on the FRF estimate. The analysis also separates nonlinear behavior from the linear behavior; the nonlinear part is then quantified and classified into even and odd nonlinear behavior. This analysis is performed in the frequency domain and is to a large extent similar to Rijlaarsdam et al. (2010), where the nonlinear behavior of a single-input industrial motion stage is studied. This section also includes a validation in the time domain, to further illustrate the model accuracy.

For the purpose of this identification and analysis, the MIMO system can be split into three separate Multi-Input Single-Output (MISO) systems. The calculations and also the analysis are performed for each output separately. To keep the notation as short as possible, subscripts to denote the individual outputs are omitted.

To help illustrate the method, Figure 4.4 schematically depicts the execution of the experiment. For each phase realization, k , a multisine input signal $u^{[k]}$ is applied to the inputs, while the output is measured for J consecutive periods. In this chapter, $K = 6$ phase realizations of the multisine are applied for $J = 6$ periods each. In this way, a total of $J \cdot K = 36$ periods of measurement data is obtained. Before measuring the periodic response, a waiting time of at least $T_t = 60$ s is used for a sufficient decay of startup transients. The measurement corresponding to a single period j of realization k is denoted $y_j^{[k]}$. The length of $y_j^{[k]}$ equals one period of the excitation signal, $T = 600$ s, and it contains $N = 60\,000$ samples. Capital

U and Y , are used to denote the DFT of respectively the inputs u and measured outputs y . Measuring multiple periods using the same excitation signal makes it possible to determine the influence of noise. Using multiple realizations of the input signal makes it possible to determine the influence of nonlinearities on the identified FRF.

4.4.1 Frequency Response Function

Using the DFT of the applied periodic inputs and measured outputs, the FRF can be calculated using a division of the transformed signals. The estimated FRF is defined only at the N_m frequencies present in the input signal: $f_0 l_{m,n}$.

For each input m , period j and realization k , the FRF is calculated as follows:

$$H_{j,m}^{[k]}(l_{m,n}) = \frac{Y_j^{[k]}(l_{m,n})}{U_m^{[k]}(l_{m,n})}. \quad (4.6)$$

Using all periods of realization k , an average FRF is determined for each realization:

$$\bar{H}_m^{[k]}(l_{m,n}) = \frac{1}{J} \sum_{j=1}^J H_{j,m}^{[k]}(l_{m,n}). \quad (4.7)$$

The use of multiple periods reduces the influence of noise on the FRF estimate. The variance of $\bar{H}_m^{[k]}$ due to noise is a factor J lower than the variance of the individual estimates $H_{j,m}^{[k]}$.

When all realizations of the multisine are used, the FRF estimate can be improved further:

$$H_{\text{BLA},m}(l_{m,n}) = \frac{1}{K} \sum_{k=1}^K \bar{H}_m^{[k]}(l_{m,n}), \quad (4.8)$$

where $H_{\text{BLA},m}$ gives the Best Linear Approximation (BLA) (Schoukens et al., 2005) using the available data. The variance of $H_{\text{BLA},m}$ due to nonlinearities is a factor K smaller than that of the single realization estimates $\bar{H}_m^{[k]}$. Also the variance due to noise decreases by a factor K . For an infinite number of random phase realizations, $H_{\text{BLA},m}$ converges to the actual best linear approximation, which depends only on the power spectrum of the excitation signal.

4.4.2 Accuracy of the Frequency Response Function

To analyze the accuracy of the FRF of a single period, $H_{j,m}^{[k]}$, two sources of distortion are separated: noise and nonlinearities.

First, the variance due to noise is quantified. Noise causes a repeated experiment with the same input signal to have a different outcome. To estimate the expected distortion of $H_{j,m}^{[k]}$ due to noise, the variance of the FRF is calculated for each realization. Next, these variances are averaged over all realizations:

$$v_{\text{H,noise},m} = \frac{1}{K(J-1)} \sum_{k=1}^K \sum_{j=1}^J \left| H_{j,m}^{[k]} - \bar{H}_m^{[k]} \right|^2. \quad (4.9)$$

The distortion due to nonlinear behavior is the same for all periods of the same realization, but changes when a different phase realization of the input signal is used. The variance of $\bar{H}_m^{[k]}$ therefore quantifies the expected distortion of $H_{j,m}^{[k]}$ due to nonlinear behavior:

$$v_{\text{H,NL},m} = \frac{1}{K-1} \sum_{k=1}^K \left| \bar{H}_m^{[k]} - H_{\text{BLA},m} \right|^2 - \frac{1}{J} v_{\text{H,noise},m}, \quad (4.10)$$

where a correction for the expected bias due to noise is used. Figure 4.5 shows $|H_{\text{BLA},m}|$ and the standard deviations $\sigma_{\text{H,noise},m} = \sqrt{v_{\text{H,noise},m}}$ and $\sigma_{\text{H,NL},m} = \sqrt{v_{\text{H,NL},m}}$ for the studied outputs.

The variances calculated in Equations (4.9) and (4.10) are the variances of $H_{j,m}^{[k]}$. The variances of $H_{\text{BLA},m}$ and $\bar{H}_m^{[k]}$ are lower and can be deduced by dividing by J and K , according to the methods provided in Section 4.4.1.

Figure 4.5 shows that the expected deviation of the FRF due to nonlinearities dominates over the expected deviation due to noise. Where $|H_{\text{BLA},m}|$ is an order of magnitude larger than the deviation due to either noise or nonlinearities, $H_{j,m}^{[k]}$ is considered an accurate estimate of $H_{\text{BLA},m}$. Which implies that an FRF that is made using a single period of ten minutes is an accurate estimate of the actual BLA. The values of $|H_{\text{BLA,VGT}}|$ are larger than those of $|H_{\text{BLA,EGR}}|$, whereas their respective standard deviations have similar values. This means that the relative accuracy of $|H_{\text{BLA,VGT}}|$ is higher. Nonlinear distortions are the largest cause of variance. Therefore, increasing the number of periods, J , is much less

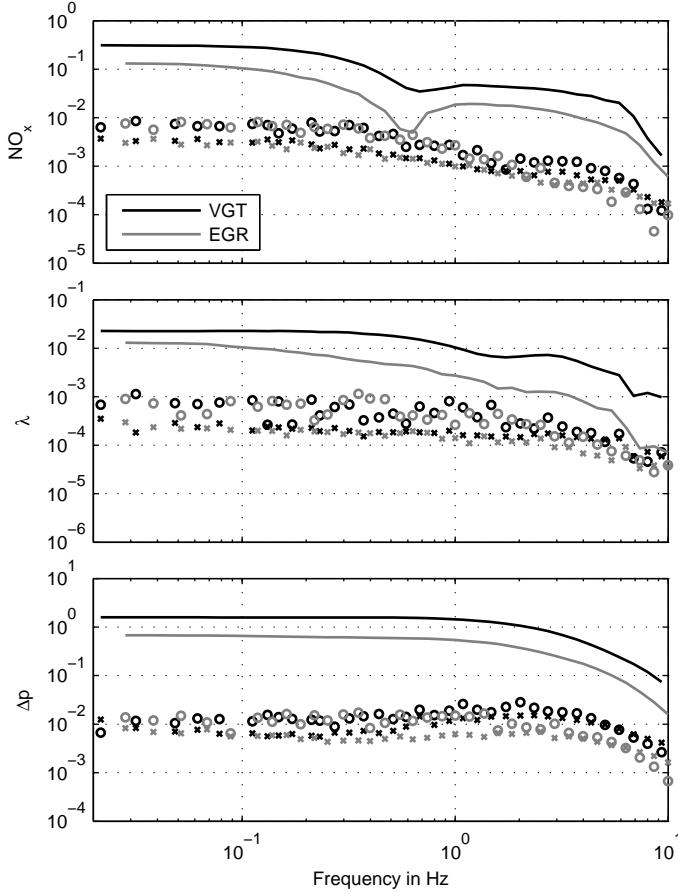


Figure 4.5: Analysis of the variance of $H_{j,m}^{[k]}$ for the operating point 1455 RPM and 120 mg/inj. The response of the VGT and EGR inputs is depicted in respectively black and gray. The lines show $|H_{BLA,m}|$; the 'x' and 'o' symbols show respectively $\sigma_{H,noise,m}$ and $\sigma_{H,NL,m}$.

effective at improving the accuracy of $H_{BLA,m}$ than increasing the number of realizations, K .

Particularly for the Δp output, the variances due to noise and nonlinearities are very low, i.e., $H_{BLA,m}$ is very accurate for the Δp output. This is also reflected in the smoothness of $|H_{BLA,m}|$ for the Δp output.

The measurement of $|H_{BLA,m}|$ for the NO_x output is, at the anti-resonance

around 0.6 Hz, of the same magnitude as $\sigma_{H,NL,m}$. A single measurement of $H_{j,m}^{[k]}$ will, therefore, not suffice to reliably determine $H_{BLA,m}$ for this frequency. However, the presence of the anti-resonance can be determined reliably from a single measurement, because $\sigma_{H,NL,m}$ is significantly smaller than the FRF values surrounding the anti-resonance.

4.4.3 Classification of Nonlinearities

The previous section dealt with determining how accurate the BLA of the FRF is determined. This section deals with determining how accurate this BLA describes the actual system behavior. Opposed to the FRF models discussed in the previous section, which only describe the linear behavior of the system, this section focusses on quantifying and classifying the remaining nonlinear part of the system. An analysis of the measured outputs at non-excited spectral lines reveals the quantity of the output power omitted from the linear model.

The response of a linear system that is excited with a periodic input signal is again a periodic signal containing only the frequencies present in the input signal. The response of a nonlinear system includes frequencies that are not present in the input signal. By analyzing the spectral content of the measured data at non-excited frequencies, the nonlinear behavior can be analyzed. The nonlinear part of the response can be classified into an even and an odd part. The frequency content of the higher-order harmonics generated by the even part of the nonlinear behavior consists of even multiples of the excitation frequencies and vice versa for the odd part.

The input signals $u_m^{[k]}$ consist of only odd frequencies (odd multiples of f_0). Odd multiples of odd frequencies result again in odd frequencies. Even multiples of the odd frequencies in the excitation signal result in even frequencies. Therefore, a separation of the spectrum of $y^{[k]}$ into even and odd multiples of the base frequency separates of the effects of even and odd nonlinear behavior.

The average DFT of the output spectrum of a single realization is given by:

$$\bar{Y}^{[k]} = \frac{1}{J} \sum_{j=1}^J Y_j^{[k]} \quad (4.11)$$

and the variance of $\bar{Y}^{[k]}$ due to noise is given by:

$$v_{\bar{Y},\text{noise}}^{[k]} = \frac{1}{J(J-1)} \sum_{j=1}^J \left| Y_j^{[k]} - \bar{Y}^{[k]} \right|^2. \quad (4.12)$$

Using $\bar{Y}^{[k]}$ and $v_{\bar{Y},\text{noise}}^{[k]}$, the power in the output spectrum due to nonlinearities, corrected for the expected bias due to noise, is:

$$P_{\text{NL}} = \frac{1}{K} \sum_{k=1}^K \left| \bar{Y}^{[k]} \right|^2 - \frac{1}{K} \sum_{k=1}^K v_{\bar{Y},\text{noise}}^{[k]}. \quad (4.13)$$

To make the results of (4.13) of the same units as the FRF ($H_{\text{BLA},m}$) and thereby easier to interpret, the square root of the power is calculated and scaled with the magnitude of the input signal. This results in D_{NL} :

$$D_{\text{NL}} = \frac{\sqrt{P_{\text{NL}}}}{\bar{U}} \quad (4.14)$$

and for the estimated noise bias of D_{NL} :

$$D_{\text{noise}} = \frac{\sqrt{\frac{1}{K} \sum_{k=1}^K v_{\bar{Y},\text{noise}}^{[k]}}}{\bar{U}}, \quad (4.15)$$

where $\bar{U} = \left| U_{j,m}^{[k]}(l_m) \right| = \frac{1}{2} N \cdot A_{m,n}$ is used to scale the results with the input amplitude. A constant amplitude is used for both inputs at all excited frequencies, therefore \bar{U} is also constant, as can be observed in Figure 4.3.

To separate the even and odd nonlinear behavior, the data of D_{NL} in (4.14) is split into two different frequency ranges, which separate the odd frequencies ($l_o \in \mathbb{L}_o = \{l \in 2\mathbb{N} + 1 \mid l \neq l_{m,n} \forall m, n\}$) from the even frequencies ($l_e \in \mathbb{L}_e = (2\mathbb{N} + 2)$).

Figure 4.6 shows a comparison between $|H_{\text{BLA},m}|$, $D_{\text{NL}}(l_e)$, $D_{\text{NL}}(l_o)$ and D_{noise} . At high frequencies D_{noise} is of similar magnitude as D_{NL} , which indicates that the values for D_{NL} are unreliable. Except for the anti-resonance in the NO_x -output and the frequency range around 10Hz, the nonlinear part of the system behavior, D_{NL} , is an order of magnitude smaller than the linear behavior, $|H_{\text{BLA},m}|$. This means that a linear FRF relevantly describes the actual dynamic system behavior. This result extends beyond multisine identification; it implies

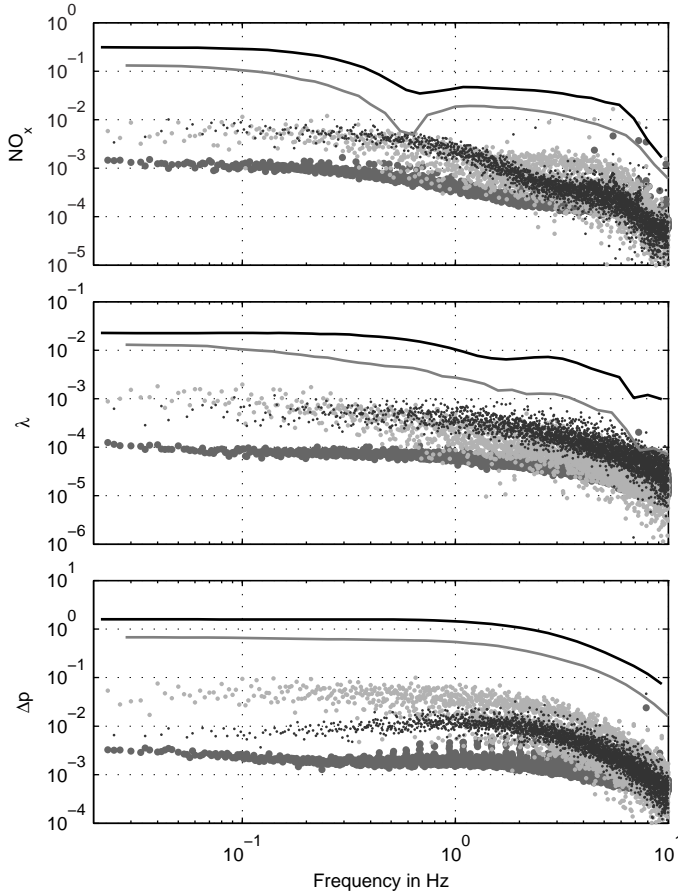


Figure 4.6: Frequency content of the non-excited spectral lines. The engine operating point is 1455 RPM and 120 mg/inj. The black and gray line show respectively $|H_{\text{BLA,VGT}}|$ and $|H_{\text{BLA,EGR}}|$. The medium gray, light gray and dark gray dots show respectively D_{noise} , $D_{\text{NL}}(l_e)$ and $D_{\text{NL}}(l_o)$.

that when the input signals are similar to those during the identification, linear techniques are relevant for analysis of the dynamics and linear control theory is suitable for the design of local controllers.

Particularly for Δp a difference between odd and even nonlinearities is observed. At low frequencies, the effect of the even nonlinearities is an order of magnitude higher. Because only odd frequencies are used for measuring the FRF,

the significantly larger even nonlinearities do not distort the FRF measurement, which is beneficial for the accuracy of the FRF.

Comparing Figure 4.5 and 4.6 shows that the odd nonlinear effects are similar at excited and non-excited spectral lines, i.e., $D_{\text{NL}}(l_o)$ is an indication for the uncertainty that is present in the FRF measurements. This is particularly interesting, because, apart from the noise bias correction, $D_{\text{NL}}(l_o)$ can also be calculated using a single measurement period j and single realization k . This enables a quick estimation of the accuracy of the FRF using only a single measurement, which will be used in Section 4.5.

4.4.4 Time-Domain Validation

In Section 4.4.3, the use of a linear model structure was shown to be relevant; the effects of the nonlinear behavior are an order of magnitude smaller than the linear behavior. Also, it was shown in Section 4.4.2 that the distortions on the FRF estimate due to noise and nonlinearities are an order of magnitude smaller than the actual estimate. Hence, the method for determining FRF models is accurate and the resulting models are an accurate representation of the measured engine behavior. To further illustrate the accuracy of the linear FRF models in the time domain, a validation experiment is performed.

For this validation, an estimate of $H_{\text{BLA},m}$ is made using five out of six realizations, where each realization contains all six periods. This model will be used to predict the results of the sixth realization. The FRF estimate is:

$$H_{\text{BLA},m}^{[1:5]}(l_{m,n}) = \frac{1}{5} \sum_{k=1}^5 \bar{H}_m^{[k]}(l_{m,n}). \quad (4.16)$$

In the discrete Fourier domain, the prediction of the sixth realization is calculated. The output change predicted by $H_{\text{BLA},m}^{[1:5]}$ as a result of input $u_m^{[6]}$ is:

$$Y_{\text{pred},m}^{[6]}(l_{m,n}) = H_{\text{BLA},m}^{[1:5]}(l_{m,n}) U_m^{[6]}(l_{m,n}). \quad (4.17)$$

This frequency-domain representation, $Y_{\text{pred},m}^{[6]}$, is converted to the time domain using the Inverse Discrete Fourier Transform (IDFT):

$$y_{\text{pred},m}^{[6]}(t) = \frac{2}{N} \sum_{n=1}^{N_m} \Re \left(Y_{\text{pred},m}^{[6]}(l_{m,n}) e^{i2\pi f_0 l_{m,n} t} \right). \quad (4.18)$$

The nominal static output is not predicted by the FRF measurements. The average output over the first five realizations is used instead:

$$y_s^{[1:5]} = \frac{1}{5N} \sum_{k=1}^5 \sum_{n=1}^N y^{[k]}(t_n). \quad (4.19)$$

Using the superposition principle, the sum of $y_s^{[1:5]}$ and $y_{\text{pred},m}^{[6]}$ evaluated for both the VGT and EGR produces the prediction of $y^{[6]}$:

$$y_{\text{pred}}^{[6]}(t) = y_s^{[1:5]} + y_{\text{pred,VGT}}^{[6]} + y_{\text{pred,EGR}}^{[6]}. \quad (4.20)$$

Figure 4.7 shows a comparison between $y_{\text{pred}}^{[6]}(t)$ and the measured output of the sixth realization averaged over all periods: $\bar{y}^{[6]}(t) = \frac{1}{J} \sum_{j=1}^J y_j^{[6]}(t)$. As expected from the earlier frequency domain results, a close match between the model prediction and measured output is observed.

Various aspects of the accuracy of the model fit are quantified. The total relative error is calculated using:

$$e_{\text{total}} = \frac{\sum_{n=1}^N \left(y_{\text{pred}}^{[6]}(t_n) - y_s^{[1:5]} - \bar{y}^{[6]}(t_n) + \bar{y}_s^{[6]} \right)^2}{\sum_{n=1}^N \left(\bar{y}^{[6]}(t_n) - \bar{y}_s^{[6]} \right)^2}, \quad (4.21)$$

where $\bar{y}_s^{[6]} = \frac{1}{N} \sum_{n=1}^N \bar{y}^{[6]}(t_n)$. A correction for the static values is used, such that e_{total} quantifies only errors in the dynamic behavior; the prediction of the static output is not of interest for FRF modeling.

The fraction of the power of the measurement signal at frequencies that are not present in the excitation signal is given by:

$$e_{o/e} = \frac{\sum_{n=1}^{N_{o/e}} \left| \bar{Y}^{[6]}(l_{o/e,n}) \right|^2}{\sum_{l=1}^N \left| \bar{Y}^{[6]}(l) \right|^2}, \quad (4.22)$$

with $l_{o/e} \in (\mathbb{L}_o \cup \mathbb{L}_e)$, the non-excited spectral lines and $N_{o/e} = N/2 - (N_{\text{VGT}} + N_{\text{EGR}})$, the number of non-excited spectral lines. The error $e_{o/e}$ indicates the relative influence of nonlinear behavior.

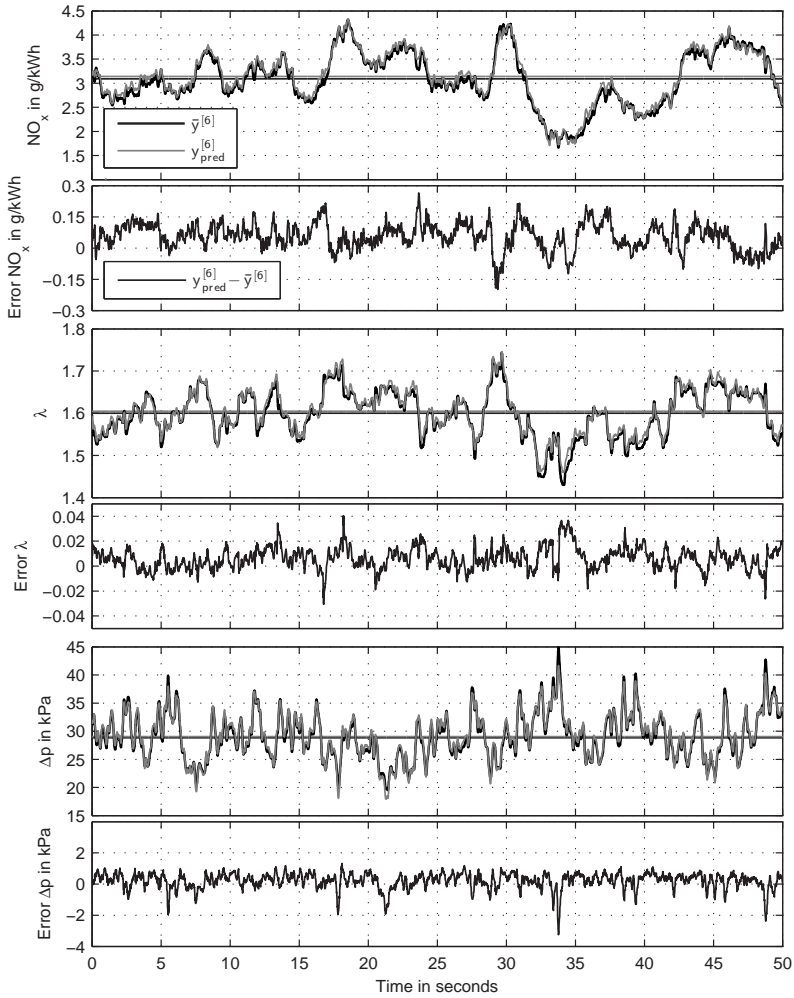


Figure 4.7: The first 50 s of $y_{\text{pred}}^{[6]}$ and $\bar{y}^{[6]}$. In the larger plots, the black line depicts the measured data, $\bar{y}^{[6]}$, and the gray line the prediction using the FRF model, $y_{\text{pred}}^{[6]}$; the straight thin lines show the $y_s^{[1:5]}$ and $y_s^{[6]}$ in black and gray, respectively. The smaller plots show the difference between the prediction and the measurement.

The relative error at the frequencies present in input signal m equals:

$$e_m = \frac{\sum_{n=1}^{N_m} \left| Y_{\text{pred},m}^{[6]}(l_{m,n}) - \bar{Y}^{[6]}(l_{m,n}) \right|^2}{\sum_{n=1}^{N_m} \left| \bar{Y}^{[6]}(l_{m,n}) \right|^2} \quad (4.23)$$

and for both inputs combined:

$$e_{\text{exc}} = \frac{\sum_{m \in \{\text{VGT}, \text{EGR}\}} \sum_{n=1}^{N_m} \left| Y_{\text{pred},m}^{[6]}(l_{m,n}) - \bar{Y}^{[6]}(l_{m,n}) \right|^2}{\sum_{m \in \{\text{VGT}, \text{EGR}\}} \sum_{n=1}^{N_m} \left| \bar{Y}^{[6]}(l_{m,n}) \right|^2}. \quad (4.24)$$

The values e_m and e_{exc} quantify the error that is made in predicting the linear behavior of the engine.

In Table 4.1, an overview of the differences between the measurement $\bar{y}^{[6]}$ and model prediction $y_{\text{pred}}^{[6]}$ is presented. Note that none of the error measures use a bias correction for noise or nonlinearities. Therefore, when a different number of periods or realizations is used, the expected values of these error measures changes. Figures 4.5 and 4.6 and Equations (4.9), (4.10), (4.14) and (4.15) provide less ambiguous error measures in this sense. The comparison also differs from the comparison in Figures 4.5 and 4.6, it is not aimed at determining the accuracy of an FRF model made using a single measurement period. Instead, the prediction of an average FRF model is compared with the expected value of a single experiment. In this comparison nonlinear effects are present mostly in the measurement. Because multiple realizations are used for determining $y_{\text{pred},m}^{[6]}$, nonlinear effects are averaged in the prediction. Noise has a very small effect on the accuracy of $y_{\text{pred},m}^{[6]}$ and averaging of six periods is used to decrease the effects of noise from the measurement.

The relative power of the error is at most 2.8 percent for all outputs. Surprisingly, the NO_x measurement is predicted more accurately than the Δp measurement, even though the relative variance of the FRF was significantly smaller for Δp . When looking at e_{exc} it can be seen that indeed the linear part of the Δp response is recreated with the highest accuracy, but nonlinear effects are the main

Table 4.1: The relative difference between model and measurement.

	e_{total}	$e_{o/e}$	e_{exc}	e_{VGT}	e_{EGR}
NO_x	1.41 %	1.23 %	0.18 %	0.11 %	0.70 %
λ	2.80 %	2.55 %	0.26 %	0.15 %	0.89 %
Δp	1.64 %	1.61 %	0.03 %	0.02 %	0.07 %

cause of e_{total} . The even nonlinear behavior observed in the Δp measurement did not disturb the FRF measurement, but does show up in $e_{o/e}$. When only e_{exc} , e_{VGT} and e_{EGR} are considered, which only quantify errors in the linear part of the response, the Δp prediction is the most accurate.

For all outputs, $e_{o/e}$ constitutes the largest part of e_{total} . Only nonlinear models can capture these effects. To significantly decrease the remaining error, a nonlinear model is needed.

The errors in Table 4.1 might be surprisingly small, but two remarks are in place here. First, the relative power of the error is considered. This means that compared to Figures 4.5 and 4.6, the relative difference is squared. Second, the parts of the FRF with high gains are identified most accurately. These parts also constitute a relatively large part of the power of the output signal. This also favors low errors in the time-domain validation compared with the frequency-domain results in Figures 4.5 and 4.6.

In the presented form, the FRF models are not directly suitable for simulating the response to a general input signal that includes different frequencies. Approximations are needed to enable a calculation of the response at frequencies that are not present in the excitation signal. Furthermore, it is known that the BLA depends on the power spectrum of the input. For inputs with smaller or larger amplitudes, the BLA will change. Using common knowledge of the nonlinear behavior of the air path, it is expected that the accuracy will degrade when larger input amplitudes are considered, because nonlinear effects will constitute a larger part of the output spectrum. When the input amplitude is decreased, the relative influence of noise and quantization will increase, but the nonlinear effects are expected to decrease. As noise and quantization currently constitute a minor effect, the approximation error is expected to decrease when the input amplitude

is decreased. For the presented identification results, the input amplitude was chosen to make the input signal resemble the output of a feedback controller. This makes the identification results and accuracy analysis particularly suited towards feedback control design.

4.5 Frequency Response Function Measurement Results

From Section 4.4, it is concluded that the standard deviation of the resulting FRF measurements is an order of magnitude smaller than the actual FRF itself, even when a single measurement period is used. When the conclusion of this analysis holds for all operating points, the FRF at a different operating point can be identified efficiently using a single 600 s period. To check this assumption, the accuracy of the FRF and encountered nonlinearities can be determined using Equation (4.14). The bias estimate cannot be included, because only one measurement period is available.

To characterize the differences in the input-output behavior of the diesel engine at different operating points, FRF measurements on a 3x3 grid of engine speeds (1011, 1455, 1700 rpm) and loads (60, 120, 200 mg/inj) are performed. Ten minutes of measurement time is used for each operating point and the FRF is calculated using Equation (4.6). Figure 4.8 shows the resulting FRFs in a Bode plot. Using Equation (4.14), it is concluded that the ratio between the linear and nonlinear contributions is similar to Figure 4.6, which implies that indeed the analysis of Section 4.4 will render similar results for all operating points.

Some salient features of the dynamic behavior of the engine in the different operating points are observed in Figure 4.8. The gain differences between different operating points are of a full order of magnitude and are present for all input and output combinations. On the other hand, the variations in phase between the different operating points are remarkably small; apart from some large variations which are discussed separately.

The FRFs of the VGT are of similar magnitude as the FRFs of the EGR for all outputs. This means that coupling is present between all inputs and outputs.

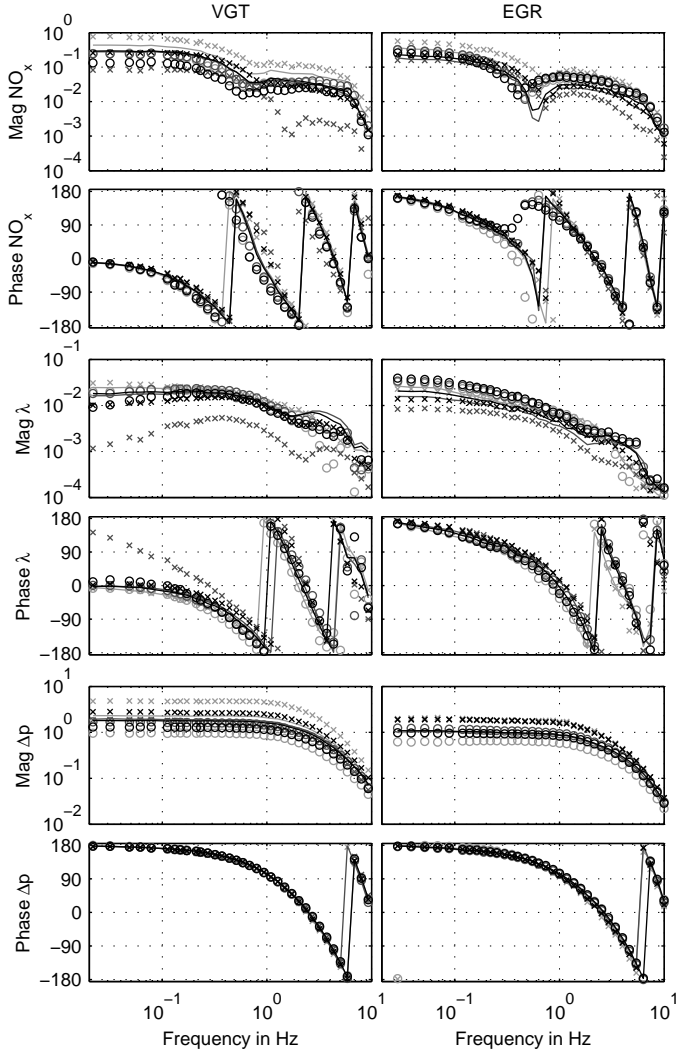


Figure 4.8: A Bode plot of the FRF of the engine measured in different operating points. Different engine speeds, ω , are plotted in different colors: light gray $\omega = 1011$ RPM; black $\omega = 1455$ RPM; dark gray $\omega = 1700$ RPM. Different symbols are used for different output torques, τ , that are obtained by varying the fuel input: 'o' denotes 60 mg/inj ; solid line denotes 120 mg/inj ; 'x' denotes 200 mg/inj .

For control design this means that MIMO design techniques are required to obtain the best performance.

In the phase plot of the VGT- λ FRF, a low frequency sign change is observed at 1700 rpm and 200 mg/inj. This potentially induces difficulties for feedback control design. In Wahlström (2009), the gain differences, coupling and sign changes are also observed, using a mean-value model of a different engine with a similar layout.

The anti-resonance found in the EGR-NO_x FRF changes between minimum and non-minimum phase. A closer analysis of the individual sensor data of the NO_x sensor and air-flow sensor explains this behavior and has shown that this anti-resonance is caused by the interaction of different sensor dynamics and is not a physical property of the engine dynamics.

The FRF measurements indicate that sensor dynamics form a significant part of the dynamic input-output behavior. In the phase plots in Figure 4.8, the delay in the response of the system can be observed. In particular for the NO_x measurement, delay has a significant influence on the phase of the FRF. For frequencies over 0.3 Hz, the phase lag due to delay largely determines the phase of the FRF. Moreover, the observed time scales are different for each output, which could also be observed in Figure 4.7. The NO_x response contains less power at high frequencies (over 1 Hz) than the Δp response. Both the delay and observed difference in time scales indicate the influence of sensor dynamics.

It should be noted that the results on the 3x3 speed-load grid are only intended to assess the global properties of the engine in a qualitative manner. Only at the selected operating points, the accuracy is comparable with the results of Table 4.1. To model the engine behavior in between the grid points, interpolation can be used, but the prediction accuracy will depend much more on the nonlinearity of the engine behavior than on the accuracy with which the local behavior at the grid points was captured.

For control applications, a different grid can be selected. The most suitable grid size depends on the type of controller. Some examples are found in literature: the controller in Ortner and Del Re (2007) uses 12 grid points and Ferreau et al. (2007) uses only two grid points. In Henningsson et al. (2012), the engine behavior is modeled only at 1200 RPM and up to mid-load. It is shown that when 4 or 6 grid points in this small range are selected, 10 % or 5 % accuracy is lost, respectively.

4.6 Discussion

The presented non-parametric modeling approach shows a high accuracy and is efficient in terms of the required measurement time, when applied to the diesel engine air path. The intended use of the FRF models is air-path feedback control design. For this purpose, the dynamic input-output response around an operating point is important. Feed-forward controllers, that bring the engine operating conditions close to the nominal conditions, are assumed to be present in the engine control system. In this case, the identified local models provide a relevant description of the dynamic behavior. Under these conditions, the identification accuracy is very high. From the results in Table 4.1, it can be deduced that the Variance Accounted For (VAF) is at least 97.2% for the considered outputs. This value can be compared with alternatives found in the literature. In Henningsson et al. (2012), a VAF between 64.3% and 93.5% is obtained. The LPV model used in Wei and Del Re (2007) obtains a VAF of 85%. The achieved accuracy with the proposed modeling approach exceeds the accuracy of alternative methods. However, for applications other than control design and analysis, the usability of the presented FRF models is limited.

The identification accuracy, as shown in this chapter, largely depends on the linearity of the input-output response. Although the local behavior (i.e. the behavior around a fixed state) of a nonlinear system is often close to linear, this is not necessarily true for a relevant input range. This dependency gives rise to a concern when different inputs or outputs are selected. Moreover, when different outputs are chosen, the noise characteristics will differ, which influences the identification accuracy. This is why it is critical that the model accuracy can be quantified, as is done in Section 4.4, and it is revealed to what extent the identified linear system description is accurate.

For accurately modeling or simulating large operating-point variations, or for modeling input variations spanning the full actuator range, the presented methodology is not well-suited. It can be expected that the analysis for nonlinearities will show that linear models no longer relevantly describe the engine behavior and the model quality will degrade. In Figure 4.7, it can be observed that the model accuracy decreases at output peaks. Modeling the engine behavior for conditions that significantly deviate from nominal is outside the scope of this article. Models that

describe this behavior accurately have to be nonlinear, e.g., mean-value models are much more valuable for this.

Despite these disadvantages, the FRF models have numerous advantages related to control design. The FRF representation used in this article is suitable to describe systems for which linear dynamics are dominant and is fit to work with broadband multisine identification. Also, classical (PID) controllers can be designed directly in the frequency domain using FRF models, which is done for air-path control in Criens et al. (2014). Moreover, the FRF models can provide strong analysis results, e.g., for decoupling control design or can be used to analyze the dynamic properties achieved with various controllers. For simulation or integration with model-based control synthesis, e.g., Linear Quadratic Gaussian (LQG) optimal control or MPC, a state-space or transfer-function representation is necessary. Software tools are available to convert the measurement data into a transfer function. The `n4sid` algorithm of the System Identification Toolbox in MATLAB[®], as applied in Henningsson et al. (2012), can be used for this. The BLA can be approximated with arbitrary accuracy by increasing the approximation order. Depending on the application, a suitable system order should be selected. In Henningsson et al. (2012), a model order of 7 is proposed and it is shown that model orders below 5 lead to a poor prediction, whereas in Wei and Del Re (2007) a model of order 3 is used to facilitate quasi-LPV control design.

4.7 Conclusions

Multisine identification is successfully used as an efficient method for determining the local dynamic behavior of a diesel engine air path, using the VGT and EGR valve as inputs. An accurate non-parametric model of the linear MIMO behavior of the engine, in the form of an FRF, is identified using ten minutes of measurement data. The FRF provides a control-relevant description of the local input-output behavior at a single operating point, naturally including sensor and actuator dynamics. The considered outputs are NO_x, air-fuel equivalence ratio and pressure difference between intake and exhaust manifold. In particular NO_x emissions are difficult to model using first-principles models, but straightforward to include using FRFs.

Quantifying the influences of noise and nonlinearities on the FRF measurement is an essential part of the presented identification method. The nonlinear part of the engine behavior is quantified and classified and the ability of linear models to describe the encountered behavior is quantified. It was discovered that the influence of nonlinear behavior is an order of magnitude smaller than the magnitude of the linear behavior. This means that linear dynamics largely determine the local engine behavior and linear techniques are relevant for system analysis and control design. It is shown that, using a linear FRF model, validation data can be reproduced with errors below 2.8%. The remaining error is largely caused by the lack of a description of the nonlinear behavior.

To characterize the global behavior of the engine, multisine identification was used to identify FRFs for a range of engine operating points. The behavior varies significantly as a function of the operating point: gain differences of a full order of magnitude, sign changes and large phase variations are captured using FRF identification.

5 Control for Disturbance Rejection, Low Emissions and High Fuel Efficiency

5.1 Introduction

With the recent introduction of EURO VI, not-to-exceed and on-road emission limits are introduced. These limits restrict the exhaust emissions of diesel engines under diverse and uncertain conditions. The WNTe and in-service emissions are affected by the uncertain drive cycle. The in-service emissions are also affected by external factors, e.g., ambient temperature, ambient pressure, humidity and fuel quality, and also internal factors, e.g., ageing, engine wear, production tolerances, engine temperature and actuator hysteresis. These uncertain factors make the measured emissions over these two tests less predictable and reproducible.

To comply with the new legislation, despite the uncertain factors, two approaches are possible. Either, additional margins between the nominal exhaust emissions and the legislation limits are introduced, such that the worst case scenario still complies with the emission legislation. Or, adaptations of the engine settings should be made, such that the engine adapts to the unknown conditions to ensure that the exhaust emissions always remain close to the nominal levels that are known to comply with legislation. The former option may seem beneficial for the environment, because the nominal pollutant emissions are reduced. But, as a result of the tradeoff between emissions and fuel efficiency, a fuel penalty is involved with reducing the engine-out emissions. This increases the operational costs and the increased CO₂ emissions and use of hydrocarbons have a negative environmental effect. Moreover, the emission limits set in EURO VI require drastic reductions of the tailpipe NO_x and PM exhaust emissions, compared with EURO V and are very challenging. This makes reducing the emissions beyond these limits

practically unacceptable. Consequently, a control strategy is needed to ensure that the achieved exhaust emissions remain close to the nominal exhaust emissions despite the influences of uncertain factors.

In this chapter, the design of an air-path control system for disturbance rejection in diesel engines is elaborated. First, the control problem is described in more detail. Next, a conceptual control design for disturbance rejection is presented and tested in simulation. Based on this conceptual design, but adapted for the current engine hardware, a second controller is designed. This controller is implemented on prototype control hardware and experimentally tested and evaluated on a modern engine.

5.2 Control Problem

The high-level goals of the engine control system in a heavy-duty diesel engine are to provide the requested amount of torque with minimum fuel consumption, while complying with emission legislation and remaining within safety and durability limits.

In this chapter, only disturbance compensation is considered. It is assumed that the operating point is quasi-stationary, such that all control aspects related to speed and load dynamics can be disregarded. Second, optimal input setting that achieve the above high-level control goal at the current stationary operating point under nominal conditions are assumed to be a priori available. When the engine behavior or the external conditions deviate from nominal, the nominal, optimal input settings should be adapted to maintain optimal performance. The aim of this chapter is to design a control algorithm that achieves this.

To minimize the fuel consumption within the emission constraints defined in legislation, a complex tradeoff between the allowed engine-out emissions and fuel efficiency is made. The emissions and fuel efficiency vary over the engine speed and load range, such that the expected in-service fuel consumption is minimized. When the nominal actuator settings are used as determined during calibration, while disturbances are present, the engine-out emissions and fuel consumption will

deviate. Unless the aftertreatment system is able to counterbalance this, compliance with legislation is no longer guaranteed. Also, an increased fuel consumption might be observed. In consequence, the high-level goals are no longer achieved.

In this chapter, a controller is designed to improve on the above situation. The high-level control goals are, however, not very suitable to be used directly in a control design. Compliance with emission legislation is determined over a cycle and cannot be determined unambiguously from measurements at a single point in time. Similarly, the fuel consumption should be evaluated over a full and realistic drive cycle, rather than instantaneously. These are unfortunate properties, as it is difficult to determine whether additional control actions are needed and also to evaluate if the current emissions and fuel consumption are optimal. Therefore, rather than aiming directly for minimum fuel consumption while achieving compliance with emission legislation, a goal that is better suited for control design is formulated:

Maintain the BSFC, NO_x emissions and PM emissions at all times as close as possible to the values obtained under nominal conditions.

After calibrating the engine, the nominal values for the BSFC, NO_x and PM will be such that a simultaneous reduction of all three aspects is not possible. Any known possibility for reducing all three performance aspects simultaneously, that does not require violating a constraint, will be exploited in the calibration process. The BSFC, NO_x and PM after calibration therefore form a Pareto optimal point. This implies that functional controllability of these three outputs is not possible. Moreover, it is likely that the exact same values for BSFC, NO_x and PM that are obtained under nominal conditions are either no longer reachable or no longer optimal, when disturbances are present. For this reason, rather than aiming for exact tracking, the goal is to remain as close as possible to the performance measures.

Disturbance rejection in this form offers the following three potential advantages.

- **Reduced variation** of the engine-out emissions and fuel consumption. This provides an opportunity to reduce the margins needed to ensure compliance with the in-service conformity legislation.

- **Reduced average emissions** as a result of preventing excessively high emissions. As a result of the exponential increase of NO_x with temperature, the increase in NO_x due to disturbances will be larger than the decrease in NO_x . Consequently, the average NO_x will increase due to uncertainties. Similarly, the PM emissions increase rapidly when the air-fuel equivalence ratios approaches unity, whereas they become relatively insensitive to increases towards higher air-fuel equivalence ratios. Disturbance rejection can therefore decrease the average NO_x and PM emissions.
- **Reduced fuel consumption** through improved calibration. As a result of both the reduced variation of the emissions and the reduced average emissions, the nominal emission levels can be allowed to increase. In consequence of the tradeoff between the emissions and fuel consumption, this provides an opportunity to reduce the fuel consumption at the expense of an increase in the nominal emissions.

The goal of this chapter is to design a controller that combines all three advantages.

An important design specification of a feedback control design is the bandwidth¹. To determine an appropriate value, the conditions where the feedback controller is used are analyzed. Several disturbances or uncertainties that potentially affect the emissions and fuel consumption are present, when a diesel engine is used in a commercial vehicle. External factors such as the ambient temperature, ambient pressure, humidity and fuel quality, and also internal factors, such as ageing, engine wear, production tolerances and engine temperature can be considered. A similarity between these disturbances is that the typical time scale on which they act is several minutes, hours or more. The target bandwidth for the feedback controller is however much faster than the time scale of the disturbances. Speed and load variations that occur in a typical drive cycle of a diesel engine have to be taken into account. The time scale associated with these speed and load variations is of the order of several seconds. In a typical control layout, feed-forward control schemes are used to accommodate these operating point variations. Nonetheless, the feedback controller should readapt the inputs after the operating point has

¹In this thesis, bandwidth is defined as the frequency up to which the magnitude of the highest singular value of the sensitivity is below 0 dB.

changed to maintain the desired disturbance rejection. Therefore, a target bandwidth of 0.2 Hz will be used. Results in the literature such as Stewart et al. (2010); Wahlström and Eriksson (2008); Alfieri (2009); Stefanopoulou et al. (2000) indicate that similar values for the bandwidth are used. A much faster bandwidth will interfere with the operating point transients; a much slower bandwidth will result in a poor tracking performance with dynamic drive cycles.

5.3 Conceptual Design

A feedback controller uses sensor measurements, a control algorithm and actuators to influence the behavior of the system. For the studied engine control problem, the choice for all three parts is nontrivial. This section motivates the choices for all three parts.

5.3.1 Actuators

The main actuators in a heavy-duty diesel engine that affect the NO_x and PM emissions and fuel efficiency are the Variable Geometry Turbine (VGT), Exhaust Gas Recirculation (EGR) valve and Start Of Injection (SOI)². To be the least conservative and have the best performance potential, generally all three available actuators should be used in the control design. However, to successfully employ an actuator in a feedback controller, sensors are equally important as actuators. For this reason the use of the SOI as an actuator is reconsidered.

The SOI can have a large effect on the engine-out emissions and fuel efficiency of a diesel engine (Guzzella and Amstutz, 1998; Brahma, 2005). Also, its fast, almost instant, dynamic response makes the SOI convenient for closed-loop control. However, sensors to measure the effects of the SOI are lacking in heavy-duty production engines, which hinders the usability of the SOI in a feedback loop. The

²Other actuators can be considered as well. A variable swirl valve or variable valve actuation can be available on some engines, but these are not available on the considered engine type. A back-pressure valve or intake throttle can be used on heavy-duty engines, but because additional throttling of the air flow has a detrimental effect on fuel efficiency, they are only used when necessary and fully opened otherwise. The rail pressure in the fuel path can also be used as an actuator. However, to simultaneously minimize the engine-out NO_x and PM emissions, the rail pressure is typically set as high as possible. This makes these actuators not very suitable for feedback control

effect of the SOI on the engine-out NO_x emissions is measured by means of a NO_x sensor, but sensors to determine the effects of the SOI on the PM emissions and fuel efficiency are not available currently. The use of equipment for measuring PM emissions or smoke (as used in Karlsson et al. (2010) and Tschanz et al. (2013)) is limited to research engines and is not available in production yet. Also, in-cylinder pressure sensors³ (as used in Karlsson et al. (2010) and Zhao et al. (2013)) or torque sensors to measure the effects of the SOI on the fuel efficiency are not available on current heavy-duty production engines. Such sensors would be required to benefit from using SOI in a feedback loop. The combustion timing is directly affected by the SOI and both early and late combustion have a detrimental impact on the fuel efficiency. Moreover, late combustion timing increases the PM emissions. When the SOI is adapted based on the measured NO_x emissions only, a simultaneous effect on the BSFC and PM emissions will be present, but this effect will not be measured by the engine sensors. Both the BSFC and the PM emissions will increase, when NO_x is reduced via the SOI. Without the proper sensors, it cannot be determined if the achieved change in NO_x outweighs the increase in PM and BSFC. And similarly if this adaptation of the SOI brings the engine performance closer to a desired situation, when all three performance measures are taken into consideration. The SOI is therefore not used as an actuator for feedback control. This reduces the available feedback actuators to the VGT and EGR valve:

$$\mathbf{u}_{\text{fb}} = \begin{bmatrix} u_{\text{fb,VGT}} & u_{\text{fb,EGR}} \end{bmatrix}^{\text{T}}. \quad (5.1)$$

Limiting the actuators used for feedback control to the VGT and EGR valve does not change that the PM emissions and BSFC cannot be measured directly. However, because the VGT and EGR valve act on the air path, measurements in the air path can be used to substitute direct PM and torque measurements, which is elaborated in Section 5.3.2. This enables a control design that takes all three performance aspects into account, despite the shortcomings of the available sensors. Similar substitutions to measure the effects of the SOI are not available.

³When in-cylinder pressure sensors are available, the control problem changes considerably. These sensors are well suited to be combined in a feedback loop with the actuators in the fuel path and provide various opportunities for combustion control. This is briefly discussed in Section 7.2.1.2. The difference in time scales that exists between the air path and fuel path likely still allows for a separate control design, without inducing a significant performance penalty.

5.3.2 Controlled Outputs

To make feedback control most effective, the controlled outputs are chosen to reflect the main performance measures: NO_x emissions, PM emissions and fuel efficiency, as directly as possible. For each performance measure, a relevant output is selected.

To quantify the engine-out NO_x emissions and PM emissions, direct measurements are used in this conceptual design. It is known that the NO_x sensor used on production diesel engines suffers from sensor dynamics, which complicates its use in feedback control systems. Moreover, on current production engines, PM measurements are not available. For this conceptual design, these shortcomings are overlooked. The engine-out NO_x and PM emissions are assumed to be measured accurately and instantaneously.

Taking into account the BSFC is more complex than the emissions. The BSFC at a certain operating point is affected by several factors; the air path, the fuel path, external disturbances and internal uncertainties all affect the fuel efficiency. It is not desirable that the VGT and EGR valve compensate for all contributing factors. Consider an example case where the friction losses increase compared with the nominal situation. Using the VGT and EGR valve, the friction cannot be influenced. But the increased BSFC can be compensated for by increasing the air-fuel ratio, decreasing the EGR flow and decreasing the pumping work. When these compensations are applied, the BSFC will decrease, but the in-cylinder conditions will deviate more from the nominal conditions than when they are not applied. This will compromise the performance elsewhere. It is therefore not an effective method for disturbance rejection; an alternative measure for fuel efficiency should be used.

The air-path affects the BSFC in two ways. First via IMEP_g and second via PMEP. IMEP_g is affected by the in-cylinder air mixture. This mixture though is largely determined to obtain low engine-out NO_x and PM emissions, rather than to maximize IMEP_g . The NO_x and PM emissions are already selected as controlled outputs and via control of these emissions the intake mixture will be adapted to have the desired composition with respect to these outputs. The remaining effect of disturbances in the air path on IMEP_g can be expected to be small and moreover necessary to maintain the emissions at the desired level.

Therefore, PMEP is the relevant measure to determine the effect of the air path on the BSFC. Controlling PMEP decreases the effect of disturbances on the BSFC and prevents that control actions to correct for NO_x and PM deviations result in excessive pumping losses. The PMEP is controlled via the pumping torque, which is available in the simulation model.

The selected controlled outputs are therefore:

$$\mathbf{y}_{\text{fb,c}} = \begin{bmatrix} y_{\text{NO}_x} & y_{\text{PM}} & y_{\tau_{\text{pump}}} \end{bmatrix}^{\text{T}} \quad (5.2)$$

Controlling these outputs corrects for all disturbances in NO_x , all disturbances in PM and the main effect of the air path on the BSFC.

5.3.3 Input-Output Controllability

With three outputs and only two inputs, the control problem is underactuated. Functional controllability can therefore not be obtained. It must be noted though that even with additional actuators, functional controllability will be very difficult to achieve. The controlled outputs BSFC, NO_x emissions and PM emissions will under nominal conditions be chosen at a Pareto optimal point. Therefore, even when additional actuators are taken into consideration, an ill-conditioned control problem will be constituted. The static input-output gain matrix will at most have two directions with a nontrivial gain. Using only two actuators will therefore not significantly hamper the achieved feedback performance. Section 5.4.2 further investigates the input-output controllability properties using measured system data.

5.3.4 Control Design

This section briefly addresses the control design. The control design is very similar to the controller in the upcoming Section 5.4.3, where the design procedure is elaborated in more detail. Further details can be also found in Criens et al. (2013b), where the current control design was originally published.

The system to be controlled can be characterised as Multi-Input Multi-Output (MIMO) and underactuated. To control this system, first a part of the system is separated that is square and does have a full-rank static gain matrix. This leaves

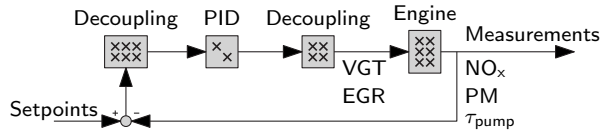


Figure 5.1: A high-level block scheme of the feedback controller.

a Two-Input Two-Output (TITO) system. For this TITO system, a multivariable feedback controller is designed. A high-level block scheme of this control layout is shown in Figure 5.1.

By converting the three-output system to a two-output system, the output direction where the inputs have no gain is separated. In this direction it is physically not possible to apply feedback control. Hence feedback control and disturbance rejection are not applied in this direction.

The multivariable feedback controller combines static SVD-decoupling with two Single-Input Single-Output (SISO) Proportional Integral Derivative (PID) controllers. The PID controllers are designed using sequential loop shaping. By combining PID control with static decoupling, a directly implementable and tuneable control design is made that combines a low implementation effort with low computational requirements.

5.3.5 Simulation Result

A selection of the results presented in Criens et al. (2013b) is shown here. The main purpose of the feedback controller is to maintain the performance of the diesel engine close to nominal when disturbances are present. This is tested using a model of a diesel engine and artificial disturbances.

The model used in the simulations is a mean-value model developed by TNO Automotive (Seykens, 2009). Mean-value models use lumped volumes to describe the dynamics in the air path of the engine. Moreover, the effects of the reciprocating behavior of the engine on the air and exhaust flows are removed by averaging. The model describes a six-cylinder 12.9 liter US2010-type engine equipped with a VGT and EGR valve. This engine type is similar to the studied EURO VI engines. The model predicts the flows, pressures, temperatures and compositions in the air path

and, through these parameters, also the fuel efficiency and engine-out emissions of NO_x and PM. The six-state engine model is described by the differential equations:

$$\dot{\mathbf{x}} = \mathbf{f}(\mathbf{x}, \mathbf{u}_{\text{fb}}, \mathbf{w}), \quad (5.3)$$

$$\mathbf{y}_{\text{fb,c}} = \mathbf{g}(\mathbf{x}, \mathbf{u}_{\text{fb}}, \mathbf{w}), \quad (5.4)$$

with states:

$$\mathbf{x} = \begin{bmatrix} p_{\text{im}} & m_{\text{air,fresh}} & m_{\text{inert}} & p_{\text{em}} & T_{\text{em}} & \omega_{\text{turb}} \end{bmatrix}^{\text{T}}, \quad (5.5)$$

external inputs:

$$\mathbf{w} = \begin{bmatrix} m_{\text{fuel}} & \omega_e & T_{\text{amb}} & p_{\text{amb}} \end{bmatrix}^{\text{T}}, \quad (5.6)$$

and inputs and outputs according to Equations (5.1) and (5.2), respectively. The symbols for the states represent the intake manifold pressure, intake manifold fresh air mass, intake manifold inert air mass, exhaust manifold pressure, exhaust manifold temperature and turbine speed, respectively. The symbols for the external inputs represent the fuel mass per injection, engine speed, ambient temperature and ambient pressure, respectively.

The emission model consists of multi-variable nonlinear functions that are implemented in the form of lookup tables or mathematical formulas. The emission model is of the form:

$$y_{\text{NO}_x} = f_{\text{NO}_x}(\omega_e, \dot{m}_f, T_{\text{coolant}}, \dot{m}_{\text{exhaust}}, \lambda, X_{\text{EGR}}, T_{\text{im}}), \quad (5.7)$$

$$y_{\text{PM}} = f_{\text{PM}}(\omega_e, \dot{m}_f, T_{\text{coolant}}, p_{\text{im}}, \dot{m}_{\text{intake air}}, \lambda). \quad (5.8)$$

The required inputs to these functions are all derived from \mathbf{x} and \mathbf{w} . The symbols of the inputs for the NO_x and PM models represent the engine speed, fuel mass per injection, coolant temperature, exhaust mass flow, air-fuel equivalence ratio, EGR rate, intake manifold temperature, intake manifold pressure and intake air flow. The EGR rate that is used is defined as $X_{\text{EGR}} = \dot{m}_{\text{EGR}}/(\dot{m}_{\text{EGR}} + \dot{m}_{\text{intake air}})$, with \dot{m}_{EGR} the EGR mass flow.

The engine is simulated around a single speed and load operating point: 1375 RPM and 775 Nm. The resulting engine power is equivalent with the power needed for driving a 40 ton commercial vehicle on a flat road at 80 km/h. To maintain the desired load, the load is controlled via the injected fuel mass. Various

Table 5.1: The disturbances applied in the comparison simulation.

	Nominal	Deviation	Unit
Ambient temperature	300	15	K
Ambient pressure	$1.1 \cdot 10^5$	$5 \cdot 10^3$	Pa
Engine speed	1375	25	RPM
Engine torque	775	25	Nm
VGT	24.5	2	%
EGR valve	68.3	2	%

disturbances are applied to the model as listed in Table 5.1. Disturbances on the ambient conditions are applied to simulate driving under diverse conditions. Disturbances on the engine speed, engine torque, VGT setting and EGR settings are applied to act in place of production tolerances and aging. Combined, this simulates driving under various conditions using an engine that can deviate from nominal. All disturbances are applied as slowly varying sinusoidal disturbances with frequencies between 0.02 Hz and 0.03 Hz. The frequencies of the disturbances are chosen as non-rational multiples of each other. This results in a non-repetitive signal, where all possible combinations of disturbances are encountered over infinite time, although a finite simulation time of 3000 s is used.

This simulation is performed twice, while applying the exact same disturbances. In the first simulation, the input settings for nominal conditions are used and no disturbance compensation is applied. In the second simulation, the feedback controller designed in this section is implemented to adapt the VGT and EGR valve to compensate for the disturbances.

The NO_x emissions, PM emissions and fuel consumption according to the engine model are analyzed. Table 5.2 shows the average emissions and their average deviation from nominal (RMS error). Figure 5.2 depicts the results graphically in a phase plot.

Figure 5.2 shows the simulation results in three dimensions, with two-dimensional projections on the axes. It is observed that with feedback control enabled, the effect of disturbances is significantly reduced in all three directions.

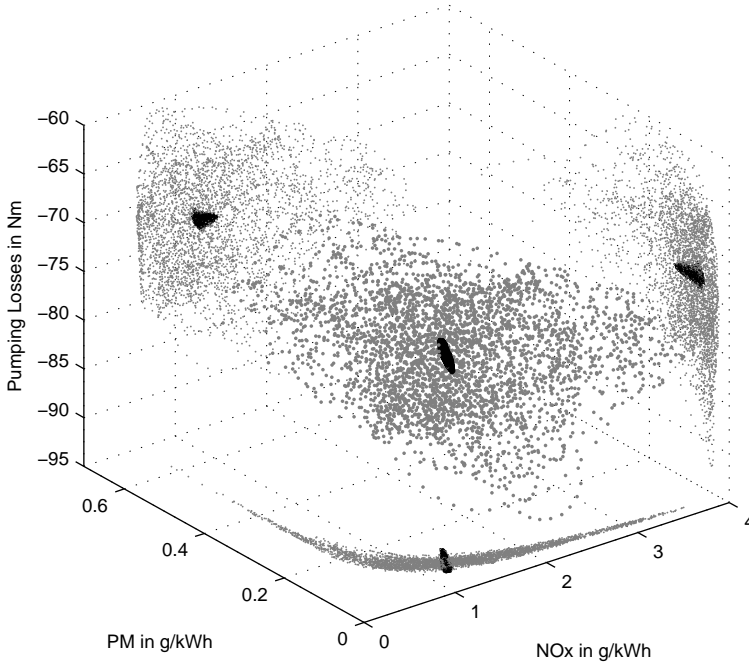


Figure 5.2: A comparison between feedback controlled (black) and open-loop controlled (gray) systems with disturbances according to Table 5.1. The large cloud in the center shows the simulation results in a three-dimensional phase plot. On the axes, smaller dots are used to project the results in two-dimensional phase plots.

Table 5.2: The effects of disturbance reduction by means of feedback control in simulation. The simulation data used to obtain these numbers is shown graphically in Figure 5.2.

	Nominal	Feedback control		Open-loop control	
		Mean	RMS error	Mean	RMS error
NO_x in g/kWh	1.3	1.304	0.05	1.464	0.695
PM in g/kWh	0.0927	0.094	0.016	0.112	0.081
Pumping in Nm	-73.56	-73.56	0.361	-74.16	5.12
BSFC in g/kWh	216.58	216.58	-	218.18	-

In Table 5.2, a comparison is made between three situations:

- **Nominal:** without disturbances
- **Feedback controlled:** with disturbances and using the feedback controller designed in this section, the black dots in Figure 5.2
- **Open-loop controlled:** with disturbances and using the nominal input values, the gray dots in Figure 5.2.

The direct goal of the feedback controller is to keep the difference between the nominal outputs and the actual outputs as small as possible. This is reflected in the RMS error, which becomes 12, 5 and 14 times smaller for NO_x , PM and pumping losses, respectively, when feedback control is applied. This shows that the controller is successful in counteracting disturbances in all three directions, even though the controlled system is underactuated, which reduces its performance potential.

Figure 5.2 shows why the two-dimensional controller achieves three-dimensional disturbance rejection. Using open-loop control only, the NO_x , PM and pumping losses do not form an evenly distributed three-dimensional cloud. Instead, all points remain in the vicinity of a two-dimensional curved surface in the three-dimensional space. The remaining error with the feedback controller enabled is largely perpendicular to this curved surface. The fact that the physical conditions for formation of NO_x and PM contradict explains that the disturbances form an approximate two-dimensional surface rather than a three-dimensional cloud. Because the uncontrolled direction is perpendicular to the curved surface, the remaining error is small in all three dimensions.

Table 5.2 also shows a comparison between the mean values in both the feedback controlled and open-loop controlled cases. In particular the emissions benefit from the use of feedback control; NO_x reduced by 14 %, PM reduced by 19 %. The pumping losses reduced as well by 0.82 %, but more importantly, the BSFC reduced by 0.74 %. When the feedback controller is used, the mean values obtained while disturbances are present are in fact very close to the nominal values. This implies that the feedback controller is successful at achieving near optimal performance.

From this simulation it is concluded that feedback control using the proposed inputs and outputs has a potential for:

- **Reduced NO_x and PM emissions**
- **Reduced fuel consumption**
- **Reduced effects of disturbances.**

These results demonstrate the performance potential of the controller concept in simulation. However, using the sensor selection of the conceptual design, an implementation on a production type engine is not possible. The required modifications for a physical implementation are discussed in Section 5.4

5.4 Experimental Design

Based on the conceptual design of Section 5.3, a modified controller is made. The controller is intended to be used for disturbance rejection around a fixed operating point. For the experiments, 1455 RPM, 1050 Nm is chosen as the nominal operating point. The new control design will feature a similar underactuated control design and will use the same actuators. The selection of controlled outputs is reconsidered, such that only sensors available on production engines are used. This modified controller is designed, analyzed and tested on a EURO VI engine mounted on a dynamometer test setup.

5.4.1 Selection of Controlled Outputs

The controlled outputs in the conceptual controller were chosen to directly reflect the main performance measures: NO_x emissions, PM emissions and BSFC. For the modified control design, available outputs are selected that reflect the original outputs as closely as possible.

Using a NO_x sensor for emission feedback control seems an obvious choice. However, due to the slow dynamic response of the sensor, or unavailability on some production engines, the NO_x sensor is sometimes dismissed as a suitable feedback signal (Waschl et al., 2012; Wahlstrom and Eriksson, 2013). On the engine used in this thesis, a production-type NO_x sensor is available. The NO_x

sensor is located downstream of the turbine and measures the engine-out NO_x concentration in parts per million (ppm). The dynamic response of the NO_x sensor is a significant concern for feedback control. The dynamic sensor response can be approximated by a time delay, combined with first-order low-pass dynamics (Mrosek et al., 2011; Alfieri, 2009). In Alfieri (2009), a time delay of 0.3 s and low-pass time constant between 0.9 s and 1.5 s are reported. A comparison between the Frequency Response Functions (FRFs) of the NO_x output and those of fast sensor measurements, e.g., pressure measurements, indicates that the NO_x sensor dynamics of the test engine are similar to those found in Alfieri (2009). When compared with the dynamics of the air path, indeed, the NO_x sensor dynamics are significant. Also, when compared with the intended closed-loop control bandwidth of about 0.2 Hz (see Section 5.2), the NO_x sensor dynamics cannot be disregarded. However, as will be shown, obtaining the desired transient feedback performance is possible, despite the slow dynamic sensor response. The benefits of using a NO_x sensor for emission feedback control are significant. Indirect indicators for NO_x , such as the EGR fraction, are less accurate for quantifying the actual NO_x emissions.

The NO_x sensor can be combined with an observer to reduce the effects of the sensor dynamics as is done in Körfer et al. (2008) and Tschanz et al. (2013). To incorporate an observer in the control structure, a reliable model of the NO_x emissions is needed. The design effort for the observer and identification effort for such a model would significantly increase the overall control design effort. Because the observer is not strictly necessary to obtain a sufficiently fast closed-loop response, as is found in Section 5.4.3 and 5.4.4, its use is dismissed and the NO_x sensor data is used directly.

A PM sensor is not available yet on current production engines. But it is known that the PM emissions are affected directly by the air-fuel equivalence ratio, λ . To measure λ , a λ -sensor is available, which provides an estimate of λ based on the exhaust oxygen concentration. The value of λ obtained via the λ -sensor shows the desired correlation with the PM emissions (obtained via an opacity sensor), when the VGT and EGR valve are varied. This is shown in Figure 5.3. The λ measurement is not representative for all aspects of PM formation. The effects of, e.g., engine speed, combustion timing or ambient humidity on the PM emissions are not accounted for. The VGT and EGR valve however mainly affect PM via λ .

Controlling λ compensates for disturbances on PM in the air path. Maintaining λ at the desired level is not only relevant for the PM emissions. The amount of excess oxygen in the exhaust is also a measure for the engine's ability to quickly respond to an increase in torque demand. Hence, control of λ is also relevant for maintaining a desired torque response.

In the conceptual design, the pumping losses were used to take into account the effects of the air path on the fuel efficiency. The pumping losses are the work transfer between the in-cylinder gases and the moving piston during the intake and exhaust stroke. This work transfer is not measured. The most direct alternative, the in-cylinder pressure, is also not available as a measurement. The pumping work can be estimated though. When it is assumed that during the intake stroke the in-cylinder pressure matches the intake manifold pressure, and similarly that during the exhaust stroke in-cylinder pressure matches the exhaust manifold pressure, an estimate for the pumping work can be made using available sensors. Pressure sensors in the intake and exhaust manifold are available on production engines. Using these sensors and the above assumptions, the torque loss due to pumping can be estimated by:

$$\tau_p = \frac{V_e}{4\pi} \Delta p, \quad (5.9)$$

where V_e is the engine displacement volume, $\Delta p = p_{ex} - p_{in}$, with p_{ex} and p_{in} the pressure in the intake and exhaust manifold, respectively. A direct and linear relation between the pumping losses and the pressure difference between the intake and exhaust manifold, Δp , exists in Equation (5.9). To quantify the effect of the VGT and EGR valve on the fuel efficiency, Δp will therefore be used. The output Δp (and also the pumping losses) is not a direct measure for the BSFC, but it does largely reflect the effect of air path on the BSFC.

To summarise the above text, the selected outputs are:

$$\mathbf{y} = \begin{bmatrix} y_{NO_x} & y_\lambda & y_{\Delta p} \end{bmatrix}^T. \quad (5.10)$$

With these outputs, the effects of air path on the three performance measures are accounted for. To verify if the relations between the measured outputs and the actual performance measures exist, an experiment is conducted. For this, the closed-loop controlled system to be designed later on in this section is used. The

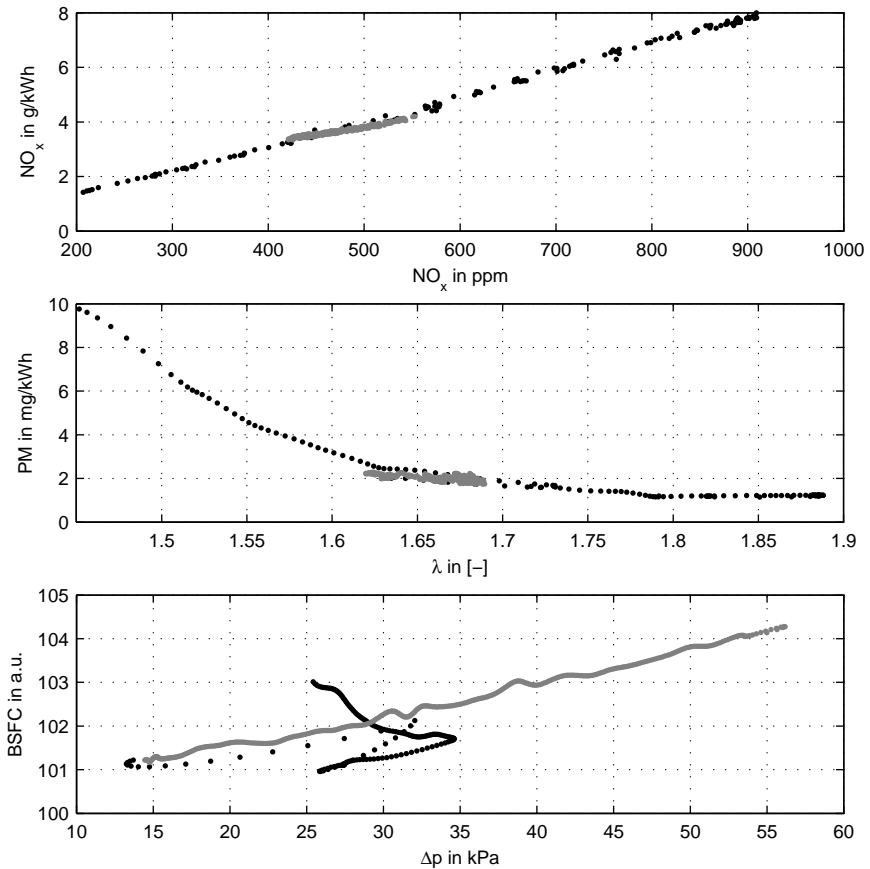


Figure 5.3: The relation between the measured outputs and the actual performance indicators. The engine speed and fuel injection during the experiment were fixed at 1455 RPM and 120 mg/inj. The BSFC is converted into arbitrary units for de-identification purposes. For this, the BSFC is multiplied with a constant, such that $\Delta p = 0$ kPa would correspond with a BSFC of 100 a.u. using a linear extrapolation of the data in gray. The black dots in the above three plots all originate from the same time-domain data sequence, and similarly for the gray dots.

setpoints for the measured outputs are manually varied while maintaining the engine speed and fuel flow constant at 1455 RPM and 120 mg/inj. The feedback controller then adapts the VGT and EGR valve in accordance with the setpoint changes, which changes the performance tradeoff. For this experiment, the sensors of the dynamometer setup were used to determine the NO_x emissions, PM emissions and BSFC. The engine sensors were used to measure the selected outputs.

Figure 5.3 shows the results of the experiment. Two data series are shown in the plots. In the black series, the variation is mostly in NO_x and λ . Here, a 538% and 696% difference between the lowest and highest value of NO_x and PM is observed, respectively. The resulting change in Δp and BSFC is relatively small, compared with the gray data series. In the gray data series, the variation is mostly in the Δp setpoint. Here, a significant variation in BSFC is observed, with relatively small changes in NO_x and PM, compared with the black data series. This shows that Δp has a significant effect on BSFC. In addition, it indicates that even large variations of the emissions as a result of changing in-cylinder conditions have a, by comparison, small effect on the BSFC. This indicates that for the considered actuators, the effect of PMEP on the BSFC is stronger than the effect of IMEP_g. The PM graph and NO_x graph also show the expected relations between the controlled outputs and the high-level performance measures. The intended relations between the controlled outputs and the performance measures are all present, which indicates that the selected outputs are indeed relevant.

The experiment of Figure 5.3 is only a partial validation of the intended relations. With only two actuators, neither the three controlled outputs, nor the three high-level objectives can be varied independently. Cross-correlations will therefore affect the results of the experiment. Moreover, it is known from theory (see Chapter 2) that the selected controlled outputs are only partially representative for the high-level objectives. For example, the start of combustion is known to affect the NO_x, PM and BSFC; and this effect will not be noticeable in the λ and Δp output. Also, when the EGR rate changes, and somehow λ and Δp maintain constant, the PM emissions and BSFC will change. These effects are not captured by the selected outputs.

The important step of modeling the input-output behavior is covered in Chapter 4. This section uses the results of Chapter 4 and continues with analyzing the resulting control problem, control design and experimental validation.

5.4.2 Input-Output Analysis

With only two inputs (VGT and EGR valve) to control three outputs (NO_x , λ , Δp), exact tracking of all outputs and, therefore, functional controllability (Skogestad and Postlethwaite, 2007) cannot be achieved. Instead, the feedback controller is intended to maintain the setpoint values as close as possible to the three outputs, using the two available actuators. The nominal input settings are chosen to result in Pareto optimal outputs under nominal stationary conditions. Keeping the outputs close to the nominal outputs therefore implies the performance is close to optimal. Due to the lack of actuators, only the two-dimensional subspace in which the VGT and EGR valve have control authority is of interest for control design. In this section, the input-output controllability properties of the two directions in which the VGT and EGR valve have a stationary gain are investigated. The third direction, where the actuators have no gain will necessarily remain uncontrolled.

As an alternative to the proposed three-output control problem, a two-output emission control problem, using only NO_x and λ as outputs, is considered in this section. This control problem is not underactuated and perfect tracking of NO_x and λ can be aimed for. This should result in a reduced spread of the engine-out emissions. Because Δp is no longer controlled, the fuel efficiency is not taken into account. The system dynamics of the two-output system are denoted $\mathbf{G}_2(s)$, whereas in this section the three-output system is denoted $\mathbf{G}_3(s)$, with s the Laplace operator. The addition of (s) is omitted in the remainder of this section for notational convenience.

To make the system outputs comparable for analysis, output scaling is applied:

$$\hat{\mathbf{y}}_i = \mathbf{S}_i \mathbf{G}_i \mathbf{u}_{\text{fb}} = \hat{\mathbf{G}}_i \mathbf{u}_{\text{fb}}, \quad (5.11)$$

where \mathbf{S}_i is the diagonal scaling matrix for system \mathbf{G}_i , the scaled system is denoted $\hat{\mathbf{G}}_i$ and the scaled outputs $\hat{\mathbf{y}}_i$, the subscript $i \in \{2, 3\}$ distinguishes between the two and three output system. The scaled static system gain is $\hat{\mathbf{G}}_{\text{ss},i} = \hat{\mathbf{G}}_i(s = j\omega = 0)$, where ω represent the frequency. Figure 5.4 visualizes the scaled static system gain for the two considered output combinations at mid speed and mid load.

Including Δp as a third control output improves both the robustness of the performance and the robustness of the closed-loop stability. These effects are discussed in the remainder of this section.

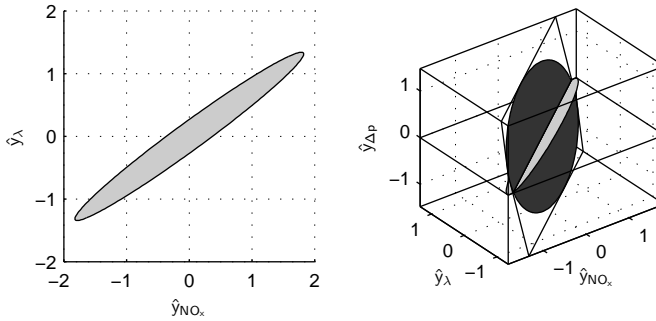


Figure 5.4: The scaled steady-state response to unit-size inputs. Two output configurations are used. The operating point is 1455 RPM and 120 mg/inj. The plots show: $\hat{\mathbf{y}}_i = \hat{\mathbf{G}}_{ss,i} \mathbf{u}_{fb}$, $\forall \|\mathbf{u}_{fb}\|_2 = 1$, for two different systems \mathbf{G}_i . On the left, the two-output emission system $\hat{\mathbf{G}}_{ss,2}$ is shown. On the right, this two-output system (light gray) is compared with the three-output system $\hat{\mathbf{G}}_{ss,3}$ (dark gray).

The BSFC is considered a fundamental part of the engine performance. Maintaining Δp close to its nominal value by means of feedback control keeps its effect on the BSFC small. This improves the robustness of the BSFC and consequently also of the engine performance. In the two-output system, where Δp is not controlled, the actions of the VGT and EGR valve to control NO_x and λ will also affect the Δp . This induces an additional disturbance on Δp and hence also on the BSFC. Including Δp as a control output therefore improves the robustness of the engine performance.

The reasoning for improved closed-loop stability, when Δp is included, is more technical. Its effect on stability can be quantified using the condition number of the scaled static-gain matrix. The condition number of the static gain matrix is an important characteristic for MIMO control. It is the ratio between the gains of the most sensitive and least sensitive input-output direction. Ideally, the condition number is close to one. A condition number much larger than one indicates that the system is close to singular and has a small response in one direction.

The condition number of the scaled static gain matrix is shown in Table 5.3 for a range of operating points and for both output configurations. For $\hat{\mathbf{G}}_2$, the system response is naturally ill-conditioned around the nominal input settings. Seven out of the nine operating points considered in Table 5.3 have a condition number after

Table 5.3: The condition number, κ_i , of the scaled static gain matrix, for a range of operating points and for both considered output configurations.

ω_{eng} RPM	Fuel mg/inj	κ_2	κ_3
1011	60	22.35	3.39
1011	120	17.79	2.20
1011	200	73.36	1.98
1455	60	8.25	2.27
1455	120	10.24	1.69
1455	200	11.07	1.35
1700	60	11.59	1.87
1700	120	10.59	1.63
1700	200	4.31	2.20

scaling, κ_2 , larger than 10, with a maximum of $\kappa_2 = 73.4$. Including Δp as a third output reduces the condition number in all operating points. For the three-output system, eight out of nine points have a condition number, κ_3 , smaller than 2.3. The maximum condition number that is encountered for the three-output system is 3.39.

The static gain of $\hat{\mathbf{G}}_{\text{ss},2}$ and $\hat{\mathbf{G}}_{\text{ss},3}$ at 1455 rpm and 120 mg/inj is visualized in Figure 5.4. The narrow ellipsoid in the left graph of Figure 5.4 shows that the two-output system has a small response in one direction. The more round ellipsoid in the right graph of Figure 5.4 indicates that the three-output system has a similar responsiveness in all directions in the depicted plane. This shows graphically why the condition numbers between the two systems differ in magnitude. It is observed that the difference in the condition numbers is not due to an ill-chosen output scaling. The magnitude of the response is similar for all three outputs. Instead, the low gain in the direction of simultaneously decreasing NO_x and increasing λ is the reason for the high condition number.

The condition number directly affects the robust stability of the closed-loop. To analyze robust stability, the system uncertainty is modeled. The uncertainty is

modeled here as a norm-bounded additive uncertainty:

$$\hat{\mathbf{y}}_i = \left(\hat{\mathbf{G}}_i + \mathbf{\Delta}_i \right) \mathbf{u}_{\text{fb}}, \quad (5.12)$$

with $\hat{\mathbf{G}}_i$ the nominal dynamic response of the input-output system and the uncertainty $\|\mathbf{\Delta}_i\|_2 < \delta \|\hat{\mathbf{G}}_i\|_2$. The parameter δ bounds the uncertainty relative to the spectral norm of the system gain. The uncertainty is only norm-bounded, the direction of the uncertainty is not specified. An uncertainty of $\delta = 0.1$ is equivalent to an uncertainty of 10% of the nominal system response. This uncertainty model only roughly approximates the actual system uncertainty, but is useful to demonstrate the effect of conditioning on the closed-loop stability.

The closed-loop system is considered more robust against uncertainties if the allowed δ for which the system is closed-loop stable is larger. Without considering a specific control design, the condition number can be used to specify a maximum δ for which the uncertain system is input-output controllable. For $\delta \geq \frac{1}{\kappa}$, the static gain may become singular and its sign is uncertain. This means that the uncertain system is not robustly functionally controllable; even locally, closed-loop asymptotic stability, taking the system uncertainty into account, cannot be guaranteed by any linear controller.

The uncertainty due to measurement noise and nonlinear behavior was extensively analyzed at the nominal operating point in Chapter 4. Combining the individual effects of noise and nonlinear behavior on the FRF measurement, and of nonlinear behavior on the actual system response gives a standard deviation of $\sigma \approx 0.05$ of the system response at low frequencies, largely due to nonlinear effects. Uncertainty due to, e.g., aging, changing ambient conditions or production tolerances is not even taken into account here. When a 2σ uncertainty range is used, which is equivalent to 95% certainty that the actual system response is within the uncertainty bounds, this results in $\delta = 0.1$. Consequently, only systems with $\kappa < 10$ are robustly functionally controllable when the identification inaccuracy is taken into account.

The \mathbf{G}_2 system is not robustly functionally controllable in the largest part of the operating range, when the model uncertainty is taken into account. For the \mathbf{G}_3 system, which has a lower condition number, robust closed-loop asymptotic stability can be achieved in two directions for the entire operating range. Because

this system is underactuated, one direction will remain uncontrolled and the system is, by definition, not functionally controllable. However, two controllable directions are present and a robustly stable controller making full use of the VGT and EGR valve can be designed.

The observations in this section are a direct consequence of having simultaneously low engine-out NO_x and PM emissions. Well chosen control actions can still simultaneously decrease NO_x and increase λ . But, as can be seen in Figure 5.4, the input direction that achieves this corresponds with a steep increase in Δp and accordingly increased BSFC. This is also the reason for the significant improvement of the condition number when Δp is included as a third output. Even when the robust stability issues are disregarded, the strong effect a NO_x - λ controller will have on Δp , and hence also on the fuel efficiency, makes NO_x - λ feedback control, using the VGT and EGR valve, undesirable. It can be expected that, when substitute measurements for NO_x , λ and Δp are used, that maintain the desired correlation with the respective high-level objectives, these conclusions hold as well.

5.4.3 Control Design

In this section, a feedback controller is designed for the 1455 RPM, 120 mg/inj operating point. For the design of the feedback controller, static SVD decoupling (i.e. decoupling based on the Singular Value Decomposition of the static system gain), combined with classical (PI) feedback control is used. The reasons for this are the following. The identified FRF model (Figure 4.8) is directly suitable for loopshaping control design of classical controllers and the resulting controllers are suitable for implementation without further processing. Typically, the design effort for classical controllers is lower than for a model-based control design, because several difficult steps that are needed to mathematically define and solve the control problem can be avoided. The use of decoupling is required due to the system behavior, which is strongly coupled as can be seen in Figure 4.8. Static decoupling will show adequate performance and is much simpler to design and implement than dynamic decoupling. In this section, the design and functioning of the decoupling and feedback controller are elaborated.

Decoupling

Decoupling serves a double purpose in the controller, both are accomplished via SVD decoupling. First, two output directions are separated from a third direction in which the VGT and EGR actuators have no influence. This solves the underactuation problem. Second, the two remaining directions are decoupled. This results in a diagonally dominant Two-Input, Two-Output (TITO) system.

The design of the decoupling matrices is based on the local static system gain. The two-input, three-output system, \mathbf{G} , describes the dynamic response of the engine:

$$\mathbf{y}_{\text{fb}} = \mathbf{G} \mathbf{u}_{\text{fb}}, \quad (5.13)$$

where $\mathbf{y}_{\text{fb}} = \begin{bmatrix} y_{\text{NO}_x} & y_\lambda & y_{\Delta p} \end{bmatrix}^\top$ and $\mathbf{u}_{\text{fb}} = \begin{bmatrix} u_{\text{VGT}} & u_{\text{EGR}} \end{bmatrix}^\top$. Now, consider the diagonal output scaling $\mathbf{S} \in \mathbb{R}^{3 \times 3}$, static gain matrix of the system response: $\mathbf{G}_{\text{ss}} = \mathbf{G}(\omega = 0) \in \mathbb{R}^{3 \times 2}$ and the following SVD decomposition:

$$\mathbf{S} = \begin{bmatrix} 0.05 & 0 & 0 \\ 0 & 50 & 0 \\ 0 & 0 & 0.7 \end{bmatrix}, \quad (5.14)$$

$$\mathbf{S} \mathbf{G}_{\text{ss}} = \begin{bmatrix} 1.4626 & -1.0914 \\ 0.8916 & -1.0040 \\ -1.2722 & -0.7582 \end{bmatrix}, \quad (5.15)$$

$$\mathbf{U} \mathbf{\Sigma} \mathbf{V}^\top = \mathbf{S} \mathbf{G}_{\text{ss}}, \quad (5.16)$$

where $\mathbf{U} \in \mathbb{R}^{3 \times 2}$ and $\mathbf{V} \in \mathbb{R}^{2 \times 2}$ are orthonormal matrices and $\mathbf{\Sigma} \in \mathbb{R}^{2 \times 2}$ is a diagonal matrix. The diagonal scaling matrix \mathbf{S} is again used to scale the outputs. It accounts for the difference in units and their importance and can be used to trade performance between the different controlled outputs. Input scaling is not applied, because both inputs are expressed in % and range between 0% and 100%. Using the results of the SVD decomposition, the TITO system \mathbf{G}_d :

$$\boldsymbol{\varepsilon} = \mathbf{U}^\top \mathbf{S} \mathbf{G} \mathbf{V} \mathbf{v} = \mathbf{G}_d \mathbf{v}, \quad (5.17)$$

with inputs $\mathbf{v} = [v_1, v_2]^\top$ and outputs $\boldsymbol{\varepsilon} = [\varepsilon_1, \varepsilon_2]^\top$, is obtained that has a diagonal static response. The block scheme of Figure 5.5 shows the implementation of the

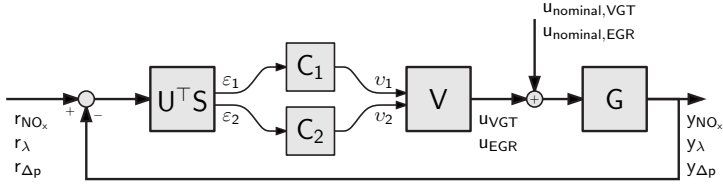


Figure 5.5: A block scheme representation of the control architecture.

decoupling in the control scheme. After SVD decoupling, a functionally controllable, decoupled TITO system remains.

The decoupling is designed to exactly match the static input-output gain of the nominal system. The dynamic decoupling quality is quantified by calculating the Relative Gain Array (RGA) (Skogestad and Postlethwaite, 2007), Λ , of the decoupled system:

$$\Lambda = \mathbf{G}_d \circ (\mathbf{G}_d^{-1})^T, \quad (5.18)$$

where the \circ -symbol is used to denote the Hadamard product (i.e. entry-wise product). Figure 5.6 shows the diagonal and off-diagonal entries of the RGA of the decoupled system. Up to and somewhat beyond the intended bandwidth of 0.2 Hz, the diagonal RGA value is close to one and the off-diagonal RGA value is close to zero, which indicates that the effects of coupling are small. For the range of frequencies that is most of interest for feedback control design, \mathbf{G}_d is close to being fully decoupled.

Feedback Control Design

Implementing two SISO feedback controllers C_1 and C_2 results in a closed-loop controlled system. For the design of C_1 and C_2 , a variation of sequential loop shaping is used. The parameters of the diagonal PI controller are designed in an iterative loop. The closed-loop effects of the already designed control elements are taken into account during the design process. Also, the effective closed-loop behavior of the controlled MIMO system is reviewed during the design process. Interaction between the diagonal terms (i.e. coupling) that remains after SVD-decoupling is thereby accounted for, both for stability and performance.

The PI controller is a good match for the system dynamics due to the low-pass characteristics found in all transfer functions and the performance requirements

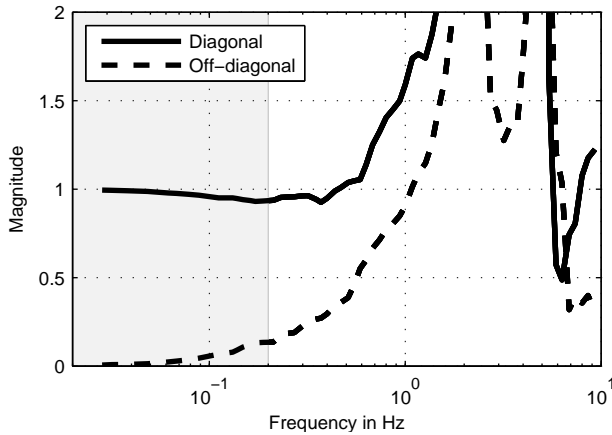


Figure 5.6: The diagonal and off-diagonal entries of the absolute values of the relative gain array, $|\Lambda|$. The frequency range up to the intended bandwidth of 0.2 Hz is shown in gray.

that focus on low frequency performance. The use of a PI controller results in smooth control actions and the controller is guaranteed to eliminate all steady-state errors in the controlled directions. The system dynamics did not give cause for using any additional dynamic elements in the controller. For C_1 , a PI controller was designed, for C_2 , only integral control was used. The use of the following controller resulted in the desired closed-loop bandwidth of 0.2 Hz:

$$\begin{bmatrix} \dot{x}_1 \\ \dot{x}_2 \\ v_1 \\ v_2 \end{bmatrix} = \begin{bmatrix} 0 & 0 & 1 & 0 \\ 0 & 0 & 0 & 1 \\ 0.6 & 0 & 3 & 0 \\ 0 & 2.5 & 0 & 0 \end{bmatrix} \begin{bmatrix} x_1 \\ x_2 \\ \varepsilon_1 \\ \varepsilon_2 \end{bmatrix}. \quad (5.19)$$

The expected transient performance can be evaluated using the closed-loop sensitivity, shown in Figure 5.7. The diagonal elements of the sensitivity show the expected transient performance level when disturbances are present. The off-diagonal elements show the effects of coupling. The singular values show the worst case and best case performance. In Figure 5.7, it can be seen that up to 0.2 Hz, the sensitivity is always below 10^0 . Up to this frequency, the feedback

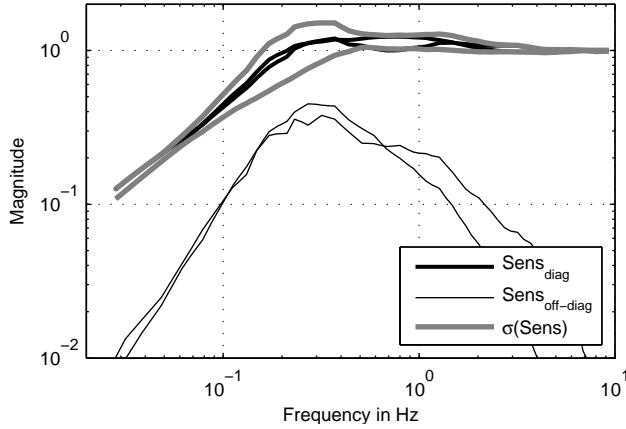


Figure 5.7: The closed-loop sensitivity: $\mathbf{Sens} = (\mathbf{I} + \mathbf{C}\mathbf{G}_d)^{-1}$ and $\sigma(\mathbf{Sens})$: the singular values of \mathbf{Sens} , denoting the best and worst case performance. The sensitivity indicates how effective the controller is at counteracting disturbances.

controller improves the tracking performance. Also, it can be observed that the off-diagonal, cross-coupling elements are relatively small when compared with the diagonal elements, i.e., decoupling was successful.

To check for closed-loop MIMO stability, the generalized Nyquist stability criterion is used. By visual inspection of the Nyquist plot, stability can be assessed. For the used MIMO control structure, the Nyquist plot consists of the real and imaginary part of:

$$N(j\omega) = \det(\mathbf{I} + \mathbf{C}(j\omega)\mathbf{U}^\top \mathbf{S}\mathbf{G}(j\omega)\mathbf{V}), \quad (5.20)$$

where \mathbf{C} is the diagonal controller of Equation (5.19). Closed-loop stability is obtained when N passes the origin to the right, while following N from low to high ω . The minimal distance of N to the origin is an indication for robustness, where a larger distance is equivalent to a more robust closed-loop. Standard practice is to use at least a radius of 0.5 around the origin. For the designed controller, a minimum distance of 0.72 was found, while obtaining the desired bandwidth. This indicates that the closed-loop stability is robust against an uncertain system response. The large robustness margin would also allow for increasing the closed-loop bandwidth beyond the target bandwidth, to further improve the high-frequency disturbance rejection. However, considering the frequency content of the

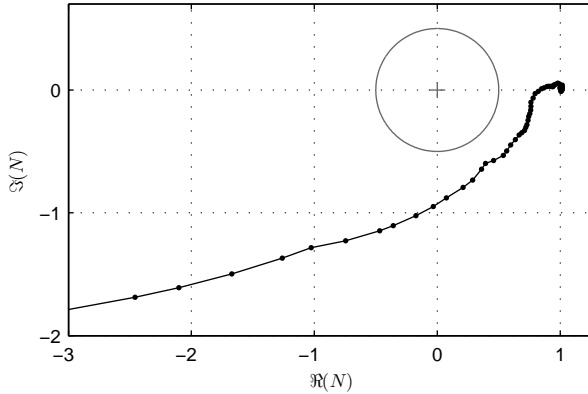


Figure 5.8: A Nyquist plot, showing the real and imaginary part of N . The circle with radius 0.5 shows the region that should be avoided to achieve robust stability with a modulus margin of at least two.

disturbances, this is not expected to bring significant improvements of the overall emissions or fuel efficiency. Therefore, the good robustness properties and smooth inputs associated with the large robustness margin are preferred over an increased bandwidth.

It is shown here that the dynamic response of the NO_x -sensor is sufficiently fast for obtaining the desired transient performance. With a faster sensor, the measured NO_x dynamics would have been faster. This would have made the static approximation used for decoupling useful in a larger frequency range, which would likely have given further improvements of the decoupling quality. Furthermore, it would have allowed for a higher closed-loop bandwidth. However, the desired performance level (closed-loop bandwidth) can be achieved using the current sensor. This makes the selection of suitable reference values and the accuracy of the measurements the most important factors that determine the resulting engine performance. Considering that the encountered disturbances are all low frequent, the current controller is sufficiently fast to adequately counteract them. Therefore, tracking the same references even more accurately, using the same sensors, but using a more advanced control algorithm with a higher bandwidth, is not expected to significantly improve the engine performance.

5.4.4 Experimental Results

The controller designed in Section 5.4.3 is implemented on a test engine mounted on a dynamometer test setup. The engine and test setup are the same as the ones used for identification in Chapter 4 and described in Section 4.2.

To test the performance of the feedback controlled engine, disturbances are applied. Aging and fouling of the engine and changing ambient conditions are always present, but difficult to influence during the experiment. Therefore, disturbances are applied in other parameters that can be influenced to act in place of the actual disturbances. Step disturbances are applied to the nominal VGT and EGR settings. Also, the engine speed and load are changed from their nominal values. These artificial disturbances do not correspond with any specific actual disturbance, but do show the response of the controlled engine to disturbances.

For this test of the feedback controlled engine, the disturbances are applied as steps, whereas the actual disturbances are slowly varying. These step-wise disturbances are more suitable for demonstrating the transient performance of the controller. When the test was executed with slowly varying disturbances, the controller would be in quasi-stationary state at all times and the actual transient response would not be visible. The transient performance of the controller is of importance despite the slowly varying nature of the disturbances. Due to the continuously changing engine speed and load, fast and dynamic adaptations are needed.

The presented experiments are conducted in the neighborhood of a nominal operating point: 1455 RPM and 1050 Nm. For the test engine, this point is close to the center of the speed and load operating range. The engine load is controlled in open loop, using the fuel flow. Because the disturbances all have a small effect on the fuel efficiency and hence the produced torque, the load is not completely constant when the disturbances are applied. Feed-forward control schemes, normally used to adapt the VGT and EGR valve during engine speed or load changes, are not active during this experiment.

The tests should experimentally verify the following questions.

- **Asymptotic stability;** does the closed-loop controlled engine converge to steady state; is the closed-loop system asymptotically stable?

- **Transient response;** how long does it take before steady state is reached; is the desired bandwidth achieved?
- **Engine performance;** does the engine performance suffer from the under-actuation?

Figure 5.9 shows the experimental results for input disturbances and Figure 5.10 shows the results for engine speed and torque disturbances. The figures show the three measured outputs, two decoupled errors, ϵ , two inputs and the speed-load operating point. In both figures, it is observed that the engine converges to a stable equilibrium after a disturbance is applied in all cases. The feedback controller makes the controlled errors, ϵ , return to zero asymptotically. The error remains close to zero as long as no new disturbance is applied. This shows closed-loop asymptotic stability. Also, it demonstrates robust stability against model uncertainty and the applied disturbances.

The transient response time that is observed after a step disturbance is applied is under 5 s in all cases. The transient response after a disturbance in torque (Figure 5.10) is slightly slower than after a disturbance in the VGT or EGR valve (Figure 5.9). The instantaneous torque disturbance evokes a dynamic effect, therefore, in the air path the disturbance is not perceived as a step.

The disturbances that are applied in the input values, VGT and EGR valve, are counteracted completely, as can be seen in Figure 5.9. These disturbances are, by definition, exactly in the direction in which the VGT-EGR valve controller has control authority. Underactuation is therefore not an issue. When the feedback controller exactly counteracts the disturbances in ϵ , the original equilibrium is recovered and perfect tracking of all three outputs is achieved. With all disturbances exactly eliminated, the achieved engine performance in terms of NO_x emissions, PM emissions and BSFC can be expected to match the nominal performance.

The disturbances in the operating point (torque and engine speed), shown in Figure 5.10, cannot be counteracted completely. When the operating point is changed, it is no longer possible to maintain the exact same NO_x , λ and Δp simultaneously by adapting the VGT and EGR valve. Nonetheless, ϵ always converges to zero, which means that within the capabilities of the VGT and EGR valve the closest possible tracking is achieved.

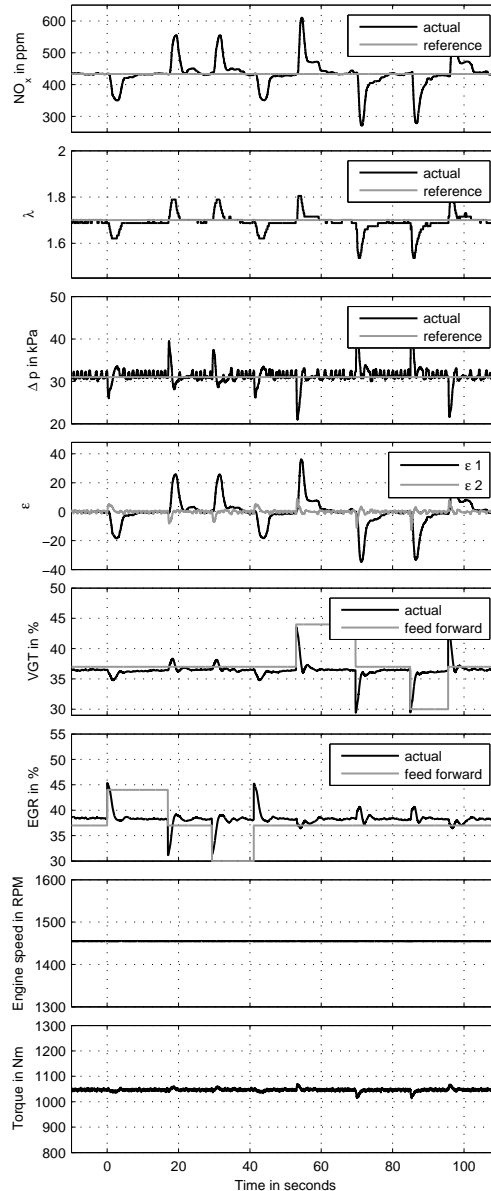


Figure 5.9: Rejection of step disturbances using feedback control. From top to bottom: the measured outputs (NO_x , λ , Δp), decoupled outputs (ϵ), inputs (VGT and EGR) and operating point (Engine Speed, τ). Disturbances are applied first in the EGR valve at time=0s and in the VGT actuator at time=50s.

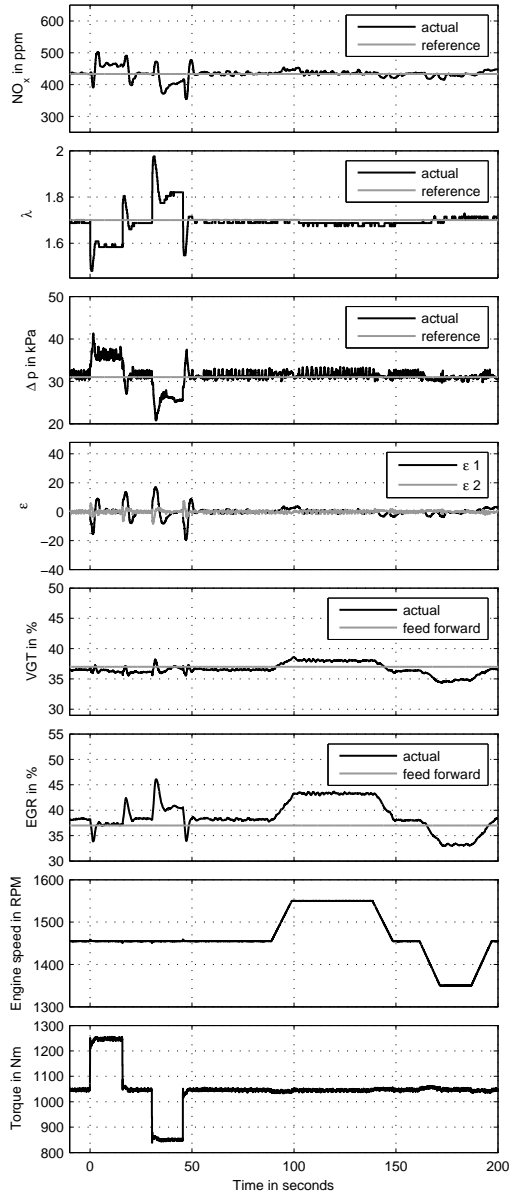


Figure 5.10: Rejection of engine speed and torque disturbances using feedback control. From top to bottom: the measured outputs (NO_x , λ , Δp), decoupled outputs (ϵ), inputs (VGT and EGR) and operating point (Engine Speed, τ). Disturbances are applied first in load at time = 0 s and in engine speed at time = 90 s.

Particularly the disturbances in torque leave a noticeable difference between the reference values and measured values for all three outputs. Increasing torque will increase NO_x , decrease λ and increase Δp . All three of these changes are undesirable, but the tradeoff between the three outputs is effectively maintained. The remaining error is distributed over all three outputs, which is preferred over exact tracking of only two outputs. Decreasing torque has the opposite effect, and simultaneous improvements in NO_x , λ and Δp are obtained and again the tradeoff between the three outputs is maintained. This is not a coincidence; the direction in which the VGT and EGR valve have no control authority is perpendicular to the dark grey ellipsoid of Figure 5.4. This direction will always correspond with the direction of the remaining static error.

The disturbances in engine speed are not applied instantaneously, because the acceleration capabilities of the test cell are physically limited. The disturbances as a result of the applied speed changes are counteracted with very small errors. The adaptations needed in VGT and EGR valve are significant, but in the NO_x , λ and Δp signals, almost no change can be observed. Apparently the direction of the disturbances matches the directions where the VGT and EGR valve have control authority. Hence, the VGT and EGR controller can almost perfectly counteract this disturbance.

To summarize the results, the three research questions posed earlier in this section are answered.

- **Asymptotic stability;** the experiments verify that the closed-loop controlled system is asymptotically stable in this operating point and robustly stable for the applied disturbances.
- **Transient response;** the transient response after a step disturbance confirms that the desired bandwidth of 0.2 Hz is achieved.
- **Engine performance;** except for the torque steps, the tracking performance is very good. The steady-state errors in NO_x , λ and Δp are very small. For torque steps, an error remains that is outside the control authority of the VGT and EGR valve, but the desired tradeoff between emissions and fuel efficiency is maintained. The engine performance therefore remains close to nominal in all tested circumstances.

The experiments show that a robustly stable and fast feedback controller is designed. The controller maintains the desired tradeoff between emissions and fuel efficiency and counteracts disturbances with small tracking errors in NO_x , λ and Δp .

6 Efficient Control Design for Low Emission, Fuel Efficient Diesel Engines

In the previous chapter, a feedback controller was designed. It is shown that this controller successfully counteracts disturbances, which reduces the spread on the NO_x and PM emissions and fuel efficiency. For practical applications, where speed and load variations are present, the controller of Chapter 5 is not directly suitable. The controller was designed to reduce the effects of disturbances, while maintaining close to a stationary speed-load operating point. Its design is based on a linear model, which is accurate only at a single operating point. Therefore, outside of this operating point, stability and performance of the controller are not guaranteed. Also, the VGT and EGR valve play an important role when the driver torque demand varies. To realize these torque variations with low emissions, fast changes in the air and exhaust flows are needed. The VGT and EGR valve should be used actively to change the air and exhaust flows in accordance with the changing torque demand. The controller of Chapter 5 does not accommodate this.

This chapter deals with efficiently designing a controller that is suitable to work on the entire speed-load operating range and addresses the above issues. The design procedure for the feedback controller is adapted, such that stability and performance in the entire operating range are taken into account. Also, a dynamic feed-forward controller is designed and implemented to provide additional air-path control actions during torque transients.

The complexity of the control design is intentionally kept low to reduce the design and implementation effort, which is a considerable problem in current engine control design. Production controllers use maps that determine actuator settings or adjustments to these actuator settings depending on the operating point and sensor

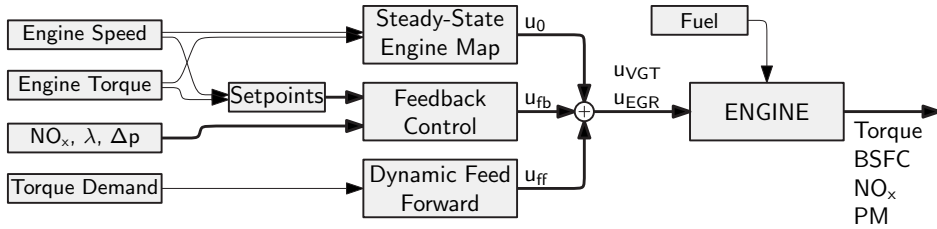


Figure 6.1: The interconnections in the air-path control scheme. Thin lines represent communicating a single signal, thick lines represent communicating multiple signals.

measurements. Each map consists of a large number of parameters, particularly when the maps are multidimensional. The liberal use of such maps is the main reason for the high design and calibration effort of current commercial engine controllers. Therefore, in contrast with the current approach, a controller with a small number of tunable parameters is aimed for.

The principal method for reducing the complexity of the control design is feedback control. When a feedback controller reliably keeps the engine state close to a desired reference situation, even when disturbances are present, the controller can be simplified drastically. The engine maps that correct for disturbances are made redundant and the number of engine maps can be reduced.

In Section 6.1, a feedback control design procedure is presented. The principles of the control design remain the same as those in Chapter 5. The design procedure is modified to ensure that the feedback controller is useable on the full speed-load range. With the adapted control design procedure, the effects of variations in the local input-output response on the closed-loop performance and stability are accounted for.

In Section 6.2, a feed-forward controller for improved behavior during torque transients is presented. The purpose of this controller is to decrease the PM emissions and improve the torque response during tip-in transients.

The control system with feedback and feed forward combined is tested on a heavy-duty engine in Section 6.3. To emulate real-life use of heavy-duty diesel engines, the controller is tested on the World Harmonized Transient Cycle (WHTC). The engine-out emissions and fuel consumption over this cycle are evaluated and

compared with the values that are achieved with a production-type EURO VI controller.

The contents of this chapter are largely based on Criens et al. (2014).

6.1 Feedback Control

The purpose and design principles of the feedback controller are the same as those in Chapter 5. To recapitulate, the purpose of the feedback controller is to maintain the BSFC, NO_x emissions and PM emissions at all times as close as possible to the values obtained under nominal conditions. The control design of Chapter 5 needs to be modified to accommodate speed and load variations, which were not considered in Chapter 5. The required modifications are discussed in this section.

In Chapter 4, it was shown that the encountered local input-output behavior can be accurately represented by a linear model (Figures 4.6 and 4.7). However, it was also shown that the local input-output behavior varies significantly, when the speed-load operating point changes (Figure 4.8). Amplitude variations of a full order of magnitude and sign changes are observed. A controller designed using only the input-output response at a single operating point can therefore not be expected to function in the entire speed-load range.

To take the nonlinear behavior into account, several control design methods can be used. In order of increasing complexity, the following control design methods can be considered.

- **Linear control design**, taking into account the variations of in the local behavior for both stability and performance, without dynamically adapting the controller properties.
- **Gain-scheduled control design**, adjusting the controller parameters online for the known variations in the local behavior.
- **(Quasi) linear parameter varying control design**, explicitly taking into account the time-varying nature of the input-output behavior.
- **Nonlinear control design**, where a nonlinear controller is designed using a nonlinear engine model, which describes the full engine behavior.

Considering the goal to produce an efficient control design, the linear control design method is preferred. Linear control is the least complex, both in terms of the design procedure and the implementation. It is however also the most conservative. Considering the large variations that are present in the input-output behavior, it might not even be possible to achieve closed-loop asymptotic stability with a linear controller. In this section, the design of a linear controller for feedback control in the entire operating range is elaborated. It is shown that stability and convergence to small tracking errors can be achieved.

Similar to the controller in Chapter 5, the new controller combines decoupling with classical control design. The design will be described briefly, focussing on the adaptations needed to accommodate the variation of the input-output behavior at different operating points.

6.1.1 NO_x Measurement

A small change is made to the selection of controlled outputs; in particular to the output representing the NO_x emissions. In Chapter 5, the feedback controller used the NO_x concentration as a controlled output, which is measured directly by the NO_x sensor. With a change in the software interacting with the engine, additional measurements became available for the control system, allowing for an adaptation. In this chapter, the brake specific NO_x emissions expressed g/kWh are controlled. Using the measured air flow, fuel flow, brake torque¹ and engine speed, the measured NO_x concentration in ppm is converted into the specific engine-out NO_x emissions in g/kWh. This conversion has the following advantages.

- **Correct for changes in air flow** The NO_x concentration decreases when the the air flow increases while NO_x mass flow remains constant. This is unwanted and the specific NO_x flow in g/kWh is not affected by this.
- **Relation with emission legislation** The EURO VI legislation for HD diesel engines imposes a limit on the tailpipe NO_x emissions expressed in g/kWh. Using the same units to control the engine-out NO_x emissions makes the values directly comparable.

¹This measurement is not available on production engines and should therefore be replaced with an estimate.

- **Interpretation** When expressed in g/kWh , the NO_x value is more natural to interpret and its nominal value changes less over the speed-load range, which makes selecting or adapting setpoint values for NO_x more insightful.

Disadvantages of using the specific NO_x emissions, rather than the NO_x concentration exist as well. In particular when the brake torque becomes low, zero or negative, even low NO_x mass flows expressed in g/s can result in very high or negative values, when expressed in g/kWh . In this region however, the use of the NO_x concentration sensor itself can be problematic as well. The NO_x sensor requires a minimum exhaust gas temperature to function, which is not always available during warm-up or at low loads. Considering that at low loads, the NO_x and PM emission flows (expressed in g/s) are very low for a wide range of input settings, feedback control is disabled below 300 Nm, which prevents these potential issues. Also, because multiple sensors are involved in the conversion of the NO_x concentration into the brake specific NO_x emissions, inaccuracies in all these sensors influence the end result. This reduces the relative accuracy of the brake specific NO_x measurement, compared with the NO_x concentration measurement. The advantages mentioned earlier make the choice for the brake specific NO_x emissions fundamentally more relevant. The inherent disadvantages are therefore accepted.

6.1.2 Decoupling

Similar to the earlier control designs, the design of the decoupling is based on the Singular Value Decomposition (SVD) of the static gain matrix. This gain matrix follows directly from the system identification. Because the input-output response is operating point dependent, the static gain matrix is as well. But, as will be shown, fixed, static decoupling matrices can again be used to effectively decouple the input-output system for the entire operating range. For the design of the controller and decoupling, 35 operating points are considered. The distribution of the operating points is shown in Figure 6.2. The operating points span the entire operating range, except for the very low torque range. The operating points are not distributed evenly over the range. To allow for a more detailed analysis of the local variation in the frequency response, the distribution is locally more dense at some points. Only nine operating points are used to graphically present the results in this chapter to prevent cluttering of the graphs with too many lines. All

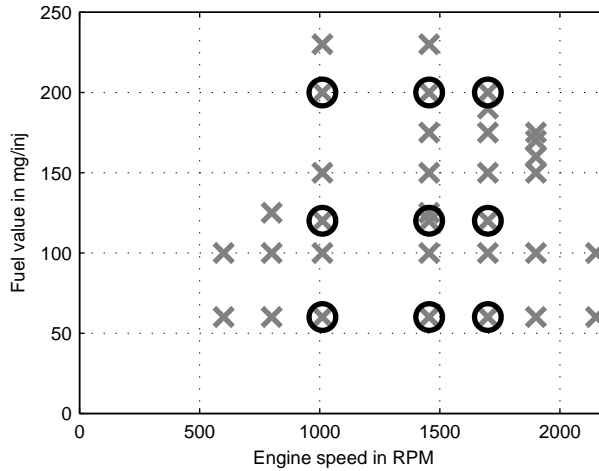


Figure 6.2: The operating points used for design and analysis of the controller. The 'x'-markers show all considered operating points. The circles indicate the selected operating points for the figures in this section.

identified points are used for design and analysis of the controller. For design of the decoupling matrix, first an average static gain matrix is calculated using:

$$\bar{\mathbf{G}} = \text{sgn}(\Re(\mathbf{G}_1(0))) \circ \left(\prod_{n=1}^N |\mathbf{G}_n(0)| \right)^{\frac{1}{N}} \approx \begin{bmatrix} 0.2548 & -0.2728 \\ 0.0130 & -0.0214 \\ -1.9714 & -1.2263 \end{bmatrix}, \quad (6.1)$$

where \circ denotes the Hadamard product (i.e. entry-wise product), also the product and the $1/N$ power are performed entry-wise. The index n represents the operating point, N the number of operating points, i.e., $N = 35$, \mathbf{G}_n the identified FRF at operating point n and $\Re(\mathbf{G}_1(0))$ the real part of the static gain matrix at a nominal operating point (1455 rpm, 120 mg/inj), which is used to recover the sign of the response that is lost when the geometric mean is calculated. The outcome $\bar{\mathbf{G}}$ is the geometric-mean static gain. To determine the static gain $\mathbf{G}_n(0)$ of system n from the measured FRF, the input-output gain at the lowest frequency excited during identification (0.028 Hz) is used. In Figure 4.8, it is observed that the system gain is close to static here.

Before decoupling, output scaling is applied, which is adapted due to the change in outputs compared with the controller of Chapter 5:

$$\bar{\mathbf{G}}_s = \mathbf{S}\bar{\mathbf{G}} = \begin{bmatrix} 5 & 0 & 0 \\ 0 & 50 & 0 \\ 0 & 0 & 0.7 \end{bmatrix} \bar{\mathbf{G}}, \quad (6.2)$$

where \mathbf{S} is again a fixed, diagonal scaling matrix. The chosen values account for the difference in units and the tracking performance tradeoff between the three different outputs.

The system \mathbf{G}_n is decoupled by pre- and post-multiplying with the appropriate scaling and decoupling matrices that are calculated via an SVD:

$$\bar{\mathbf{G}}_s = \mathbf{U} \boldsymbol{\Sigma} \mathbf{V}^\top, \quad (6.3)$$

$$\boldsymbol{\varepsilon} = \mathbf{G}_{d,n} \mathbf{v} = \mathbf{U}^\top \mathbf{S} \mathbf{G}_n \mathbf{V} \mathbf{v}, \quad (6.4)$$

where $\mathbf{U} \in \mathbb{R}^{3 \times 2}$, $\mathbf{V} \in \mathbb{R}^{2 \times 2}$ and $\boldsymbol{\Sigma} \in \mathbb{R}^{2 \times 2}$, such that $\mathbf{U} \mathbf{U}^\top = \mathbf{I}$, $\mathbf{V} \mathbf{V}^\top = \mathbf{I}$ and $\boldsymbol{\Sigma}$ is diagonal. The variables $\boldsymbol{\varepsilon}$ and \mathbf{v} represent the outputs and inputs of the decoupled system, $\mathbf{G}_{d,n}$, respectively. When the system response, \mathbf{G}_n , is close to $\bar{\mathbf{G}}$, $\mathbf{G}_{d,n}$ is close to the diagonal matrix $\boldsymbol{\Sigma}$ and the system is close to being completely decoupled.

The system gain is both frequency and operating-point dependent, which affects the decoupling quality. To quantify to what extent the actual system is decoupled, the relative gain array, $\boldsymbol{\Lambda}$ (Skogestad and Postlethwaite, 2007), of the decoupled system is calculated for all operating points and frequencies:

$$\boldsymbol{\Lambda}_n(j\omega) = \mathbf{G}_{d,n}(j\omega) \circ (\mathbf{G}_{d,n}^{-1}(j\omega))^\top. \quad (6.5)$$

Figure 6.3 shows $\boldsymbol{\Lambda}_n(j\omega)$, using the local responses shown in Figure 4.8. It shows that for frequencies up to 0.5 Hz, the local behavior is diagonally dominant at all operating points. The large differences in the local behavior, even including a sign change in the input-output gain, do not significantly affect the low-frequency decoupling quality. A closed-loop bandwidth of around 0.2 Hz is aimed for, and up to this frequency, neither the dynamic behavior, nor the operating point variations significantly decrease the decoupling quality for the purpose of feedback control,

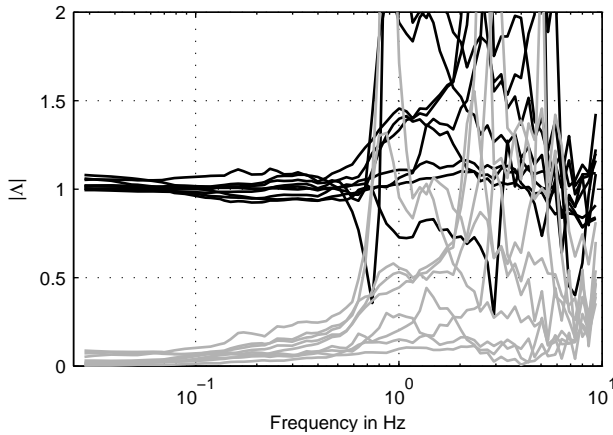


Figure 6.3: The relative gain array of the decoupled system, $G_{d,n}$. In black the diagonal elements, in gray the off diagonal elements. The operating points are the same as in Figure 4.8.

as is shown in Figure 6.3. Hence, static SVD decoupling with the chosen, fixed matrices effectively decouples the local input-output dynamics in all operating points.

6.1.3 PI control

The PI feedback controller is designed to achieve maximum bandwidth, while satisfying the Nyquist stability criterion, and keeping the sensitivity peak below 2 for the entire operating range. Similar to the local control design of Chapter 5, sequential loop-shaping is used to design two PI controllers. Considering the low-pass behavior that characterizes the local input-output response in all operating points, PI control is a suitable structure. The main difference with the design in Chapter 5 is that the PI controller is designed to work in the entire operating range. Instead of shaping only the frequency response at a single operating point, the frequency response at all identified operating points is shaped simultaneously, according to the above criterion. This way, local stability and performance in all operating points is accounted for.

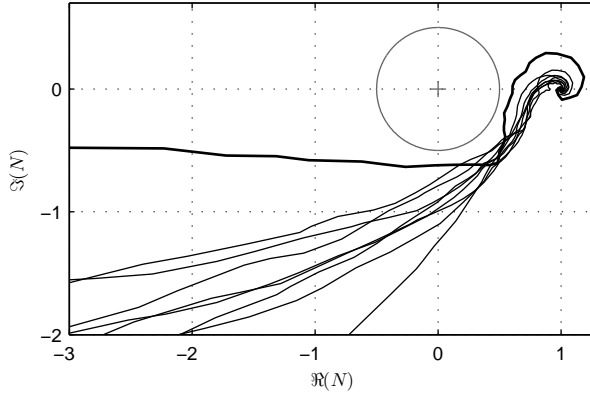


Figure 6.4: The Nyquist plot, calculated on the 3x3 grid of operating points used also in Figure 4.8. The black line closest to the circle corresponds with the low speed, high load operating point. This operating point is the closest to the stability margins.

The controller is described by:

$$\begin{bmatrix} \dot{x}_{fb,1} \\ \dot{x}_{fb,2} \\ v_1 \\ v_2 \end{bmatrix} = \begin{bmatrix} 0 & 0 & 0.6 & 0 \\ 0 & 0 & 0 & 1.2 \\ 1 & 0 & 0.5 & 0 \\ 0 & 1 & 0 & 0.05 \end{bmatrix} \begin{bmatrix} x_{fb,1} \\ x_{fb,2} \\ \varepsilon_1 \\ \varepsilon_2 \end{bmatrix}. \quad (6.6)$$

Using this controller, the maximum singular value of the sensitivity is below 0 dB up to a frequency of 0.16 Hz for all operating points. The maximum singular value of the sensitivity is below 2 for all operating points and all frequencies. The 0.2 Hz bandwidth target that was formulated in Chapter 5 is not met. But the achieved 0.16 Hz bandwidth still results in a closed-loop response that is much faster than the considered disturbances (see Section 5.2). The generalized Nyquist criterion is used for visually checking stability and robustness against uncertainties in the local dynamic response. The Nyquist plot of:

$$\mathcal{N}_n(j\omega) = \det(\mathbf{I} + \mathbf{C}(j\omega)\mathbf{U}^T\mathbf{S}\mathbf{G}_n(j\omega)\mathbf{V}), \quad (6.7)$$

shown in Figure 6.4, passes the origin to the right, with an amplitude margin of a factor two to provide the desired robustness, when following the line from low to

high frequency. The closed-loop system is therefore locally stable in all considered operating points. This is not a definitive proof of stability for the actual system with time-varying engine speed and load. A mathematically conclusive proof of stability with time-varying operating points requires an accurate model of the engine behavior during operating point transients. The identified FRF models used for control design only capture the local input-output dynamics and are not very suitable for modeling the effects of time-varying operating points. Even a common Lyapunov function that shows stability in all operating points is not a sufficient proof of stability. During speed and load changes, the input-output response will be different than the response at stationary operating points. Stability with time-varying operating points is therefore tested and shown experimentally.

6.1.4 Implementation

Nominal Inputs and Setpoint Values

A practical implementation of the feedback controller requires nominal input settings and setpoint values for all outputs. The nominal input settings are designed for optimal stationary performance. The accompanying setpoints reflect the achieved engine performance under nominal conditions. Both the nominal inputs and the setpoint values are provided in the form of a lookup table with engine speed and torque as inputs and the corresponding setpoint value as output. In between the grid points of the lookup table, linear interpolation is used.

For the VGT and EGR valve inputs and the Δp and λ outputs, a map with nominal values in the form of the above described lookup table was available. For the NO_x -output, such a map was not available. Instead, the setpoint value was fixed at 3.5 g/kWh . This value does not exactly match to the nominal engine calibration over the operating range. Considering that the controlled output value is expressed in g/kWh , and thereby scaled for the engine power, the selected constant value is suitable in the entire operating range. The remaining difference acts as a disturbance during the experiments.

Safety

To ensure safe and stable operation under all encountered circumstances, some modifications to the feedback controller are made for the practical implementation. This way, a proof-of-concept experiment can be conducted safely, without risking engine damage in case of controller failure. The feedback controller is disabled in the low torque range and safety limits are implemented to prevent feedback control actions that can potentially damage the engine. This is discussed below.

In Section 6.1.1, it was already noted that to prevent issues with the NO_x measurement, the controller should be disabled at low loads. Therefore, at loads below 300 Nm and whenever a required sensor measurement is not available, the feedback controller is disabled. This is implemented by overriding the value of ϵ and setting it to zero, whenever the load is below 300 Nm or any of the sensors does not output a measurement. By setting the input to the controller to zero, the controller states \mathbf{x}_{fb} and hence the integral action of the controller remain at a fixed value. It can be assumed that by using constant integral action, the controller is still partly effective at counteracting the effects of constant disturbances. Maintaining the integral effect is therefore favorable, compared with setting the output of the feedback controller to zero. In this low torque range, a low NO_x mass flow (in g/s) is combined with a high λ and low Δp . This can be verified in Section 6.3. In a typical drive cycle that combines low, medium and high torque, it can be expected that the contribution of the low torque range to the overall emissions and fuel consumption is relatively small. Therefore, the overall emissions and efficiency of the engine are not significantly influenced by disabling the feedback controller in the low-load operating range.

Also, two precautions are taken that limit the allowed range of the feedback control actions. First, the outputs of the feedback controller are limited to $u_{\text{fb},i} \in (-10\%, 10\%)$. This ensures that the actuators remain in the range where the engine behavior is close to linear. Sensor measurements that deviate enough from the nominal situation to require feedback actions outside of this range can occur during fast torque transients, when large disturbances are present, or when an actuator or sensor is malfunctioning. In case of malfunctioning, the implemented output limits reduce the probability and consequences of unstable closed-loop behavior.

Second, anti-windup is applied to ensure that the internal state of the integrators in the controller cannot reach excessive values when the controller is saturated. The state of the integrators is limited to $x_{fb,i} \in (-10\%, 10\%)$.

The output saturation and anti-windup can limit the effectiveness of the feedback controller when large disturbances are present that require control actions outside of the allowed range. However, to ensure safe operation, they are essential.

6.1.5 Experimental Results

To test the functioning of the feedback controller, the controller is implemented on the dynamometer test setup described in Section 4.2. The dSPACE Autobox[®] is used as an I/O board for both controlling the actuators and collecting the sensor signals. The inputs and outputs of the engine are monitored, while the operating point is varied.

Figure 6.5 shows a typical sample from these tests, where the operating point changes from medium torque at high engine speed towards high torque at low engine speed with various in-between points. Linear interpolation with a 20 s slope time is used when changing the operating point.

In the ε signal, it is observed that ε remains close to zero, when the operating point is constant; and converges to zero quickly after the operating point has changed. This indicates that the closed-loop behavior is asymptotically stable for the studied conditions. In the NO_x , λ and Δp signals, it is observed that the actual outputs follow their respective setpoint values. Considering the 0.16 Hz closed-loop bandwidth, approximate first-order behavior at low frequencies and 20 s operating-point changes, a remaining error in the order of 31 % can be expected during the applied operating point changes.

At some points, particularly between 450 s and 475 s, an oscillation in the VGT, ε and Δp signals can be observed. It was found that this oscillation is related to the VGT actuator. It is however not caused by the new feedback controller; the oscillation can also occur when fixed input settings are used, or even when a Notch filter is used to actively counteract input oscillations at the particular frequency.

The discrepancy between the NO_x setpoint value and the engine-out NO_x value using nominal input settings acts as a disturbance on the closed loop, which

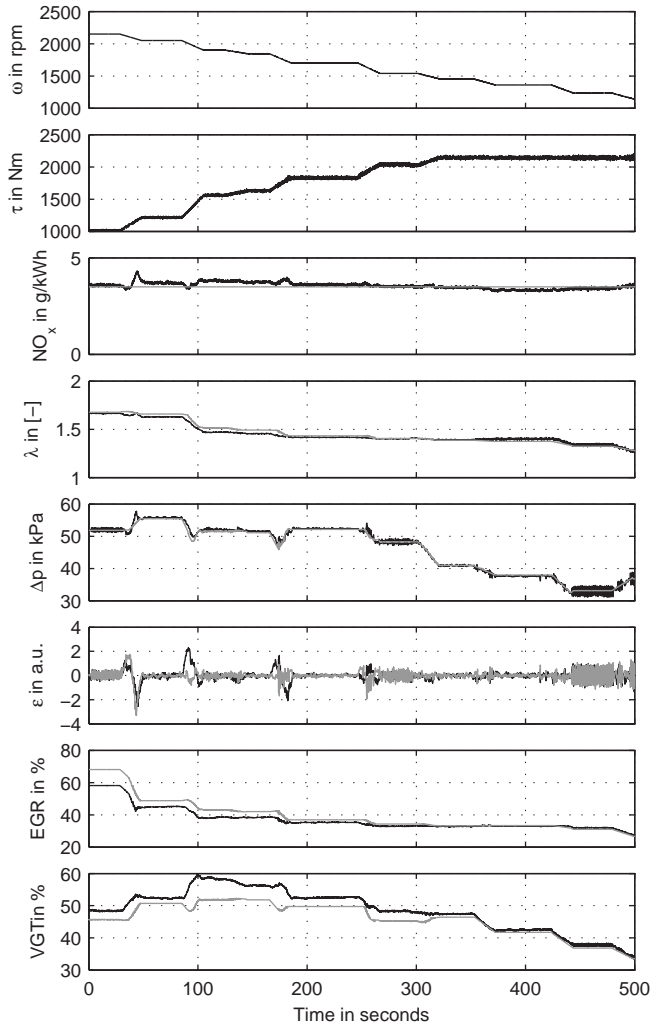


Figure 6.5: Testing the behavior of the closed-loop controlled engine. In the NO_x , λ and Δp plots, the gray line denotes the reference value, the black line the actual value. In the ε plot, the gray and black line denote ε_1 and ε_2 , respectively. In the EGR valve and VGT plots, the gray line denotes the nominal value, u_0 , the black line the actual value, $u_0 + u_{fb}$.

is compensated for by the VGT and EGR valve. The inputs therefore do not necessarily remain very close to their nominal settings, even in steady state. In both inputs, smooth behavior is observed. No signs of oscillations, or other indicators of being on the verge of instability are observed.

The experiments indicate that the expected stable closed-loop behavior and disturbance rejection are achieved, albeit only in the torque range above 300 Nm due to the applied restrictions on the feedback controller. Only relatively slow changes of the operating point were considered in this section. Fast changes of the operating point are considered in Section 6.2, where additional control components are designed and implemented to better accommodate these fast changes.

6.2 Feed-Forward Control

During fast tip-in transients, torque buildup can be hampered by the availability of oxygen, while the turbocharger is accelerating. The injection of fuel is restricted by a smoke limiter, which prevents the injection of more fuel than can be combusted without visible smoke. This limitation can prevent compliance with the driver torque demand, in particular during fast tip-in transients, which has a negative impact on the drivability. Besides activating the smoke limiter, the lack of oxygen during these transients also increases the engine out PM emissions. By adapting the VGT and EGR valve, the flow of fresh air, and thereby the availability of oxygen, can be increased. This way, air-path control can improve the drivability and decrease the PM emissions.

Control for improved transient performance differs significantly from the disturbance rejection considered in the previous section. The encountered disturbances due to changes in operating point can be much larger and their timescale is much faster. Moreover, the operating point changes are known with the availability of pedal position and engine speed. These properties favor the use of feed-forward control over feedback control. Feed-forward control, here, means that control actions are based directly on the operating point, rather than on internal engine sensor measurements.

The goal of the feed-forward controller is to achieve a fast, smooth and monotonic torque response, while avoiding excessive NO_x or PM emissions. For a HD

diesel engine, a two second response time to a step change in torque demand is considered acceptably fast. To achieve this, a temporary increase in the engine-out NO_x and PM emissions must be tolerated. Although without additional control actions, a temporary increase in the EGR flow and decreased availability of oxygen reduce the NO_x emissions during tip-in transients; as a result of control actions required to increase the fresh air flow, an increase in NO_x emissions will be observed. The feed-forward controller should ensure that a suitable tradeoff between the NO_x and PM increase is made. In this thesis, a moderate increase in the engine-out NO_x emissions (up to 25% compared with the steady-state value), combined with a necessarily larger increase in the PM emissions is considered a suitable tradeoff during a fast transient. The feed-forward controller will be designed such that via tuning of its parameters the NO_x -PM tradeoff can be influenced and a range of NO_x -PM combinations can be achieved. This makes the structure of the feed-forward controller applicable independent of the desired tradeoff.

Using the VGT and EGR valve, two measures can be taken to improve the torque response and decrease the PM emissions. First, decrease the time needed for the turbocharger to spin up by temporarily increasing the turbine flow and increasing the pressure difference over the turbine, which increases the turbine power. Second, increase the fresh air flow by temporarily decreasing the EGR flow until the turbocharger speed is sufficient to provide the required boost pressure. These measures improve the torque response and reduce the PM emissions. Simultaneously, as a result of these actions, the pumping work increases and the EGR flow decreases. Consequently, temporarily the BSFC and NO_x emissions increase. Therefore, a tradeoff between low PM emissions and a fast torque response versus low NO_x emissions and a low BSFC exists.

It is worth noting that the goal of feed-forward control is not to improve the tracking of the stationary setpoints during the torque transient. The optimal steady-state tradeoff between NO_x , λ and BSFC, that is reflected by the NO_x , λ and Δp setpoints, is necessarily shifted to improve the fresh air flow and turbocharger response during torque transients. Exact tracking of these steady-state setpoints is therefore not equivalent with achieving the optimal transient response. This is also found in Grahn et al. (2013).

Various solutions for improved transient control found in literature are described in Section 3. With a goal of optimizing for the emissions, fuel consumption

and torque response directly, while aiming for a fast and efficient control design, model based approaches become impractical. The emissions are difficult to model accurately during large transients and for a large range of actuator settings. The necessary complexity of such an emission model complicates direct control design using this model. Also, the large identification effort that can be expected increases the control design effort. Moreover, model based approaches that are found in literature use numerical optimization (Benz, 2010; Sequenz et al., 2011), but these solutions are not suitable for real-time implementation. Also, the optimal control design of Alberer and Del Re (2009) is not suitable for real-time implementation, without prior optimization on the specific drive cycle.

As a solution, manual calibration of the parameters of a dynamic feed-forward controller is proposed. The general structure of the controller is chosen such that it can emulate results obtained via optimal control (Sequenz et al., 2011; Tienstra, 2013). The design and calibration of the feed-forward controller are further described in the remainder of this section.

6.2.1 Control Design

The general structure of the proposed feed-forward controller is a linear second-order high-pass filter. This filter is used to generate a feed-forward signal based on the torque demand. The response of a high-pass filter to a step change in the input is an immediate output change followed by a smooth decay to zero. This resembles the shape of the desired response of both the VGT and EGR to a step in torque (Sequenz et al., 2011; Tienstra, 2013). To facilitate online tuning of the feed-forward characteristics, two parameters are available that determine the properties of the high-pass filter. The filter takes the following form:

$$\begin{bmatrix} \dot{x}_{\text{FF},1} \\ \dot{x}_{\text{FF},2} \\ u_{\text{FF},i} \end{bmatrix} = \begin{bmatrix} -1.5\alpha_{\text{T},i} & -\alpha_{\text{T},i} & \alpha_{\text{T},i} \\ \alpha_{\text{T},i} & 0 & 0 \\ 0 & -\alpha_{\text{g},i} & \alpha_{\text{g},i} \end{bmatrix} \begin{bmatrix} x_{\text{FF},1} \\ x_{\text{FF},2} \\ \tau_{\text{d}} \end{bmatrix}. \quad (6.8)$$

The torque demand in %, τ_{d} , is the input to the filter and the feed-forward control signal, $u_{\text{FF},i}$, is the output for actuator $i \in \{\text{EGR}, \text{VGT}\}$. The two parameters $\alpha_{\text{T},i}$ and $\alpha_{\text{g},i}$ are used to adapt respectively the gain and time scale of the

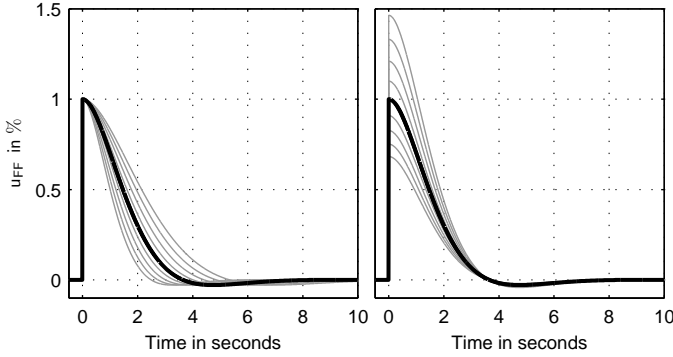


Figure 6.6: The effect of changing the parameters $\alpha_{T,i}$ (left) and $\alpha_{g,i}$ (right) on the step response of the feed-forward filter. The black line corresponds with unity parameters, the gray lines represent consecutive changes of 10% in the parameters. Increasing $\alpha_{T,i}$ decreases the decay time, increasing $\alpha_{g,i}$ increases the gain.

response. The states $x_{FF,1}$ and $x_{FF,2}$ are used only internally in the filter. The value 1.5 that is used in the filter determines its damping coefficient. Figure 6.6 shows the step response of the filter and the effects of $\alpha_{T,i}$ and $\alpha_{g,i}$. Via tuning on the engine, appropriate values for $\alpha_{T,i}$ and $\alpha_{g,i}$ are selected, such that the transient engine response has the desired characteristics. Two similar feed-forward filters are implemented, which produce the control actions for the VGT and EGR valve, respectively. Both filters are described by the state-space equation (6.8), but use different parameters.

6.2.2 Tuning Process

To find the appropriate values for $\alpha_{T,i}$ and $\alpha_{g,i}$ tuning on the engine is needed. For this, the dynamometer test setup is used. The to-be-calibrated feed-forward controller is implemented in parallel with the feedback controller designed in the previous section. Since the feed-forward control actions can be expected not to affect the closed-loop stability, the parameters can be varied freely, while monitoring the engine performance. The additional sensors that are available on a dynamometer setup are used to evaluate the emissions, fuel consumption and torque response.

For the initial calibration of the four feed-forward parameters, a 400 Nm to 1400 Nm torque step at 1455 RPM is applied repetitively. On this torque step, the

turbo lag is clearly visible, but it can be completed without excessive emissions for a range of parameters, which makes it suitable to use for initial calibration. The performance of the engine is monitored, while the feed-forward parameters are manually adjusted. The main signals that are monitored during this tuning process are the turbine speed, air-fuel equivalence ratio, Δp , engine-out NO_x emissions, smoke emissions and torque.

The turbine speed and air-fuel equivalence ratio provide insight during tuning. The desired response in these measurements is a monotonic increase to the value corresponding with stationary operation in the new operating point. Overshoot² in either of these measurements indicates that the feed-forward controller is overcompensating and smaller values for $\alpha_{T,i}$ and $\alpha_{g,i}$ should be selected.

The combination of an increase in the fuel flow, closing the VGT and EGR valve, and a low turbine speed results in a high exhaust manifold pressure. Consequently, the momentary pressure difference between intake and exhaust manifold can reach high values of several bar. The high exhaust manifold pressure increases the turbine power, which, eventually, is beneficial for the air flow and reduces the turbo lag. However, momentarily, a high pumping work reduces the engine torque. This adds to the perceived turbo lag. To monitor this effect, the pumping work is measured via the closely related Δp .

The NO_x and smoke value, sk , (to represent the PM emissions) are important to consider during a tip-in transient. The sudden increase of the fuel-oxygen ratio increases the smoke emissions. Increasing the fresh air and oxygen flow by decreasing the EGR flow improves the torque response and lowers the smoke emissions. However, because of the reduced EGR flow, the NO_x emissions increase. To obtain the desired balance between NO_x and PM, they are monitored.

Finally, the produced engine torque is measured. The ability of the engine to quickly meet a change in torque request is the main reason for implementing the feed-forward controller. A smooth and fast torque response within two seconds is aimed for.

The parameter values are tuned to obtain the fastest smooth torque response, while preventing peaks in the NO_x and PM emissions emissions that exceed the

²Overshoot in λ is observed when after the initial decrease in λ due to the sudden fuel increase, λ peaks above the steady-state value.

Table 6.1: The selected feed-forward parameters.

	VGT	EGR
$\alpha_{T,i}$	0.80	0.67
$\alpha_{g,i}$	0.18	0.42

defined criterion. After the initial tuning on the single, repetitive torque step, the engine performance (emissions, fuel consumption and torque response) is evaluated on a purpose-built cycle, which consists of a series of different torque steps, with variations in engine speed, torque step size, and rate of increase in torque demand. In this cycle, the engine speed varied between 1000 RPM and 1700 RPM; torque steps up to 100 % are considered; and the rate of increase of the torque demand varied between instantaneous and 2s. It was found that fixed values for α_T and α_g give an adequate performance for this entire cycle considering driveability as well as emissions and fuel efficiency. Scheduling of the feed-forward parameters can therefore be dismissed, which keeps the design effort of the feed-forward controller low. Small adjustments to the initial parameters were made to improve the performance on this cycle. The final parameter values can be found in Table 6.1.

6.2.3 Torque Step Experiments

Figure 6.7 shows the experimental performance of the engine during an instantaneous step change to maximum torque demand. The instantaneous step to maximum torque is the most challenging step that can be applied. Smaller or slower steps will be affected less by turbo lag and also show lower emissions. The results exemplify that by selecting different feed-forward parameters, the performance tradeoff can be shifted between PM (i.e. smoke), NO_x and torque.

A noticeable torque dip is observed shortly after the torque increase. This is the result of the Δp peak, which is largely caused by the peak in the VGT input. The Δp peak of 100 kPa is equivalent with a 70.8 Nm increase in the pumping loss. The VGT peak in this case is the result of the combined effects of the dynamic feed forward, which responds to torque demand, and the steady-state feed forward, which responds to the actual torque. Coincidentally, on this torque step the two

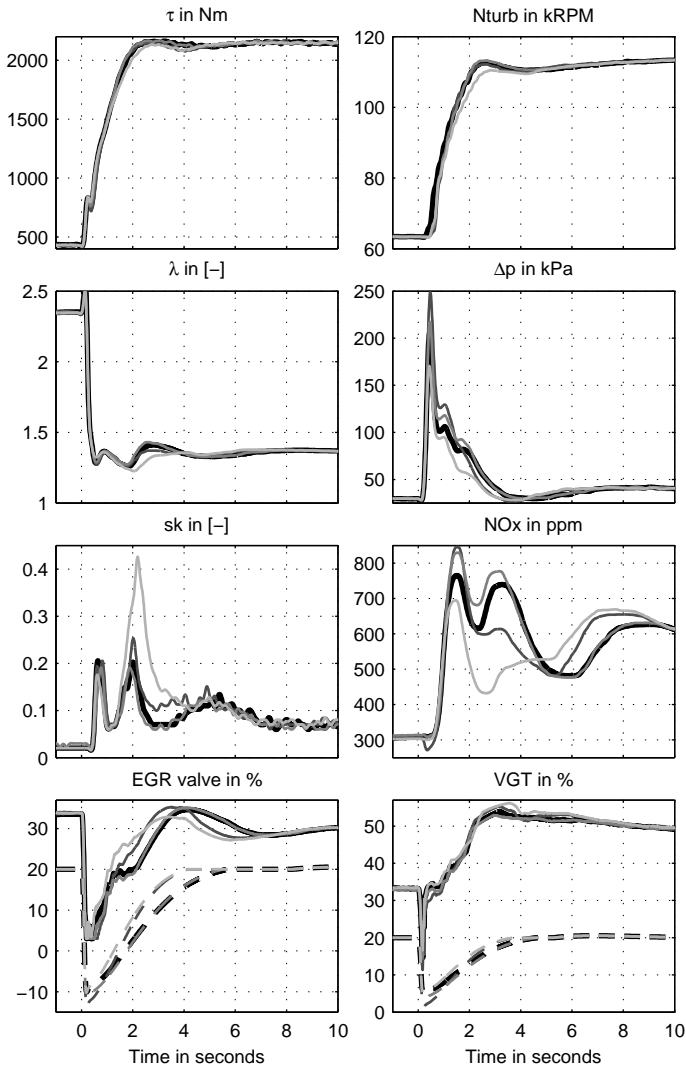


Figure 6.7: Experimental feed-forward results; the effects of four possible variations on the feed-forward parameters during a large torque step at 1455 RPM. The different shades of gray indicate the parameter versions. The black line corresponds with the parameters listed in Table 6.1. In the two bottom plots, both the individual effect of the feed-forward controller (u_{FF} , dashed) and the actual control signal (u_{VGT} , u_{EGR} , solid) are shown. In the figure, the VGT and EGR feed-forward signal are shifted with 20% relative to the actual value, to allow for a more compact vertical axis. A 4 Hz second-order zero-phase Butterworth low-pass filter was used on the measured data to reduce the noise for better discrimination between the lines.

effects cancel each other out shortly after the step in torque demand. Such a sharp change can occur only during instantaneous steps in torque demand. When, the increase in torque demand occurs more gradually over, e.g., 1 second, the changes in the steady-state and dynamic feed forward also occur more gradually. This smooths the input changes and removes its noticeable effect on the torque response. Considering that this more smooth step change is a more likely real-world scenario, the observed torque dip is acceptable.

It is important to make allowance for the the sensor dynamics in the results of Figure 6.7. Particularly the emission measurements are affected by sensor dynamics. Also, the results are affected by the fuel controller. The fuel controller limits the injected fuel quantity, when insufficient fresh air is available and determines the Start Of Injection (SOI). This controller is implemented in the engine ECU. Both the torque response and the emissions are affected by the fuel controller. The design of the fuel controller is however not a topic of this thesis.

6.3 Experimental WHTC Tests

The World Harmonized Transient Cycle (WHTC) is the official transient test cycle used for the EURO VI type approval tests. It is designed to be representative for the world-wide on-road usage of commercial vehicles. The WHTC is therefore the most suitable and representative test cycle for testing to what extent the achieved engine performance using the new control system can match the performance that is achieved using the controller on the engine ECU. In this section, only WHTC tests using a warm engine are conducted. The WHTC test for the EURO VI legislation is more elaborate. More details on the WHTC and its usage for emission legislation can be found in Section 2.3.1 and in (European Commission, 2011).

The full control system, as shown in Figure 6.1, is implemented on the engine dynamometer setup. The dSPACE Autobox[®] was again used as an I/O board; it calculates all control actions for the VGT and EGR valve, outputs the control commands to the engine and collects the sensor signals. Using the dynamometer setup, it is possible to switch between the new controller and the controller of the original ECU. This enables an objective comparison between the performance that is achieved with the two controllers, on the same engine, using the same measurement equipment and under the same conditions. With each controller,

three WHTC tests are executed. After each cycle, the controllers are switched, which reduces the effects of possibly changing ambient conditions. Again, the sensors of the dynamometer setup are used to evaluate the engine performance. This way, the torque can be measured and using an opacimeter, the PM emissions can be estimated.

Two parts of the WHTC tests using the controller designed in this thesis are shown in Figures 6.8 and 6.9. The full WHTC contains more details than can be distinguished in a single figure. The two figures respectively show a low-load (urban) and a high-load (motorway) part of the WHTC. In the low-load part, feedback control is largely inactive, whereas in the high-load part, feedback control is constantly active.

In the low-load part of the WHTC, Figure 6.8, the emission mass flow in g/s of both NO_x and PM is very low, compared with Figure 6.9. This supports the assumption made earlier that the potential absolute benefit of emission feedback control is small in the low torque region. Without feedback, the obtained values for NO_x , λ or Δp do not remain close to their nominal setpoints, but this does not result in large emissions. For a small part around 160 seconds, the engine torque exceeds the threshold value of 300 Nm to enable feedback control. The feedback error does not converge to zero error here, because the interval is both short and very dynamic.

Figure 6.9 shows a high-load part of the WHTC. The feedback controller is constantly active and the control error in ϵ remains close to zero. This ensures that the NO_x - λ - Δp tradeoff is maintained, which implies that also the desired NO_x -PM-BSFC tradeoff is closely maintained. The engine performance is as close as possible, i.e., within the capabilities of the selected actuators, to the nominal engine performance. Despite the underactuated control architecture, close tracking is obtained for all three outputs.

In both Figure 6.8 and 6.9, the VGT and EGR inputs show that the steady-state controller has the largest contribution to the final input value. In the high-load plot, Figure 6.9, the feedback controller has a notable contribution as well. The offset between the nominal and actual EGR valve position is mostly due to a correction made by the feedback controller. As can be seen in Figure 6.9, this results in close tracking of the references.

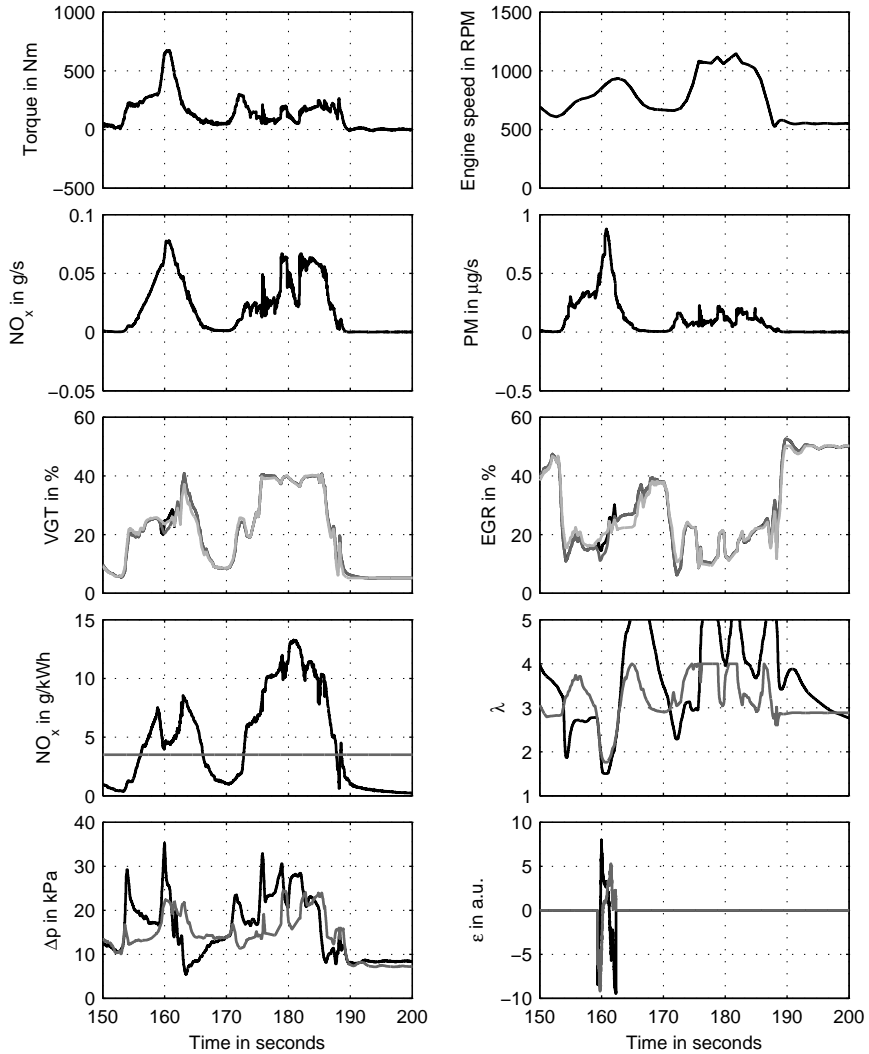


Figure 6.8: A low-load part of the hot WHTC cycle. In the VGT and EGR plot, the black line shows the output of the combined controller \mathbf{u} , the dark-gray line shows the combined effect of steady-state \mathbf{u}_0 and dynamic feed forward \mathbf{u}_{FF} , the light-gray line shows the steady-state feed forward only \mathbf{u}_0 . In the NO_x , λ and Δp graphs, the black line shows the sensor measurement and the gray line the reference value. In the ε plot, the black and gray line show ε_1 and ε_2 respectively. When the feedback controller is disabled, ε is shown as exactly zero.

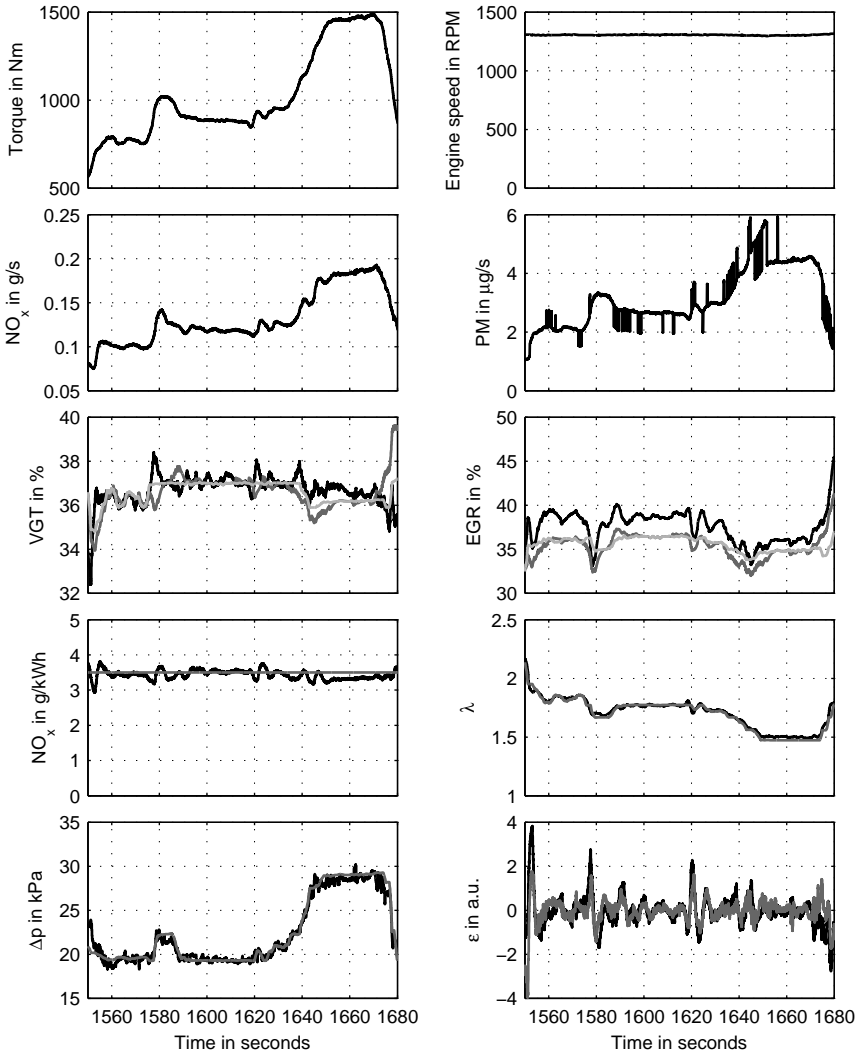


Figure 6.9: A high-load part of the hot WHTC cycle. In the VGT and EGR plot, the black line shows the output of the combined controller \mathbf{u} , the dark-gray line shows the combined effect of steady-state \mathbf{u}_0 and dynamic feed forward \mathbf{u}_{ff} , the light-gray line shows the steady-state feed forward only \mathbf{u}_0 . In the NO_x , λ and Δp graphs, the black line shows the sensor measurement and the gray line the reference value. In the ε plot, the black and gray line show ε_1 and ε_2 respectively. When the feedback controller is disabled, ε is shown as exactly zero.

Table 6.2: WHTC performance comparison of the normalized average brake specific NO_x , PM and BSFC. The baseline controller is the controller as implemented on the engine ECU. The new controller is the controller designed in this chapter using both feed-forward and feedback control.

	Baseline	New
NO_x	100 %	96.09 %
PM	100 %	88.30 %
BSFC	100 %	100.06 %

The purpose of the new controller is to simultaneously achieve good drivability, robustness against disturbances and uncertainties, low emissions and a low fuel consumption. In the new control system, the drivability is accounted for by means of the feed-forward controller; robustness by means of the feedback controller. To investigate if indeed low emissions and a low fuel consumption are obtained, the total engine-out emissions and fuel consumption of the engine were measured over three WHTC cycles. This test is performed with both the new control system and the original control system of the engine, which serves as a benchmark. To avoid using the same measurements for feedback control as for the performance evaluation, which might bias the experiment, the emission measurement equipment of the dynamometer setup, rather than the internal engine sensors, were used for accurately measuring the emissions and fuel consumption.

The normalized NO_x emissions, PM emissions and BSFC, averaged over three WHTC cycles, are shown in Table 6.2. With the new controller, the average engine-out NO_x emissions decreased with 3.9 %, while the engine-out PM emissions decreased with 11.7 %. In this test, the average BSFC remained approximately unchanged with a negligible increase of 0.06 %. Compared with the original engine controller, the new controller achieves a reduction of the engine-out NO_x and PM emissions without affecting the low fuel consumption.

7 Conclusions & Recommendations

7.1 Conclusions

In this thesis, the design of a control system for the air path of a EURO VI heavy-duty diesel engine is elaborated, which uses the Variable Geometry Turbine (VGT) and Exhaust Gas Recirculation (EGR) valve as actuators. Compared with alternative methods for air-path control design, the work in this thesis focusses in particular on reducing the effects of disturbances on the engine-out emissions and fuel efficiency, and on reducing the control design effort.

7.1.1 Disturbance Rejection

Reducing the effects of disturbances has gained great importance with the introduction of the in-service conformity limits in the EURO VI legislation. This legislation imposes emission limits for real-life usage of diesel powered vehicles. Because varying external conditions, ageing and production tolerances all affect the produced emissions, a control strategy that reduces the effects of these disturbances is needed to guarantee compliance with the new legislation.

In this thesis, a new method for disturbance rejection is elaborated. A new selection of controlled outputs is proposed: the engine-out NO_x emissions, the air-fuel equivalence ratio (λ), and the pressure difference between the intake and exhaust manifold (Δp). These outputs are selected for their direct relation with the high-level objectives: NO_x emissions, PM emissions and fuel efficiency, respectively, which is beneficial for the effectiveness of the feedback controller.

The addition of Δp as a controlled output is particularly important for the robustness. It is shown that control of NO_x and λ only, using the VGT and EGR valve, constitutes an ill-conditioned control problem. With the addition of Δp , a well-conditioned control problem can be constituted. Moreover, with control of Δp , the effect of disturbances on the fuel efficiency is reduced, and in addition the effect of control actions for disturbance rejection on NO_x and λ on the fuel efficiency is reduced. For heavy-duty diesel engines, the fuel efficiency is very important, and with the anticipated fuel efficiency legislation, its importance will further increase.

Via Singular Value Decomposition (SVD) decoupling, the two-input three-output configuration is converted into a decoupled two-input two-output system. For this system, a diagonal PI controller is designed using loopshaping. The controller is tested in simulation and experiments. In simulation, its effectiveness at reducing the effects of disturbances is shown. With the controller enabled, the deteriorating effect of the disturbances on the average NO_x and PM emissions and fuel consumption is neutralized and the variation of the NO_x and PM emissions, and Δp is reduced by an order of magnitude. In experiments, the effectiveness of the controller for disturbance rejection and its functioning over the operating range of the engine are shown.

7.1.2 Design Effort

The control design effort for diesel engines is a bottleneck in the overall engine design. With new generations of diesel engines, the number of sensors and actuators increased. This enlarged the potential for performance improvements by means of control, but a simultaneous increase in control design effort is observed. Taking into account the control design effort, when designing control techniques for diesel engines, is therefore increasingly relevant.

In this thesis, three measures are taken to reduce the control design effort.

- **Use feedback control for disturbance rejection.** With an effective feedback controller, the effects of disturbances are diminished. The need for engine maps that compensate for disturbances is thereby reduced. This reduces the number of parameters that require calibration, and thereby reduces the control design effort.

- **Use a systematic, offline control design.** A design path is followed that consists of: model identification, control design, and performance evaluation. A time-efficient and accurate procedure for modeling the engine behavior is experimentally applied and extensively analyzed. The identified FRF models characterize the dynamic input-output behavior of the engine. The design of the feedback controller is based entirely on these FRF models. This way, the controller is designed such that it works well in conjunction with the input-output behavior of the engine, without the time-consuming process of manually adapting the controller parameters and empirically determining its effect on the engine performance. After control design, the performance is experimentally evaluated to determine if indeed the expected performance level is realized.
- **Use low-complexity control elements.** A range of control design techniques (see Chapter 3) is suitable to fulfill the above two requirements. The proposed control design consists of PI control and SVD decoupling. Compared with the alternatives, this has the advantage that the complexity of the controller and its design process is low. Various alternative methods for linear control design are used in literature, but these require some form of gain-scheduling to work on the entire operating range. By focussing on robustness in the system layout, scheduling of the control parameters is not required. An LTI feed-forward controller combined with a PI controller with static decoupling matrices, both with fixed parameters, is sufficient to control the engine over its entire operating range.

7.1.3 Summary of the Main Results

The control design process, as elaborated in this thesis, is divided into system identification, disturbance rejection around a fixed operating point, and control over the full operating range. The main conclusions resulting from these parts are separately addressed in the following.

Identification

In Chapter 4, a method for identification of the sensor response to variations in the actuators, i.e., the input-output response, is elaborated. For this, the local Frequency Response Function (FRF) at a fixed speed-load operating point is

measured using multisine excitation. Compared with alternative modeling methods, the ability to include any measured output in the model, without complicating the modeling procedure, is an advantage. Also, the natural inclusion of sensor and actuator dynamics into the model is an advantage for the application of control design. The considered actuators are the VGT and EGR valve, the measurements are the engine-out NO_x emissions, air-fuel equivalence ratio and pressure difference between the intake and exhaust manifold. It is found that using only ten minutes of identification data, the local input-output behavior can be captured accurately. The effects of noise and nonlinearity on the local engine behavior are individually quantified and it is shown that these effects are an order of magnitude smaller than the linear effects. Using the linear FRF models, the actual engine measurements in a single speed-load point are reconstructed with average squared errors smaller than 3 % of the actual response.

Disturbance Rejection

Chapter 5 discusses control design to reduce the effects of disturbances. The goal of the controller is to keep the engine-out emissions of NO_x , PM and the fuel efficiency close to their respective nominal values, despite the effects of external influences. To realize this, a feedback controller is designed. A new selection of controlled outputs is made: NO_x , λ and Δp . These outputs are selected because they reflect the engine-out NO_x emissions, PM emissions and fuel efficiency, respectively. With two actuators and three measured outputs, the resulting input-output system is underactuated. It is argued that the expected Pareto-optimality of the combination of NO_x , PM and fuel efficiency implies that regardless of the number of actuators, only two controllable directions are available. This means that the underactuation does not induce an additional limitation. Using SVD-decoupling and loopshaping, a feedback controller is designed to control the underactuated input-output system. In a simulation, where disturbances are applied in the inputs, operating point and ambient conditions, the controller is shown to reduce the variation of the NO_x and PM emissions and Δp with a factor 12, 5 and 14, respectively. In addition, the increase of the average emissions and fuel efficiency is neutralized, resulting in a reduction of the average NO_x and PM emissions with 14 % and 19 %, respectively, and a reduction of 0.74 % of the BSFC. The controller is also tested experimentally, while step disturbances are applied in the inputs and the engine speed and load. It is again shown that the feedback controller maintains the tradeoff between NO_x ,

λ and Δp and reduces the effects of the applied disturbances on the individual outputs.

Full Operating Range

In Chapter 6, an air-path control system is designed that can be used on the full engine speed-load range and features a particularly low design effort. The identification method of Chapter 4 is used to efficiently model the local input-output behavior in a grid of operating points covering the full speed-load range. The feedback control design of Chapter 5 is reused and modified to accommodate different engine speeds and loads. An additional dynamic feed-forward controller is designed to reduce the PM emissions and improve the torque response during tip-in torque transients. This feed-forward controller is calibrated manually on a dynamometer setup. This enables the evaluation of the transient NO_x emissions, PM emissions and torque response during calibration. Both the feedback controller and the feed-forward controller are of low-order LTI form and do not require scheduling of their parameters. Therefore, they have a particularly low design complexity and implementation footprint. The combined controller is experimentally tested on the World Harmonized Transient Cycle (WHTC). Compared with the controller originally implemented on the engine ECU, the emissions over the WHTC of both NO_x and PM are reduced with 3.9% and 11.7%, respectively. The fuel consumption over the WHTC remained approximately unchanged.

Summarising, a control design procedure for air-path control of clean diesel engines was formulated. The design procedure comprises system identification, a feedback controller for disturbance rejection and a feed-forward controller for improved transient performance. The designed controller is tested both in simulation and experimentally on a modern EURO VI engine. It is shown that due to the feedback controller, the performance of the engine remains close to the nominal performance when disturbances are applied. On WHTC experiments, it is shown that with the newly designed controller, the NO_x and PM emissions are reduced, compared with the original controller. The presented control design procedure is time efficient and the resulting controller has a small implementation footprint.

7.2 Recommendations for Future Research

The current work presents a proof of concept for a new diesel engine control design using the air-path actuators. Several potential improvements to the control design framework can be considered and are outlined below. First, adaptations to improve on the limitations of the proposed control design are addressed. Because the applied modeling procedure is also useful outside of the proposed control design framework, recommendations for adapting the modeling procedure are addressed separately. When reconsidering the use of air path control in the overall engine control problem, including the aftertreatment system, further opportunities for improvement are discerned, which are discussed at the end of this section.

7.2.1 Improved Air Path Control

Control Algorithm

The current control design has a low design effort. When the process of optimizing the steady-state engine performance is completed; and assuming that the necessary preparations to process and evaluate the data are made and an I/O-board to interface with the engine is available. Identification and design of the feedback and feed-forward controller can optimistically be completed in a single day.

The choice to minimize complexity, rather than to maximize the performance induces a performance penalty. To quantify to what extent this affects the emissions and fuel consumption, a comparison with a less conservative control design should be made. For example, a gain-scheduled \mathcal{H}_∞ controller can replace the current feedback controller and serve as a high-performance benchmark. This removes the conservatism introduced by the decoupling and linear PI control design and adapts the control behavior to the local engine behavior. Depending on the achieved performance increase, an increase in the controller complexity may be justified and a more complex control design can be considered. The gain-scheduled \mathcal{H}_∞ controller is likely too complex to implement in production. But implementing, e.g., scheduling of the PI parameters requires only a moderate increase in the controller complexity and design effort. Similarly, scheduling can also be applied to the parameters of the feed-forward controller, e.g., based on the engine speed. The added flexibility can be used to control the emission tradeoff more closely.

Controlled Outputs

The BSFC, NO_x and PM are considered the main performance measures that require feedback control. To increase the effectiveness of the feedback controller with regards to disturbance rejection on these measures, the use of alternative sensors that more directly reflect these measures can be considered.

When a PM sensor becomes available, direct control of measured PM emissions is possible. This enables more direct control of the emissions and more tight compliance with the emission legislation. The use of λ instead of PM, as used in this thesis, also has advantages. The λ output is also a relevant measure for the engine's ability to quickly respond to an increase in torque demand. Controlling λ , rather than PM, is therefore beneficial for maintaining the desired torque response when disturbances affect the engine. It is therefore not obvious whether controlling PM, rather than λ , improves the engine performance.

When the in-cylinder pressure is measured, a number of different control applications become possible. The fast dynamic response of the in-cylinder measurements is well suited to be combined with the fast actuators in the fuel path. Some examples that become possible are: control of the combustion timing via the injection timing; control of the combustion profile via the injection profile; and control of IMEP via the injection quantity. Also, the indicated specific fuel consumption can be determined using the in-cylinder pressure. This information can be used to further improve the air-path controller. In the control design in this thesis, only the PMEP effect on the BSFC is used for disturbance rejection. This can be complemented with the IMEP effect, when the in-cylinder pressure is measured. This enables more direct control of the BSFC.

With the current control design, the sensor dynamics of the NO_x sensor are a bottleneck for the achieved closed-loop bandwidth. This limitation can be surmounted either by using a sensor that does not suffer as much from sensor dynamics (Karlsson et al., 2010) or by using an additional observer (Tschanz et al., 2013). When the limitations of sensor dynamics are removed, the internal air-path dynamics limit the closed-loop bandwidth. This enables the design of a feedback controller that achieves faster disturbance rejection.

Experiments

Further testing of the controller in more realistic scenarios is advised to determine if the controller and disturbance rejection remain effective in real-world scenarios. When a series of engines is tested, the effects of production tolerances on the engine performance, and the effectiveness of the feedback controller on reducing the performance differences can be quantified. Similarly, engines of a different age and maintenance state, and the effects of fuel quality, ambient temperature, pressure and humidity should be tested. The presented simulation results in Chapter 5 indicate that the controller can be expected to handle these disturbances well. An experimental validation is, however, much more convincing.

Transients

The engine performance during fast operating-point transients is not well reflected in the design of the feedback controller. The proposed sensor layout and feedback bandwidth are designed to reduce the effects of slowly varying disturbances and maintain close to optimal performance in steady state. Ideally, a feedback controller should improve the transient performance as well as achieve disturbance rejection.

The time scales relevant for evaluating emissions and fuel consumption are much longer than those for evaluating performance during an operating point transient. A temporary 20% difference between the nominal emissions and the actual emissions during a tip-in transient can well be tolerated if this averages out over time. Nonetheless feedback control can also be relevant for improving the performance during fast transients. When, during transients, a feedback controller assists in controlling, e.g., the fresh air flow, turbine speed or both, the transient engine response can become less sensitive to how well the feed-forward characteristics match the actual engine characteristics. This can reduce the calibration effort needed for improving torque transients and reduce the effects of disturbances on the torque response.

7.2.2 Modeling

The presented modeling procedure is both accurate and fast for the considered use case and is suitable for the proposed control design. A further improvement of the accuracy or a reduction of the required identification effort will therefore not significantly improve the overall modeling process. The range of applications for which the resulting models can be used with high accuracy is however rather limited. A modified identification procedure that results in more versatile models, that are suitable for more applications, would be an improvement. Additional applications that can be considered are described below. The challenge when adapting the modeling procedure is to maintain the strong features of the current modeling procedure, i.e., the high and quantifiable accuracy, ability to model any input-output combination and the inclusion of sensor and actuator dynamics. Recommendations for changes to the modeling procedure that can be considered are discussed next.

The number of actuators that are considered can be extended. When in addition to the excitations in the VGT and EGR valve, also excitations in the engine speed or fuel quantity are applied, these effects can be modeled as well. This can be useful, e.g., for calculating control actions during operating point changes. When the use of, e.g., the SOI or BPV for feedback control is considered, an excitation signal can be added here as well. Adding excitation signals to additional actuators does come at the expense of either the identification accuracy or the required identification time. Additional outputs, e.g., the mass air flow or exhaust temperature, can be modeled without modifying the identification experiment and without compromising the identification accuracy or identification time. The frequency response of any sensor signal that was measured during the identification experiment can be determined the using analysis procedure in Chapter 4.

The conversion of the FRF into a different model type can also make the models more suitable for (quasi) linear model-based control design, which is used in most of the control design methods described in Chapter 3. A conversion of the FRF into to a different model type, such as a linear state-space model makes the models more suitable to be used for this.

For simulating drive cycles, large speed and load transients must be considered and included in the modeling process. During these transients, the effects of

nonlinear behavior can be expected to become dominant over the linear behavior. Significant changes to both the modeling and identification process are required to accurately capture this. A different model structure should be selected, such that the nonlinear behavior can be modeled accurately. Also, the identification experiment should be changed. The current experiment was designed to accurately identify the local input-output response. By maintaining close to a fixed operating point, the effects of operating point variations are excluded from the experimental results as much as possible. Therefore, the current experiment is not suitable for identifying the dynamic effects of operating point variations. In literature, mean-value models, which are based on approximate physical relations, are often used for simulating drive cycles. These models are more suitable for this purpose. Compared with the FRF models, the local accuracy and the ability to easily include any available input-output combination in the model are compromised.

7.2.3 Integrated Engine Control

A further synergy between the control system of the air path and the aftertreatment system presents opportunities for improvements in two ways. First, control of the air path can be used to increase the conversion efficiency of the SCR system. Second, the state of the SCR system can be used to dynamically schedule the allowed engine-out emissions. This is explained below in more detail.

The exhaust gas temperature, which is affected by the VGT and EGR valve, affects the conversion efficiency of NO_x in SCR catalysts. When the exhaust gas temperature is controlled to be at its optimal level for NO_x conversion, increased engine-out NO_x emissions can be allowed, without increasing the tailpipe-out emissions. This presents an opportunity to further reduce the PM emissions and BSFC. It is worth noting that an increased exhaust gas temperature also implies an increase of the BSFC. It is therefore not a priori clear if the allowed increase in engine-out NO_x also results in a reduced BSFC.

When the conversion efficiency of the SCR catalyst is known, this information can be used to dynamically schedule the allowed engine-out NO_x emissions. When the conversion efficiency is high, increased engine-out NO_x emissions can be allowed, without increasing the tailpipe-out emissions. The allowed increase in engine-out emissions can be used to further optimize the fuel efficiency. In Willems et al. (2013),

the potential to reduce the fuel consumption using this method is experimentally demonstrated.

Bibliography

- ACEA. Commercial vehicles and CO₂. Technical report, ACEA, 2010.
- D. Alberer and L. Del Re. Optimization of the transient diesel engine operation. *Proceedings of the 9th International Conference on Engines and Vehicles, Capri, Naples, Italy, SAE Technical Paper 2009-24-0113*, 2009.
- D. Alberer and L. Del Re. On-line abatement of transient NO_x and PM diesel engine emissions by oxygen based optimal control. *SAE paper 2010-01-2201*, 10 2010.
- D. Alberer, H. Hjalmarsson, and L. Del Re. System identification for automotive systems: Opportunities and challenges. In D. Alberer, H. Hjalmarsson, and L. Del Re, editors, *Identification for Automotive Systems*, volume 418 of *Lecture Notes in Control and Information Sciences*, pages 1–10. Springer London, 2012.
- E. Alfieri. *Emissions-controlled diesel engine*. PhD thesis, ETH Zurich, Switzerland, 2009.
- M. Benz. *Model-based optimal emission control of diesel engines*. PhD thesis, ETH Zurich, Switzerland, 2010.
- A. Brahma. *Methodologies for Modeling and Feedback Control of the NO_x-BSFC Trade-Off in High-Speed, Common-Rail, Direct-Injection Diesel Engines*. PhD thesis, The Ohio State University, USA, 2005.
- J. Chauvin, G. Corde, N. Petit, and P. Rouchon. Motion planning for experimental airpath control of a diesel homogeneous charge-compression ignition engine. *Control Engineering Practice*, 16(9):1081–1091, 2008.

- C. Criens, F. Willems, T. van Keulen, and M. Steinbuch. Experimental control design for robust low emission, fuel efficient diesel engines. *Submitted for Journal Publication*, 2014.
- C. Criens, T. van Keulen, F. Willems, and M. Steinbuch. A control oriented multivariable identification procedure for turbocharged diesel engines. *Submitted for journal publication*, 2013a.
- C. Criens, F. Willems, and M. Steinbuch. Under actuated air path control of diesel engines for low emissions and high efficiency. In *Proceedings of the FISITA 2012 World Automotive Congress*, pages 725–737. Springer, 2013b.
- H. Dekker and W. Sturm. Simulation and control of a HD diesel engine equipped with new EGR technology. *SAE Technical Paper 960871*, 1996.
- L. Del Re, P. Ortner, and D. Alberer. Modeling alternatives for automotive predictive control. In *Proceedings of the ECOSM09*, 2009.
- DieselNet. Emission standards, European Union, heavy-duty truck and bus engines, 2013. URL <http://www.dieselnet.com/standards/>.
- T. Dobrowiecki and J. Schoukens. Linear approximation of weakly nonlinear mimo systems. *Instrumentation and Measurement, IEEE Transactions on*, 56 (3):887–894, 2007.
- European Commission. Commission regulation (EU) No 582/2011 of 25 May 2011 implementing and amending regulation (EC) No 595/2009 of the European parliament and of the council with respect to emissions from heavy duty vehicles (Euro VI) and amending annexes I and III to directive 2007/46/ec of the European parliament and of the council text with EEA relevance, May 2011.
- European Environment Agency. European union emission inventory report 1990-2011 under the UNECE convention on long-range transboundary air pollution (Irtap). Technical Report 10/2013, European Union, 2013.
- H. J. Ferreau, P. Ortner, P. Langthaler, L. Del Re, and M. Diehl. Predictive control of a real-world diesel engine using an extended online active set strategy. *Annual Reviews in Control*, 31(2):293–301, 2007.

-
- S. García-Nieto, M. Martínez, X. Blasco, and J. Sanchis. Nonlinear predictive control based on local model networks for air management in diesel engines. *Control Engineering Practice*, 16(12):1399–1413, 2008.
- N. Gense, C. Such, and L. Ntyiachristos. Euro VI technologies and costs for heavy duty vehicles. *TNO Science and Industry report*, 6(06.OR.PT.023.2/NG), 2006.
- M. Grahn, K. Johansson, and T. McKelvey. A diesel engine management system strategy for transient engine operation. In *7th IFAC Symposium on Advances in Automotive Control*, pages 1–6, 2013.
- C. Guardiola, A. Gil, B. Pla, and P. Piqueras. Representation limits of mean value engine models. In D. Alberer, H. Hjalmarsson, and L. Del Re, editors, *Identification for Automotive Systems*, chapter 11, pages 185–206. Springer Berlin / Heidelberg, 2012.
- L. Guzzella and A. Amstutz. Control of diesel engines. *Control Systems, IEEE*, 18(5):53–71, 1998.
- L. Guzzella and C. Onder. *Introduction to modeling and control of internal combustion engine systems*. Springer, 1 edition, 2004.
- M. Henningsson. *Data-Rich Multivariable Control of Heavy-Duty Engines*. PhD thesis, Department of Automatic Control, Lund University, Sweden, 2012.
- M. Henningsson, K. Ekhölm, P. Strandh, P. Tunestål, and R. Johansson. Dynamic mapping of diesel engine through system identification. In D. Alberer, H. Hjalmarsson, and L. Del Re, editors, *Identification for Automotive Systems*, chapter 13, pages 223–240. Springer, 2012.
- M. Herceg, T. Raff, R. Findeisen, and F. Allgöwe. Nonlinear model predictive control of a turbocharged diesel engine. In *Computer Aided Control System Design, 2006 IEEE International Conference on Control Applications, 2006 IEEE International Symposium on Intelligent Control, 2006 IEEE*, pages 2766–2771, 2006.

- M. Hirsch, K. Oppenauer, and L. Del Re. Dynamic engine emission models. In L. Del Re, F. Allgöwer, L. Glielmo, C. Guardiola, and I. Kolmanovsky, editors, *Automotive Model Predictive Control*, chapter 5, pages 73–87. Springer Berlin / Heidelberg, 2010.
- M. Jankovic, M. Jankovic, and I. Kolmanovsky. Constructive Lyapunov control design for turbocharged diesel engines. *Control Systems Technology, IEEE Transactions on*, 8(2):288–299, 2000.
- M. Jung and K. Glover. Calibratable linear parameter-varying control of a turbocharged diesel engine. *Control Systems Technology, IEEE Transactions on*, 14(1):45–62, 2006.
- M. Karlsson, K. Ekholm, P. Strandh, R. Johansson, and P. Tunestal. Multiple-input multiple-output model predictive control of a diesel engine. In *Proceedings of the Sixth IFAC Symposium in Automotive Control, Munich, Germany*, volume 1, pages 124–129, 2010.
- T. Koji and Y. Kazuhiro. A study on the cell structure and the performances of wall-flow diesel particulate filter. *Energy*, 48(1):492–499, 2012.
- I. Kolmanovsky, P. Moraal, M. Van Nieuwstadt, and A. Stefanopoulou. Issues in modelling and control of intake flow in variable geometry turbocharged engines. *Chapman and Hall CRC research notes in mathematics*, pages 436–445, 1999.
- T. Körfer, L. Ruhkamp, O. E. Herrmann, R. Linssen, and D. Adolph. Verschärfte anforderungen an die luftpfadregelung bei nutzfahrzeug-motoren. *MTZ - Motortechnische Zeitschrift*, 69(11):958–965, 2008.
- L. Ljung. *System identification, Theory for the User*. Wiley Online Library, 2 edition, 1999.
- M. Mrosek, H. Sequenz, and R. Isermann. Identification of emission measurement dynamics for diesel engines. In *18th IFAC World Congress, Italy*, pages 11839–11844, 2011.
- M. van Nieuwstadt, I. Kolmanovsky, P. Moraal, A. Stefanopoulou, and M. Jankovic. EGR-VGT control schemes: experimental comparison for a high-speed diesel engine. *Control Systems, IEEE*, 20(3):63–79, 2000.

-
- P. Ortner and L. Del Re. Predictive control of a diesel engine air path. *Control Systems Technology, IEEE Transactions on*, 15(3):449–456, 2007.
- P. Ortner, R. Bergmann, H. Ferreau, and L. Del Re. Nonlinear model predictive control of a diesel engine airpath. In *IFAC Workshop on Control Applications of Optimisation, Jyvaskyla*, pages 91–96, 2009.
- D. Pachner, D. Germann, and G. Stewart. Identification techniques for control oriented models of internal combustion engines. In D. Alberer, H. Hjalmarsson, and L. Del Re, editors, *Identification for Automotive Systems*, chapter 15, pages 257–282. Springer, 2012.
- R. Pintelon and J. Schoukens. *System identification: a frequency domain approach*. Wiley-IEEE Press, 1 edition, 2001.
- D. Rijlaarsdam, B. van Loon, P. Nuij, and M. Steinbuch. Nonlinearities in industrial motion stages - detection and classification. In *American Control Conference, 2010*, pages 6644–6649, 2010.
- J. Schoukens, R. Pintelon, T. Dobrowiecki, and Y. Rolain. Identification of linear systems with nonlinear distortions. *Automatica*, 41(3):491–504, 2005.
- H. Sequenz, M. Mrosek, S. Zydek, and R. Isermann. Model based optimisation of a step in acceleration for a CR-diesel engine. In *World Congress*, volume 18, pages 13016–13021, 2011.
- X. Seykens. Engine simulation tool DYNAMO. Technical report, TNO Automotive, 2009.
- X. Seykens. *Development and validation of a phenomenological diesel engine combustion model*. PhD thesis, Eindhoven University of Technology, The Netherlands, 2010.
- S. Skogestad and I. Postlethwaite. *Multivariable feedback control: analysis and design*, volume 2. Wiley, 2007.
- I. Stamati, D. Telen, F. Logist, E. Van Derlinden, M. Hirsch, T. Passenbrunner, and J. Van Impe. Optimal experimental design for mechanistic nonlinear dynamic models using multisine inputs: Application to a diesel engine. In *American Control Conference, 2012*, pages 4227–4232, 2012.

- A. Stefanopoulou, I. Kolmanovsky, and J. Freudenberg. Control of variable geometry turbocharged diesel engines for reduced emissions. *Control Systems Technology, IEEE Transactions on*, 8(4):733–745, 2000.
- G. Stewart, F. Borrelli, J. Pekar, D. Germann, D. Pachner, and D. Kihás. Toward a systematic design for turbocharged engine control. In L. Del Re, F. Allgöwer, L. Glielmo, C. Guardiola, and I. Kolmanovsky, editors, *Automotive Model Predictive Control*, chapter 14, pages 211–230. Springer Berlin / Heidelberg, 2010.
- T. Tienstra. Optimization of tip-in transients for a heavy duty diesel engine. Masters Thesis CST 2013.045, Eindhoven University of Technology, 2013.
- F. Tschanz, A. Amstutz, C. Onder, and L. Guzzella. Feedback control of particulate matter and nitrogen oxide emissions in diesel engines. *Control Engineering Practice*, 21(12):1809–1820, 2013.
- R. Van Helden, R. Verbeek, F. Willems, and R. van der Welle. Optimization of urea SCR deNOx systems for HD diesel engines. *SAE Technical Paper*, 1(SAE 2004-01-0154), 2004.
- K. Vanhoenacker, T. Dobrowiecki, and J. Schoukens. Design of multisine excitations to characterize the nonlinear distortions during FRF-measurements. *Instrumentation and Measurement, IEEE Transactions on*, 50(5):1097–1102, 2001.
- A. S. Verma. Airpath modelling of turbocharged diesel engine in transient operation and investigation. *International Journal of Advanced Technology and Engineering Research*, 3(1):1–10, 2013.
- J. Wahlström. *Control of EGR and VGT for emission control and pumping work minimization in diesel engines*. PhD thesis, Department of Electrical Engineering, Linköpings universitet, 2009.
- J. Wahlström and L. Eriksson. Robust nonlinear EGR and VGT control with integral action for diesel engines. In *17th IFAC World Congress, Korea*, 2008.
- J. Wahlstrom and L. Eriksson. Output selection and its implications for MPC of EGR and VGT in diesel engines. *Control Systems Technology, IEEE Transactions on*, 21(3):932–940, 2013.

-
- J. Wahlström, L. Eriksson, and L. Nielsen. EGR-VGT control and tuning for pumping work minimization and emission control. *Control Systems Technology, IEEE Transactions on*, 18(4):993–1003, 2010. ISSN 1063-6536.
- J. Wahlström and L. Eriksson. Modelling diesel engines with a variable-geometry turbocharger and exhaust gas recirculation by optimization of model parameters for capturing non-linear system dynamics. *Proceedings of the Institution of Mechanical Engineers, Part D: Journal of Automobile Engineering*, 225(7):960–986, 2011.
- X. Wang, H. Waschl, D. Alberer, and L. Del Re. A design framework for predictive engine control. *Oil & Gas Science and Technology—Revue d’IFP Energies nouvelles*, 66(4):599–612, 2011.
- H. Waschl, D. Alberer, A. Kerschbaummayr, and L. Del Re. Reliable reference determination for diesel engine emission control. In *American Control Conference, 2012*, pages 4215–4220, 2012.
- X. Wei and L. Del Re. Gain scheduled H_∞ control for air path systems of diesel engines using LPV techniques. *Control Systems Technology, IEEE Transactions on*, 15(3):406–415, 2007.
- F. Willems and R. Cloudt. Experimental demonstration of a new model-based SCR control strategy for cleaner heavy-duty diesel engines. *Control Systems Technology, IEEE Transactions on*, 19(5):1305–1313, 2011.
- F. Willems, P. Mentink, F. Kupper, and E. van den Eijnden. Integrated emission management for cost optimal EGR-SCR balancing in diesels. In *7th IFAC Symposium on Advances in Automotive Control*, pages 701–706. Japan : IFAC, September 2013.
- D. Zhao, C. Liu, R. Stobart, J. Deng, E. Winward, and G. Dong. An explicit model predictive control framework for turbocharged diesel engines. *Industrial Electronics, IEEE Transactions on*, PP(99):1–1, 2013.

Summary

Air-Path Control of Clean Diesel Engines

for disturbance rejection on NO_x , PM and fuel efficiency

This thesis deals with the design of a control system for heavy-duty diesel engines, which makes use of the Variable Geometry Turbine (VGT) and Exhaust Gas Recirculation (EGR) valve. The goal of this control system is to simultaneously achieve a low fuel consumption and low engine-out NO_x and PM emissions, and to maintain these properties when disturbances are present. In addition, a control design method with a low design effort and complexity is aimed for.

The new EURO VI emission legislation for heavy-duty diesel engines requires a reduction of the Nitrogen Oxides (NO_x) and Particulate Matter (PM) emissions of 80 % and 50 %, respectively, compared with the EURO V legislation. Moreover, it requires that these low emissions are achieved under real-world conditions, which implies that the effects of, e.g., production tolerances, ageing and changing ambient conditions have to be accounted for. This can in part be achieved via improved control using the VGT and EGR valve. A VGT can adapt the flow area of the turbine, which influences the power generated by the turbine as well as the flow through the turbine. The EGR system is used to dilute the intake air with cooled exhaust gas. This reduces the temperatures reached during combustion, which reduces the NO_x emissions. The EGR flow is throttled by a controllable EGR valve, such that a favorable balance between the positive effects (reduced NO_x emissions) and the negative effects (increased PM emissions, decreased combustion efficiency, increased pumping work) of EGR can be maintained. Combined, the

VGT and EGR valve determine the pressures and flows in the air path and thereby they influence the emissions and fuel efficiency.

The control design process, which is elaborated in this thesis, can be divided into three parts: system identification, disturbance rejection around a fixed operating point, and control over the full speed-load range of the engine. In the following, these parts are individually addressed.

Multisine Frequency Response Function (FRF) identification is used as an accurate and time-efficient method for modeling the input-output dynamics at a fixed engine speed-load point. The considered inputs are the VGT and EGR valve; the considered outputs are the engine-out NO_x emissions, the air-fuel equivalence ratio, and the pressure difference between the intake and exhaust manifold. The resulting model accuracy is extensively analyzed. The effects of noise and nonlinearities on the local system behavior and the distortion of the FRF as a result of these effects are separated and individually quantified as a function of frequency. It is found that with ten minutes of identification data, an accurate Multi-Input Multi-Output (MIMO) model of the local behavior in a single speed-load point is identified. That is, the effects of the above mentioned distortions are an order of magnitude smaller than the modeled linear behavior. The identification procedure is used repeatedly to model the local behavior on a grid of engine speed-load points that covers the full operating range of the engine. Large difference in the local behavior at different speed-load points are identified that include variations in the input-output gain of a full order of magnitude.

A feedback controller is designed, that is aimed at maintaining the brake specific fuel consumption (BSFC), NO_x emissions and PM emissions at all times as close as possible to the values obtained under nominal conditions. It is found that for the performance of this feedback controller, the selection of the controlled outputs is critical. Outputs that reflect the main performance measures: NO_x , PM and BSFC, are preferable. For this reason, three outputs are selected as controlled outputs: the engine-out NO_x sensor measurement, air-fuel equivalence ratio (λ), and pressure difference between intake and exhaust manifold, respectively. Using SVD-decoupling, the three-output system is reduced to a decoupled Two-In, Two-Out (TITO) system. A diagonal PI controller is designed to control this TITO system. It is shown in a simulation with various disturbances that, despite these disturbances, the engine with the controller can achieve near-nominal average

NO_x and PM emissions and fuel efficiency. For comparison, the same simulation is repeated without feedback control. With feedback enabled, the average NO_x and PM emissions and fuel consumption are reduced with 14 %, 19 % and 0.74 %, respectively. Moreover, the feedback controller reduced the variation as a result of disturbances of the NO_x and PM emissions and pressure difference with a factor 12, 5 and 14, respectively. The controller is also tested experimentally, while step disturbances in the inputs and engine speed and load are applied. Its effectiveness at reducing the effects of disturbances is again demonstrated.

To control the air path over the full engine speed-load range, the effects of nonlinear behavior have to be accounted for. It is shown that despite the encountered nonlinear behavior, a linear feedback controller of the same structure as used for local disturbance rejection and with fixed parameters can also be effective for disturbance rejection in the full operating range; using a linear controller, asymptotic stability and a sufficient closed-loop bandwidth are achieved. To improve the torque response and decrease the PM emissions during tip-in torque transients, a complementary feed-forward controller is designed. This controller accelerates the turbine response and increases the fresh air flow during tip-in transients. For the feed-forward controller, a control design with a fixed structure and two tunable parameters is used for each actuator. The emission measurement equipment that is available at the dynamometer test setup is used to evaluate the engine performance while tuning the controller parameters. It is shown experimentally that a two-second torque response can be combined with acceptable NO_x and PM emissions. The combination of the feedback and feed-forward controllers constitutes a control system that satisfies the performance requirements and features the desired low design effort.

The performance of the engine, using the new feedback and feed-forward controller, is demonstrated experimentally on a modern six-cylinder, heavy-duty, EURO VI engine. On the hot World Harmonized Transient Cycle (WHTC), which is part of the EURO VI approval tests, reduced NO_x (-3.9 %) and PM (-11.7 %) emissions are obtained, while maintaining the low fuel consumption that is obtained with the original engine controller.

Samenvatting

Ontwerp van een Luchtpadregeling voor Schone Dieselmotoren voor verstoringsonderdrukking op NO_x , PM en brandstofverbruik

Het onderwerp van dit proefschrift is het ontwerp van een regelsysteem voor dieselmotoren in vrachtauto's. De regelaar maakt gebruik van de Variabele Geometrie Turbo (VGT) en uitlaatgasrecirculatieklep (EGR klep). Het doel van het regelsysteem is om een laag brandstofverbruik te combineren met een lage uitstoot van NO_x en PM (Particulate Matter, ofwel fijnstof) en bovendien deze eigenschappen te behouden als er verstoringen aanwezig zijn. Een tweede doelstelling voor het nieuwe regelaarontwerp is dat het in korte tijd geïmplementeerd kan worden.

De nieuwe EURO VI emissiewetgeving voor vrachtauto dieselmotoren schrijft een vermindering van de NO_x en PM uitstoot voor van respectievelijk 80 % en 50 %, ten opzichte van het EURO V niveau. Daarbij wordt ook voorgeschreven dat deze lage uitstoot tijdens bedrijf gehaald moet worden, wat impliceert dat de invloeden van bijvoorbeeld productiever verschillen, veroudering en veranderingen in de atmosferische condities meegenomen moeten worden. Een verbeterde aansturing van de VGT en EGR klep kan hier een bijdrage aan leveren. Een turbo die is uitgevoerd met VGT kan de geometrie van de turbine inlaat aanpassen. Hiermee verandert de stroming door de turbine en ook het door de turbine opgewekte vermogen. Middels het EGR systeem wordt de aangezogen lucht verdund met gekoelde uitlaatgassen. Hierdoor loopt de temperatuur tijdens verbranding minder hoog op, waardoor de NO_x uitstoot vermindert. De EGR stroom wordt beperkt door een regelbare EGR klep, zodat de balans tussen de positieve effecten (verminderde NO_x uitstoot) en de negatieve effecten (verhoogde PM uitstoot, slechtere verbranding, toegenomen

pompverliezen) van EGR gunstig blijft. De instellingen voor de VGT en EGR klep beïnvloeden zo de NO_x en PM emissies en het brandstofverbruik van dieselmotoren.

Het ontwerpproces van de regelaar, zoals uitgewerkt in dit proefschrift, is in drie onderdelen op te splitsen: systeem identificatie, verstoringsonderdrukking rond een vast werkpunt, en regelacties over het volledige werkgebied. Deze onderdelen zullen nu individueel besproken worden.

Frequentie Response Functies (FRF), gemeten door middel van multisinus identificatie, worden gebruikt als een nauwkeurige en efficiënte methode om het dynamisch gedrag van de motor rond een vast werkpunt te modelleren. De gebruikte systeemingenangen zijn de VGT en EGR klep; de gemodelleerde uitgangen de NO_x uitstoot, lucht-brandstof verhouding, en het drukverschil tussen het inlaat- en uitlaatspruitstuk. Het model bevat alle dynamica tussen ingang en uitgang, inclusief sensor- en acuatorodynamica. De verkregen modelnauwkeurigheid is uitgebreid geanalyseerd. De effecten van ruis en niet-lineariteiten op het lokale systeemgedrag en de vervorming van de gemeten FRF als gevolg van deze effecten worden onderscheiden en individueel gekwantificeerd als functie van de frequentie. Met een meting van tien minuten kan een nauwkeurig Multi-Input Multi-Output (MIMO) model van het lokale systeemgedrag worden geïdentificeerd, waarmee wordt bedoeld dat de effecten van de eerder genoemde verstoringen minstens één orde grootte kleiner zijn dan het gemodelleerde lineaire gedrag. De identificatie procedure is meermaals toegepast om zo het lokale systeemgedrag op een raster van werkpunten te modelleren. Grote onderlinge verschillen tussen het lokale systeemgedrag bij verschillende motortoerentallen of verschillende koppels worden gevonden, waaronder een orde grootte verschil in de magnitude van de FRF.

Er is een feedback regelaar ontworpen met het doel het brandstofverbruik en de uitstoot van NO_x en PM zo dicht mogelijk bij de nominale waarden te houden. Voor de prestaties van deze feedbackregelaar is de keuze voor de geregelde uitgangen van groot belang. Uitgangen die een sterk verband houden met de prestatie-indicatoren: NO_x , PM en brandstofverbruik, zijn het meest geschikt. Om die reden worden drie uitgangen gekozen: de gemeten NO_x uitstoot, lucht-brandstof verhouding en het drukverschil tussen het inlaat- en uitlaatspruitstuk, respectievelijk. Het systeem met drie uitgangen wordt gereduceerd tot een ontkoppeld systeem met twee ingangen in twee uitgangen (TITO) met behulp van een singuliere waarden decompositie. Om dit systeem te regelen wordt een diagonale

PI regelaar ontworpen. In een simulatie met verschillende verstoringen wordt aangetoond dat de emissies en het brandstofverbruik met deze regelstructuur, ondanks de aangebrachte verstoringen, vrijwel overeenkomen met de nominale waarden. Een vermindering van de gemiddelde NO_x (-14%) en PM (-19%) emissies en het gemiddelde brandstofverbruik (-0.74%) is behaald, ten opzichte van de versie zonder feedback regelaar. Bovendien vermindert de regelaar de spreiding van de NO_x en PM emissies en het drukverschil met, respectievelijk, een factor 12, 5 en 14. De regelaar is ook experimenteel getest, waarbij stapverstoringen in de ingangen en het motortoerental en koppel zijn aangebracht. De effectieve verstoringsonderdrukking is hier opnieuw aangetoond.

Om een regelaar te ontwerpen die effectief is over het volledige werkgebied van de motor, moet er rekening gehouden worden met het niet-lineaire gedrag. In dit proefschrift wordt aangetoond dat ondanks de aanwezigheid van niet-lineair gedrag, een lineaire regelaar gebruikt kan worden. De voorgestelde regelaar gebruikt dezelfde structuur als voor verstoringsonderdrukking rond een vast werkpunt, en is ook met constante parameters effectief voor verstoringsonderdrukking in het volledige werkgebied van de motor. Met deze lineaire regelaar wordt asymptotische stabiliteit en een voldoende snelle bandbreedte van de regellus verkregen. Om de koppelrespons te verbeteren en de PM uitstoot te verminderen als een snelle toename van het koppel wordt gevraagd, wordt er een feed forward regelaar toegevoegd. Deze regelaar verkort de tijd die de turbo nodig heeft om op te toeren en vergroot de instroom van verse lucht. Deze regelaar gebruikt een lineaire tijdinvariante structuur met twee instelbare parameters per actuator. Het emissie meetsysteem, dat beschikbaar is in de dynamometer testopstelling, wordt gebruikt om de prestaties van de motor te evalueren, terwijl de juiste waarden voor de parameters worden bepaald. Experimenten laten zien dat binnen twee seconden aan de koppelvraag kan worden voldaan, terwijl de uitstoot van schadelijke stoffen acceptabel blijft.

De prestaties van de motor met het nieuwe feedback en feed forward regelsysteem worden experimenteel gedemonstreerd. Hiervoor wordt een moderne zescilinder vrachtauto-motor gebruikt die geschikt is voor de EURO VI emissienorm. De warme World Harmonized Transient Cycle (WHTC), een onderdeel is van de EURO VI testprocedure, wordt gebruikt als testcyclus. Door het gebruik van het nieuwe regelsysteem neemt de uitstoot van NO_x af met 3.9% en de uitstoot van PM met 11.7%. Het lage brandstofverbruik van de motor blijft hierbij behouden.

Dankwoord

Met dit proefschrift wordt meer dan vier jaar onderzoek afgerond. Hoewel er maar een auteur op de omslag staat, hebben veel meer mensen een bijdrage aan dit onderzoek gehad. Deze mensen wil ik graag bedanken; niet alleen vanwege hun inhoudelijke bijdrage, maar ook omdat ik dankzij hen een erg mooie tijd heb gehad.

Als eerste wil ik graag mijn promotor Maarten Steinbuch en copromotor Frank Willems bedanken.

Maarten, bedankt voor de kans om in jouw groep een promotieonderzoek uit te voeren en de vrijheid die je me binnen dit onderzoek hebt gegeven. Ik waardeer je open doch kritische blik, brede kennis en enthousiasme.

Frank, je hebt een grote bijdrage geleverd aan de totstandkoming van dit proefschrift. Onze scherpe discussies zorgden ervoor dat de praktische relevantie niet uit het oog werd verloren. Steeds vroeg je me in hoeverre mijn ideeën daadwerkelijk voor prestatieverbeteringen zorgden. Steeds liet je me mijn beschrijvingen verduidelijken, om zo steeds beter neer te zetten wat er bedoeld werd.

I would like to thank Luigi del Re, Johan Schoukens, Lars Eriksson, Paul van den Hof and Thijs van Keulen for reviewing my thesis in detail, suggesting improvements and taking part in the defense committee.

Graag wil ik DAF Trucks N.V. bedanken voor het beschikbaar stellen van een state-of-the-art motor en testopstelling. Dankzij hen was het voor mij mogelijk om na drie jaar simulaties, mijn onderzoek een meer experimentele en praktische wending te geven. Tijdens deze experimenten was de hulp van in het bijzonder Thijs onmisbaar, waarvoor ik hem graag wil bedanken. Ook de eerdere input van

Ignace heeft mij veel verder geholpen. Ook wil de afstudeerders die betrokken zijn geweest bij mijn project: Gerard en Tomas, bedanken voor het gedane werk.

Naast iedereen die een inhoudelijke bijdrage heeft geleverd aan dit proefschrift wil ik graag de (oud)collega's van de D&C, CST en H&NS groepen bedanken. Mede dankzij de goede sfeer op vloer -1 ben ik altijd met plezier naar het werk gegaan. In het bijzonder wil ik mijn kamergenoten bedanken. We hadden de gezelligste kamer van -1 en dat was allemaal aan hen te danken. Dennis, Bart, Menno, Nick en Emanuel, bedankt voor alle gezelligheid en de leuke tijd.

Ook wil ik graag mijn ouders en twee zussen bedanken voor hun steun. Papa, mama, Josine en Maud, bedankt voor alles. Mijn laatste bedankje is voor mijn lieve vriendin Malaika. Mede dankzij jouw steun en liefde is het gelukt om dit proefschrift af te ronden.

Curriculum Vitae

Chris Criens was born on September 11th, 1984 in Roermond, The Netherlands. He finished his secondary education (*Atheneum*) at the *Sg. St. Ursula* in Horn in 2002. Subsequently, he started his academic education in Mechanical Engineering at the Eindhoven University of Technology, for which he received his Master's degree (with great distinction) in 2008. As a part of his studies he performed a traineeship at the University of Southampton, where he worked on *Iterative Learning Control (ILC) for Functional Electrical Stimulation (FES) of Human Arms*. His Master's project was entitled *Linear Parameter Varying (LPV) control of an active vibration isolation system* and was performed at the Dynamics and Control Technology group of the Eindhoven University of Technology.

In September 2008, Chris Criens started his PhD research within the Control Systems Technology group of the department of Mechanical Engineering at the Eindhoven University of Technology. The subject of this research was the design of control algorithms for upcoming clean and fuel efficient heavy-duty diesel engines. The main results of his research are presented in this thesis.

